Towards 6G-Enabled Internet of Things with IRS-Empowered Backscatter-Assisted WPCNs

by

Parisa Ramezani

A thesis submitted in fulfilment of the requirements

for the degree of Doctor of Philosophy

at

Wireless Networking Group

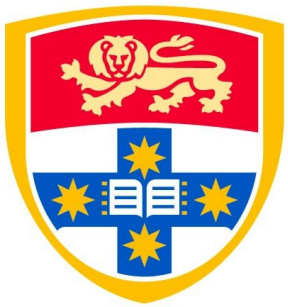

THE UNIVERSITY OF SYDNEY

Faculty of Engineering and Information Technologies

The University of Sydney

September 2021

Declaration

This is to certify that to the best of my knowledge and belief, all material presented in this thesis is the original work of the author, unless otherwise referenced or acknowledged. The content of this thesis has not been previously submitted as a part of any academic qualification to any other university or institution.

_____

Parisa Ramezani

September 2021

To my beloved parents and my lovely brother

Acknowledgment

First of all, my deepest gratitude goes to my supervisor, Prof. Abbas Jamalipour. His continuous support, encouragement, and guidance helped me progress in my studies and find the right research problems. From the very first day, he gave me motivations, provided me with his invaluable advice, believed in me and helped me believe in myself. He patiently guided me through this challenging journey and followed each stage of my research with attention and dedication. The completion of this thesis would not have been possible without his sincere help and support.

I would like to thank my friends in the Wireless Networking Group (WiNG) for making the lab a friendly environment. A very special thank you to Forough for being an awesome friend and helping me in my difficult times. Many thanks to the Head of School of Electrical and Information Engineering at the University of Sydney and all the administrative staff, who helped me with numerous issues.

My Ph.D. experience would not have been this perfect without the experience of working with Dr. Yong Zeng, Dr. Bin Lyu, and Dr. Hoang Dinh Thai. I wholeheartedly thank them for sharing their valuable knowledge with me and teaching me new problem solving skills.

I am eternally grateful to my beloved parents and my lovely brother for their unconditional support and endless love. Without their sacrifices, prayers, and inspirations, I would have never been the person I am today. I am forever thankful to my uncles, aunts, and cousins whose everyday caring and love made me feel at home in Australia. Words cannot express my appreciation for their never-ending kindness and support.

Abstract

Radio Frequency (RF)-enabled wireless energy transfer (WET) is a reliable and controllable technique for powering energy-constrained devices in the emerging Internet of Things (IoT)/Internet of Everything (IoE) era. Thanks to its promising and preeminent properties, RF-enabled WET has notably attracted research interests during the past decade, the consequence of which has been the advent of the far-reaching wireless powered communication technology. A wireless powered communication network (WPCN), as its name implies, is a system where devices rely on RF-enabled WET from dedicated and ambient RF sources for powering their information transmission. This self-sustainable operation of devices in WPCN has useful implications for the envisioned IoT/IoE networks of the future, where massive number of devices are expected to be present, actively communicating with each other and with their designated access points (APs). The extraordinary and unrivaled features of WPCNs have given rise to extensive research efforts from academia and industry for improving the performance of these networks and fulfilling the goals promised by WPCNs. However, now that almost a decade has passed since the introduction of WPCN, a large gap exists between research works and practical implementations, and we have not yet seen any plausible and realistic deployment of WPCN. The major reason for the limited practicality of WPCNs is their poor performance in real-life scenarios, mainly due to the high attenuation of RF power over distance which limits the harvested energy of devices and degrades the network throughput. Despite the substantial research endeavors for enhancing the efficiency of RF power transfer, the performance of WPCNs is still far from acceptable and the integration of WPCNs in their current form into the IoT/IoE environment of the sixth generation (6G) systems does not seem realistic.

Besides what has been done for upgrading WPCN elements and enhancing their ef-

ficiency (e.g., improving the energy conversion efficiency of devices, improving the energy transfer efficiency of RF sources, etc.), the integration of other novel technologies into WPCNs can also be helpful for boosting their performance. In this regard, the incorporation of backscatter communication into WPCN is a promising strategy, where WPCN devices are enabled to use the technique of backscattering for transmitting their information. As backscatter transmission consumes much less power than active wireless powered transmission, devices can utilize part of the incident signal for powering their backscatter-related operations, while using the remaining part for modulating and transmitting their own information. As a result, the traditional harvest-then-transmit (HTT) protocol of WPCNs can be modified to harvest/backscatter-then-transmit (HBTT) protocol in which devices take advantage of the energy signals transmitted by RF sources for two purposes: energy harvesting and backscattering. This way, the energy signals can be utilized more efficiently and the throughput can be significantly improved.

Intelligent reflecting surface (IRS) is another prominent technology which has been lately applied to various networks and proved effective for improving the performance of wireless systems in a multifaceted manner. With its unique capability of reconfiguring the wireless propagation environment, IRS can be helpful for overcoming the limitations of WPCNs by enhancing the efficiency of both energy transfer and information transmission. Specifically, IRS elements can collaboratively modify the incident signals in a way that the signals reflected from the surface are constructively combined at the intended receiver(s), thus significantly boosting the power of the received signal and improving both the harvested energy and signal-to-noise ratio (SNR) in energy and information transmission phases.

Bearing in mind the beneficial features of backscatter communication and IRS, the main contributions of this thesis can be summarized as follows:

- Backscatter communication is incorporated into the traditional WPCN model and a backscatter-assisted WPCN (BS-WPCN) is proposed, enabling WPCN users to utilize the energy signals transmitted by a power station (PS) for both energy harvesting and backscatter transmission. The conventional HTT protocol is modified to HBTT protocol, where the users first harvest energy and backscatter their modulated information to the AP, and then transmit information to the AP by active wireless powered information transmission using their harvested energy.

- Inspired by the unprecedented characteristics of IRS, an IRS-empowered WPCN is studied with an IRS being added to the traditional WPCN model to improve the performance of both energy and information transfer. With the help of IRS, the energy signal transmitted by the PS is boosted in power so that the harvested energy of the users is substantially improved. Furthermore, IRS elements modify the information signals of the users in the information transmission phase; thus, the power of the received signals at the AP is enhanced, resulting in improved SNR and throughput.

- The simultaneous integration of backscatter communication and IRS into WPCN is then investigated where the previously presented BS-WPCN is enhanced by the addition of an IRS. In the proposed IRS-empowered BS-WPCN, IRS elements assist in backscatter and active information transmission of the users to the AP by applying amplitude changes and phase shifts to the users' information signals and reflecting them to the AP. It is noteworthy that unlike most of the existing works on IRS-aided systems which only optimize IRS phase shifts, we study the joint optimization of IRS amplitude reflection coefficients and phase shifts. Optimizing the amplitude reflection coefficients is essential when users simultaneously transmit their information signals and the AP receives a com-

bination of the information of all users. In such a case, the optimal amplitude reflection may be smaller than one.

- Sensitivity and saturation are two important characteristics of practical energy harvesting circuits. To be precise, sensitivity means that the energy harvesting circuit cannot be activated with small amounts of received power and the input power of the energy harvester must be greater than a determined threshold. Saturation implies that there exists a limitation on the maximum power that can be harvested by energy harvesting circuits and if the received power goes beyond that specific limit, the harvested power gets saturated. While it is common to ignore these two characteristics in theoretical analyses, taking them into account can make the theoretical studies more realistic. To this end, a practical and tractable energy conversion model is presented, able to capture the sensitivity and saturation effects of realistic energy harvesters. This model is applied to several real measurements, where it is shown that the difference between real measured values and the estimated values via this model is negligible. The presented energy conversion model is subsequently used to calculate the harvested power of the users in the proposed IRS-empowered BS-WPCN.

The main objective of this thesis is to solve total throughput maximization problems in the proposed BS-WPCN, IRS-empowered WPCN, and IRS-empowered BS-WPCN models. The techniques of successive convex approximation (SCA), alternating optimization (AO), semidefinite relaxation (SDR), and block coordinate descent (BCD) are mainly used for solving the throughput maximization problems. The performance of the proposed schemes are assessed via extensive numerical results which corroborate the effectiveness of the presented models and algorithms and reveal useful insights on how the proposed schemes behave in different network scenarios.

Publications

Published Papers Directly Related to this Thesis:

[P1] **P. Ramezani** and A. Jamalipour, "Backscatter-Assisted Wireless Powered-Communication Networks Empowered by Intelligent Reflecting Surface," in *IEEE Transactions on Vehicular Technology*, vol. 70, no. 11, pp. 11908-11922, November 2021.

[P2] B. Lyu, **P. Ramezani**, D. T. Hoang, and A. Jamalipour, "IRS-Assisted Downlink and Uplink NOMA in Wireless Powered Communication Networks," in *IEEE Transactions on Vehicular Technology*, 2021.

[P3] B. Lyu, **P. Ramezani**, D. T. Hoang, S. Gong, Z. Yang, and A. Jamalipour," Optimized Energy and Information Relaying in Self-Sustainable IRS-Empowered WPCN," in *IEEE Transactions on Communications*, vol. 69, no. 1, pp. 619-633, January 2021.

[P4] **P. Ramezani** and A. Jamalipour, "Optimal Resource Allocation in Backscatter-Assisted WPCN With Practical Energy Harvesting Model," in *IEEE Transactions on Vehicular Technology*, vol. 68, no. 12, pp. 12406-12410, December 2019.

[P5] **P. Ramezani** and A. Jamalipour, "Throughput Maximization in Backscatter Assisted Wireless Powered Communication Networks," *ICC 2019 - 2019 IEEE International Conference on Communications (ICC)*, Shanghai, China, 2019, pp. 1-6.

Other Published Papers:

[P6] **P. Ramezani** and A. Jamalipour,"Two-Way Dual-Hop WPCN With A Practical Energy Harvesting Model," *IEEE Transactions on Vehicular Technology*, vol. 69, no. 7, pp. 8013- 8017, June 2020.

[P7] **P. Ramezani**, Y. Zeng, and A. Jamalipour, "Optimal Resource Allocation for Multiuser Internet of Things Network With Single Wireless-Powered Relay," *IEEE Internet of Things Journal*, vol.6, no. 2, pp. 3132 - 3142, April 2019.

Papers Under Review:

[P8] **P. Ramezani**, B. Lyu, and A. Jamalipour, "Toward RIS-Enhanced Terrestrial/Non-Terrestrial Connectivity in 6G-Enabled IoE Era," Submitted to *IEEE Network*.

Authorship Attribution Statement

Papers [P1], [P4]-[P8] are my original work, where all stages of the paper writing, including the development of the ideas, reviewing the related works, modeling the system, formulating the problems, solving the problems, analyzing the solutions, and conducting the simulations have been performed by me, under the supervision of Prof. Abbas Jamalipour.

In writing papers [P2] and [P3], I have collaborated with Dr. Bin Lyu from Nanjing University of Posts and Telecommunications (NJUPT), where my contributions include reviewing the related works and cooperating with Dr. Lyu and his team in modeling the system, solving the problems, and analyzing the solutions. The simulations of these two papers have been completely done by Dr. Lyu. It is worth mentioning that in Chapter 4 of this thesis, which is partly based on [P3], I have used a slightly different model than the one in [P3] and re-conducted all the simulations by myself.

Contents

List of Figures

List of Tables

Glossary

AF	Amplify-and-Forward
AMPS	Advanced Mobile Phone System
AO	Alternating Optimization
AP	Access Point
AR	Augmented Reality
BCD	Block Coordinate Descent
BS-WPCN	Backscatter-Assisted Wireless Powered Communication Network
D2D	Device-to-Device
DC	Direct Current
DF	Decode-and-Forward
DH-WPCN	Dual-Hop Wireless Powered Communication Network
EM	Electromagnetic
eMBB	Enhanced Mobile Broadband
FD	Full-Duplex
FD-WPCN	Full-Duplex Wireless Powered Communication Network
HAP	Hybrid Access Point
HBTT	Harvest/Backscatter-Then-Transmit
HD	Half-Duplex
HTT	Harvest-Then-Transmit
IoE	Internet of Everything
IoT	Internet of Things
IRS	Intelligent Reflecting Surface
ITS	Intelligent Transmitting Surface
KPI	Key Performance Indicator
LoS	Line-of-Sight

MEMS	Micro Electromechanical Systems
MMSE	Minimum Mean Square Error
mMTC	Massive Machine-Type Communication
MRC	Maximum Ratio Combining
MSE	Mean Square Error
NEMS	Nano Electromechanical Systems
NLoS	Non-Line-of-Sight
OFDM	Orthogonal Frequency Division Multiplexing
PB-WPCN	Power Beacon-Assisted Wireless Powered Communication Network
PS	Power Station
QCQP	Quadratically-Constrained Quadratic Program
RF	Radio Frequency
RFID	Radio Frequency Identification
RIS	Reconfigurable Intelligent Surface
SCA	Successive Convex Approximation
SDMA	Space Division Multiple Access
SDP	Semidefinite Programming
SDR	Semidefinite Relaxation
SIC	Self-Interference Cancellation
SINR	Signal-to-Interference-plus-Noise Ratio
SNR	Signal-to-Noise Ratio
SWIPT	Simultaneous Wireless Information and Power Transfer
TDMA	Time Division Multiple Access
uRLLC	Ultra-Reliable Low-Latency Communication
WET	Wireless Energy Transfer
WPCN	Wireless Powered Communication Network

Chapter 1

Introduction

This chapter briefly reviews the generations of wireless communication systems and discusses the new requirements of the next generation. The motivations, objectives, and contributions of this thesis are clarified in this chapter, followed by presenting the chapter-wise outline of the thesis. Notations used and assumptions made throughout this thesis are provided at the end of this chapter.

1.1 Wireless Powered Communication for 6G

1.1.1 Wireless Network Generations

It all started in the late 1970s where the first generation of mobile networks (1G), referred to as advanced mobile phone system (AMPS) emerged, allowing people to make analog voice calls. In the early 1990s, the second generation networks (2G) were introduced, replacing the analog signaling system with the digital signaling technology, thereby offering short messaging and multimedia messaging services in addition to the traditional voice calls. The third generation (3G), launched in 2000, enabled mobile internet access and allowed mobile users to use their devices for video calling,

web surfing, online gaming, etc. for the first time. These unprecedented services offered by the 3G internet connectivity sparked the smart phones revolution but it was not until the unfolding of the fourth generation (4G) in 2009 that smart phones truly found their place in people's everyday lives. Supporting high-speed internet access, instant messaging services, quality streaming, and social networking, 4G has fundamentally reshaped the society and made Internet an indispensable part of billions of people's lives around the world. With the everyday-increasing dependency of modern life on the Internet and its associated services, and the emergence of ground-breaking applications such as augmented reality (AR), eHealth, etc., 4G soon proved insufficient to cater to the needs of very high data rate, extremely low latency, ultra-high reliability, and massive connectivity. New applications in enhanced mobile broadband (eMBB), massive machine-type communications (mMTCs), and ultra-reliable low-latency communications (uRLLCs) have driven the research and development of the fifth generation of wireless systems (5G) [1]. Now in 2021, 5G has already been deployed in many countries around the world, promising to provide data rates of up to 20 Gbps, latencies as low as 1 ms, and massive device-to-device (D2D) connectivity [2].

1.1.2 What's New in 6G?

Despite the substantial performance improvements that 5G offers over the previous generations, the requirements for the long-awaited Internet of Things (IoT) are yet to be fulfilled. Besides, many applications envisioned for 2030s require another 1000x increase in data rates and latencies of less than 0.1 ms [3, 4], and new key performance indicators (KPIs) also need to be defined for the successful implementation of the groundbreaking technologies of the next decade. More importantly, these new applications and use cases require the simultaneous fulfillment of several KPIs and the

Table 1.1: Comparison between KPIs in 5G and 6G [6].

KPI	**5G**	**6G**
Peak Data Rate	20 Gb/s	1 Tb/s
Experienced Data Rate	0.1 Gb/s	1 Gb/s
Peak Spectral Efficiency	30 b/s/Hz	60 b/s/Hz
Experienced Spectral Efficiency	0.3 b/s/Hz	3 b/s/Hz
Maximum Bandwidth	1 GHz	100 GHz
Area Traffic Capacity	10 Mb/s/m^2	1 Gb/s/m^2
Connection Density	10^6 devices/km^2	10^7 devices /km^2
Energy Efficiency	not specified	1 Tb/J
Latency	1 ms	10 μs
Reliability	1-10^{-5}	1-10^{-9}
Jitter	not specified	1 μs
Mobility	500 km/h	1000 km/h

traditional trade-offs present in previous generations may no longer be acceptable [5]. It is thus safe to say that we must expect an overhaul of the existing wireless systems for the sixth generation (6G), much more than only incremental improvement over the current 5G systems. Table 1.1 provides a comparison between the KPIs of 5G and the expected KPIs of 6G defined by the 6G flagship research team [6].

Applications and use cases which are envisioned to be seamlessly supported by the 6G wireless systems include but are not limited to super-smart city, holographic communication, wireless brain-computer interactions, tactile/haptic-based communications, chip-to-chip communications, five senses information transfer, precision agriculture, connected autonomous vehicles, Internet of Everything (IoE), and telesurgery [1, 4, 5, 7–11].

Besides the requirements on data rate, latency, reliability, connectivity, etc. which were defined and specified in previous generations of wireless systems, 6G applications are expected to have stringent requirements in terms of energy efficiency. Traditionally, energy efficiency has been largely overlooked when delineating the performance targets of different applications; that's because improving the energy efficiency is

conventionally bound with the conservative use of energy, the direct consequence of which is sacrificing other performance metrics, e.g., throughput, reliability, coverage, etc. 6G, however, seeks solutions which can guarantee the energy-efficient operation of devices and applications, while ensuring the fulfillment of other performance targets at the same time.

1.1.3 The Role of Wireless Powered Communication in the 6G Era

In recent years, energy harvesting has been raised as an effective solution for satisfying the energy efficiency requirements of wireless communication networks and addressing the undesirable trade-offs between energy efficiency and other key performance metrics. Through energy harvesting, devices will be able collect their required energy from the ambient environment, which allows them to operate without being concerned about battery depletion issues. Since devices have the chance to replenish their batteries via harvesting energy, there will be no need for them to be prudent in energy usage. This energy availability offered by energy harvesting techniques is pivotal for responding to the strict and multifaceted quality of service requirements of 6G systems. Therefore, the impeccable fulfillment of the newly-added energy efficiency performance target of the next generation largely depends on the maturity of the energy harvesting technology [4].

Besides conventional energy harvesting methods such as solar, thermal, flow-based, and vibration energy harvesting, the relatively new technology of radio frequency (RF) energy harvesting is a promising paradigm with huge potentials to be a 6G facilitator. Along with inductive coupling and magnetic resonant coupling, RF-based energy transfer is a sub-class of wireless energy transfer (WET) technologies. As compared to the other two WET techniques, RF-based energy transfer is regarded

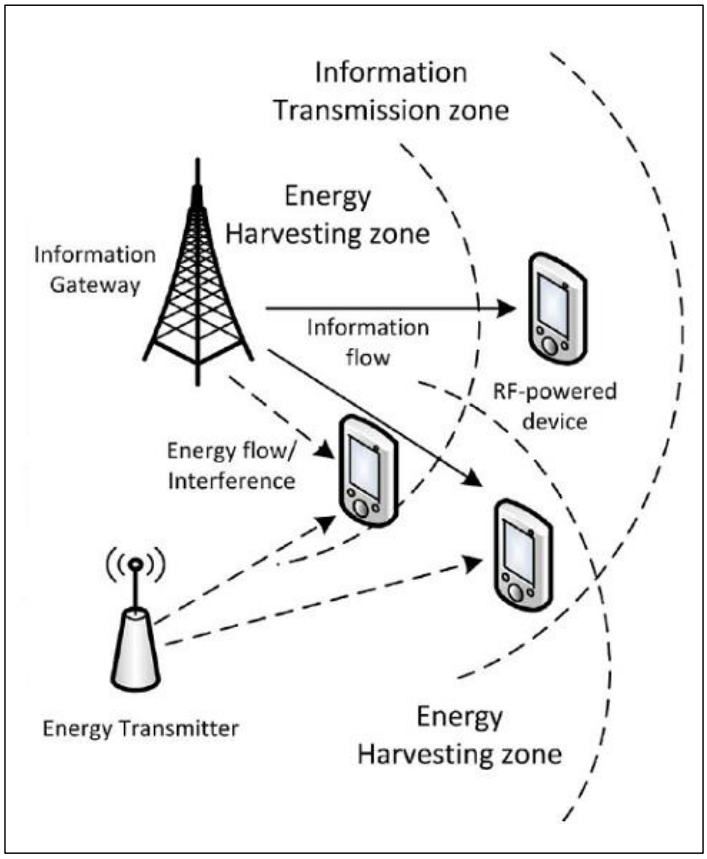

Figure 1.1: A WET-enabled network [12].

as a scalable and reliable solution for powering the massive number of devices in the 6G-enabled IoT/IoE era as it admits a small form-factor and its functioning is not contingent on the alignment between the transmitter and the receiver. Hereinafter, we simply use the term WET to refer to the RF-based WET.

Figure 1.1 shows an example architecture of a WET-enabled network, where devices are powered through RF energy harvesting [12]. In addition to the dedicated energy transmitter which transfers on-demand wireless energy, the information gateway can also act as an ambient energy source for RF-powered devices. In other words, the information signals of the gateway also carry energy which can be scavenged by devices which are not intended to be the receiver of information. This

way, the unwanted information signal which has been traditionally deemed as undesirable interference can now be a useful source of energy with RF energy harvesting technique.

During the past decade, we have seen extensive efforts, especially from the research community, for investigating the application of WET to wireless communication networks. There are numerous works and publications in the literature proposing WET-assisted network models and presenting novel methods and algorithms for improving the efficiency of WET [13–17]. The emergence of the innovative concept of wireless powered communication networks (WPCNs) [18–23] also stems from the substantial research works on WET-enabled communication. Despite the notable research endeavor, WET and WPCN have found limited practical implementation, mainly due to the severe attenuation of RF power over distance, which imposes strict constraints on the placement of energy transmitters and receivers and limits the available energy for collection. Though considered a crucial component for the sustainable operation of devices in 6G networks [24], WET technologies are not yet mature and WPCNs are more imaginary than realistic at the moment. The research in this area is thus far from done and comprehensive studies and novel ideas are urgently called for in order to enable wireless powered operation of future communication networks.

1.1.4 How Can Wireless Powered Communication Be Improved?

WPCN is envisaged to be an essential building block of 6G wireless systems. However, considering the current status of this important technology, there is still a long road ahead before we can rely on fully wireless powered communication for devices and networks. It is thus imperative to investigate novel methods and techniques to improve the performance of WPCNs in order to facilitate their inclusion into the

imminent 6G era. The integration of WPCN with other 6G enabling technologies can be a stepping stone for putting an end to the impracticality and inefficiency of WET-enabled communication and networking. In this regard, backscatter communication and intelligent reflecting surface (IRS) - which will be briefly introduced in the following and discussed in more detail in the next chapter - are two prominent candidates that can bring their unique features and functionalities into WPCNs and improve the performance of both energy and information transfer in these networks.

Backscatter communication is a momentous technology which can smooth the way for energy-efficient operation of 6G wireless networks. Allowing the transmitter to communicate with its intended receiver without generating RF signals, the backscattering technique consumes significantly lower power as compared to active information transmission, which makes it an apt choice for enabling the communication of the large number of low-power devices (e.g., sensors) in IoT/IoE and a major player for realizing the massive connectivity in 6G systems [5, 10]. This technique, however, is only suitable for very short-range communications and due to the double attenuation of the signals (i.e., attenuation in the RF source - backscatter transmitter - backscatter receiver links), the throughput drastically degrades with increasing the distance between the transmitter-receiver pair. As two potential enabling technologies for 6G, backscatter communication and WPCN can be integrated into one framework, letting us reap the benefits of both techniques, while alleviating their shortcomings [25, 26].

Very recently, the novel IRS technology has come on the scene, promising to bring unprecedented performance gains into wireless communication networks, while embracing a simple and cost-effective design. IRS has lately inspired considerable research for its distinctive capability of smartly modifying the time-varying propagation environment. Able to dynamically change the the attributes of the impinging

signals, IRS allows for instantaneous reconfiguration of propagation channels by reshaping wireless signals in the mid-way of communication. Thanks to its unparalleled features and functionalities, IRS is foreseen to be a decisive player in the design and planning of 6G systems and catalyze the establishment of avant-grade applications of the next generation [27, 28]. If integrated with IRS, WPCNs can benefit from multi-dimensional performance enhancements. On the one hand, the channel modification capability of IRS can provide favorable energy harvesting conditions for network devices and overcome the traditional challenges pertaining to the low-efficiency of WET. On the other hand, creating strong transmission paths, IRS allows devices to consume much lower transmit powers and yet enjoy remarkable throughput gains. This way, IRS helps WPCNs find their place in real-life scenarios and contributes to the fulfillment of strict requirements of 6G applications by clearing away the barriers of WET and enhancing the performance of communication without inflicting extra energy burden on networks.

The integration of WPCN with backscatter communication and IRS constitutes the main theme of this thesis.

1.2 Motivations

Since the emergence of WPCN in 2014 [19], we have observed an upsurge of research in this area. Extensive efforts have been made for extending WPCNs and improving their performance, among which we can name designing energy beamforming vectors [29–32], adding full-duplex (FD) operation for simultaneous downlink energy and uplink information transfer [33–41], optimizing the placement of energy transmitters and data receivers [20], using stochastic geometry tools for analyzing large-scale WPCNs [42], enabling cooperation mechanisms [43–46], using power beacons to enhance the

efficiency of WET [47], using ambient energy harvesting techniques (e.g., solar energy harvesting) for minimizing dedicated transmission of RF signals [48], and integrating this technology with relay-based communication [22, 23, 49–51] and cognitive radio networks [52–55].

Despite the appreciable contributions in this field, WPCNs have not been practically implemented on a wide scale so far. The main reason for this limited practicality is that the power of RF signals drastically falls with distance, as a result of which the efficiency of both energy and information transmissions is negatively impacted. Wireless powered devices are assumed to rely solely on the harvested energy from ambient and dedicated RF signals for their operation. The severe attenuation of the signal power over distance causes the available energy for harvesting to be very low, especially if devices are not in an ideal position with respect to power stations (PSs). In a WPCN environment where the time resources are divided between energy transfer and information transmission, the low level of harvestable power inevitably degrades the performance. On the one hand, accumulation of sufficient energy without dedicating much time to energy harvesting is not possible. On the other hand, allocating most of the time resources to energy harvesting shortens the information transmission time and lowers the throughput. It is therefore difficult to implement WPCNs at a large scale in practice because an acceptable performance cannot be easily achieved.

With the growing attention towards the utilization of RF signals for powering the communication of devices, backscatter communication entered the research limelight as a technique which not only observes RF signals as a source of energy but also recovers them for transmitting information. Backscatter communication allows devices to communicate without needing to generate active RF signals by themselves. Specifically, a backscatter transmitter absorbs part of the existing RF signals to power

its circuit operations and exploits the remaining part for information transmission by modulating its data onto the signals and reflecting them towards its destined receiver. As no active signal generation is required in this type of transmission, backscatter communication consumes much less power than active wireless communication. Integrating backscatter communication into WPCNs can efficiently improve the performance of these networks. Particularly, if WPCN devices are enabled to use the transmitted energy signals of the PS for the dual purpose of energy harvesting and backscattering, the throughput of WPCN can be greatly improved. To elaborate more, the energy needs of devices in a WPCN can be very dissimilar; for example, devices closer to the PS need less time to accumulate enough energy while farther devices have to spend long periods on energy harvesting. By enabling backscatter transmission at WPCN devices, the signals sent by the PS can be more efficiently utilized and the network throughput can be significantly enhanced. This is the motivation of Chapter 3 of this thesis, where the performance of a WPCN assisted by backscatter communication is studied.

IRS, also dubbed as reconfigurable intelligent surface (RIS), consisting of a large number of low-cost reflecting elements, has recently emerged as a revolutionary solution to improve the performance of wireless communication networks. IRS can modify the propagation environment and create favorable conditions for energy and information transfer without using energy-hungry RF chains. The integration of IRS technology with WPCNs can remarkably boost the performance of both energy transfer and information transmission, thereby improving the throughput of WPCNs by orders of magnitude. This is the motivation behind Chapter 4 of this thesis, where the performance improvement resulted from the inclusion of IRS into a WPCN is investigated.

Confirmed by numerical simulations in Chapter 3 and Chapter 4, backscatter

communication and IRS can considerably enhance the performance of WPCNs. It is thus worthwhile to study the scenario where both backscatter communication and IRS are simultaneously integrated into WPCNs. However, analytical studies cannot be accredited unless they are performed with practical assumptions and considerations. An important design consideration in energy harvesting-enabled networks is the model used for energy conversion. Most of the works in the area of WPCN assume a linear model for energy conversion in which the harvested power linearly increases with the received power boundlessly. In practice, however, there are limitations on the minimum required received power and the maximum harvested power in energy harvesting circuits, known as sensitivity and saturation, respectively. Using an over-simplified linear energy conversion model, though useful for analytical tractability, may lead to mismatches between theoretical studies and real-life implementations. Also, the well-known sigmoidal energy conversion model [56–59] which considers the saturation effect of energy harvesters has tractablity issues and its implementation is not straightforward. Therefore, there is a compelling need for a simple and tractable way for modeling the behavior of energy harvesting circuits. The above-mentioned points constitute the main motivations behind Chapter 5, where the incorporation of both backscattering and IRS technologies into a WPCN is inspected. A piece-wise linear energy conversion model with three pieces is adopted at the users which accounts for the two important characteristics of practical energy harvesters, namely, sensitivity and saturation.

1.3 Objectives and Methodologies

The objective of this thesis is to investigate the performance enhancements that can be achieved by integrating the novel technique of backscatter communication

as well as the pioneering technology of IRS into WPCNs. To achieve this objective, we first study a backscatter-assisted WPCN (BS-WPCN), where the traditional WPCN model is upgraded by introducing the backscattering capability at WPCN users and enabling them to use the energy signals, which were formerly used for the mere purpose of energy harvesting, to transmit their information to an access point (AP) by backscatter-based transmission. We investigate the maximization of network throughput which is the total throughput obtained through both backscatter-based and active information transmissions by optimizing the energy beamforming at the PS as well as the time allocation for energy harvesting, backscattering, and active information transfer.

We then study an IRS-assisted WPCN, where an IRS is included in the conventional WPCN model, responsible for empowering the downlink energy transfer from the PS to the users and the uplink information transmission from the users to the AP. IRS elements modify the energy and information signals to boost the power of the received signals at the destined receivers. Under this setup, we formulate the throughput maximization problem and study the optimization of reflection matrices at the IRS, beamforming vectors at the PS, and the time allocation for energy and information transfer.

Finally, we present an IRS-empowered BS-WPCN model in which the simultaneous integration of backscattering and IRS technologies into WPCN is explored. This new model enhances the previous BS-WPCN model by adding an IRS which aids backscatter and active information transmission of the users to the AP. Further, by equipping the AP with multiple antennas, we allow users to concurrently transmit their information to the AP in the active information transmission phase. With users transmitting information to the AP at the same time, it is very important to jointly optimize both amplitude reflection and phase shifts of the IRS. A realistic energy

conversion model is considered at the users which is able to capture the sensitivity and saturation behaviors of practical energy harvesting circuits. Again, the objective is to maximize the total network throughput by optimizing the values of the related variables. Specifically, we seek the optimal solution to IRS amplitude reflection coefficients and phase shifts, energy beamforming vectors of the PS, receive beamforming vectors of the AP, power allocation for the users' active information transmission, and the time allocation for energy harvesting, backscattering, and active information transfer.

Successive convex approximation (SCA), alternating optimization (AO), semidefinite relaxation (SDR), and block coordinate descent (BCD) techniques are the main methods used in this thesis for solving the optimization problems. We also use the MATLAB-based convex optimization toolbox CVX [60] for solving convex optimization problems. At the end of each chapter, we conduct extensive numerical simulations in MATLAB to evaluate the performance of the proposed algorithms and verify the superiority of our proposed designs over the benchmark schemes.

1.4 Thesis Contributions

We expect to see the unification and convergence of different networks and technologies in the forthcoming 6G environment. WPCN, backscatter communication, and IRS are innovative paradigms which can play vital roles in the realization of 6G applications and use cases, especially the fulfillment of the much-anticipated IoT/IoE environments. As all these three technologies are enablers of self-sustainable wireless communication, studying their integration is paramount for bringing together their individual merits while mitigating their weak points. The main contribution of this thesis is to study and analyze this integration and investigate the performance en-

hancements that can be attained by leveraging the above-mentioned technologies in a unified framework.

In what follows, we delineate the contributions of this thesis in detail.

- **Integration of backscatter communication into WPCN:**

  Devices in a WPCN usually need a long energy harvesting time to collect their needed energy for actively generating RF signals on which they can carry information. Conventional WPCN assigns part of the transmission block for the energy transfer process, where all devices are involved in energy harvesting during the assigned time duration. Introducing backscatter transmission capabilities at WPCN devices can help them utilize time and energy resources more efficiently. Motivated by the gains of integrating backscatter communication with WPCN, we propose a BS-WPCN in this thesis, consisting of a PS, a number of users, and an AP. In the proposed BS-WPCN, the users communicate with the AP via both backscatter and active wireless information transmissions. The PS acts as a signal and energy source for the users by transmitting downlink signals which are exploited by the users for backscattering and energy collection purposes. The collected energy of the users is then consumed for active generation of RF signals on which users' information is modulated and transmitted to the AP. We investigate the optimization of energy beamforming vector at the PS and the time durations for users' backscatter information transmission, energy harvesting, and active information transmission, in order to maximize the total achievable throughput.

- **Integration of IRS into WPCN:**

  The newly-arisen IRS technology has been proved propitious for performance enhancement of different wireless communication systems [61–70]. Accordingly, the introduction of IRS into WPCNs has the potential to boost the performance

of these networks and tackle the issues WPCNs are facing. With its channel modification properties, IRS can improve the efficiency of both energy transfer and information transmission, thereby enhancing the overall performance. Inspired by the evident benefits of employing IRS for bettering the performance of WPCNs, another contribution of this thesis is to inspect and study an IRS-assisted WPCN, where an IRS is deployed for empowering the energy transfer from the PS to the users as well as the information transmission from the users to the AP. The throughput maximization problem is then formulated which seeks the optimal solution to IRS reflection coefficients in both energy and information transfer phases, energy beamforming vectors at the PS, and time allocation. We propose a two-stage solution for solving the throughput maximization problem where the optimal IRS phase shifts for assisting each user's information transmission are given in closed-form in the first stage and near-optimal values of other variables are obtained in the second stage.

- **Simultaneous integration of backscatter communication and IRS into WPCN:**

  As verified by extensive numerical simulations, both backscatter communication and IRS can noticeably improve the performance of WPCNs. Their simultaneous integration into WPCN is thus worthy of investigation. In light of this, we propose an IRS-empowered BS-WPCN in which the previously studied BS-WPCN is extended by the addition of IRS and equipping the AP with multiple antennas. The IRS supports backscatter and active information transmissions of the users to the AP by inducing amplitude changes and phase shifts to the signals transmitted by the users such that the signals reflected by the IRS towards the AP are coherently combined with those directly sent from the users to the AP. A time division multiple access (TDMA) scheme is considered for the

backscatter transmission of the users while the users simultaneously transmit in a space division multiple access (SDMA) manner in the active information transmission phase. Under this setup, we are interested in maximizing the total throughput by optimizing the amplitude reflection coefficients and phase shifts of the IRS, energy beamforming vectors at the PS, receive beamforming vectors at the AP, users' power allocation in the active information transfer phase, and time allocation. Optimizing the IRS amplitude reflection is very important in the active information transfer phase when the users concurrently transmit to the AP and the AP receives a combination of the signals of all users. In such a case, we cannot simply assume that the amplitude reflection coefficients are equal to 1 because the amplitude of each user's received signal affects the performance of all users and the whole network. A two-stage scheme is proposed for solving the problem where the IRS reflection coefficients for assisting the backscatter transmission of the users are optimized in the first stage and the optimization of other variables is carried out in the second stage.

- **Practical and tractable piece-wise linear energy conversion model:** Considering realistic models which account for practical limitations of network elements is essential for the proper design of optimization algorithms. Although simplified and idealistic models make the analysis tractable, they can cause mismatches between expected and actual outcomes. One clear example is the model used for energy conversion in energy harvesting-enabled networks. If we neglect the sensitivity and saturation effects of practical energy harvesting circuits and use the traditional linear model for energy conversion, the implementations based on the theoretical optimal design may fail to produce convincing outcomes. We propose to use a piece-wise linear energy conversion model with three pieces at the users, which accounts for the sensitivity and saturation ef-

fects of practical energy harvesters. We verify the accuracy of this model by applying it to several real measurements and comparing the real measured values with the ones estimated via this model.

1.5 Thesis Organization

This thesis is organized as follows:

Chapter 1 briefly overviews different generations of wireless communication networks and discusses why the newly-deployed 5G systems are incapable of meeting the requirements of groundbreaking applications of the next decade. WPCN is introduced as an enabling technology for 6G communication networks and the limitations that WPCNs are challenging with are explained. The integration of the recent technologies of backscatter communication and IRS with WPCN is suggested as a means for enhancing the performance of WPCNs and addressing their limitations. We then present the motivations, objectives, and contributions of this thesis along with a detailed discussion on the importance of each contribution we have made.

Chapter 2 reviews the literature on WPCNs, starting from the very basic WPCN model and continuing to the extended models of WPCNs and the techniques used for improving their performance. A comprehensive survey of the recent research on backscatter communication and IRS is also provided and the advantages of IRS over conventional relays are thoroughly discussed.

Chapter 3 presents the BS-WPCN model in which the backscatter communication has been added to the basic WPCN model to enable users to communicate with the AP not only via active information transmission but also by the technique of backscattering. The chapter investigates how to design the energy beamforming and allocate the time resources for different network operations such that the over-

all network throughput is maximized. The performance of the proposed BS-WPCN is assessed via numerical simulations which reveal the considerable gain of the integrated BS-WPCN framework over the schemes which either employ active information transfer or backscatter-based information transfer.

Chapter 4 studies the inclusion of IRS into the basic WPCN model, where the IRS is employed to assist in downlink energy transfer and uplink information transmission. Besides energy beamforming and time allocation, the reflection matrices of IRS are also optimized for the sake of maximizing the network throughput. Numerical evaluations confirm that the proposed scheme for IRS-assisted WPCN remarkably outperforms the conventional WPCN. The importance of optimizing the IRS phase shifts for further performance enhancement is also illustrated by comparing the cases with optimized and non-optimized phase shift values for IRS elements. The scenario where the IRS itself needs to harvest energy for sustaining its operations is also numerically studied in order to observe the effect of using an energy harvesting IRS on the network performance.

Chapter 5 investigates the simultaneous incorporation of backscatter communication and IRS into WPCN and proposes a practical energy conversion model with three pieces for capturing sensitivity and saturation modes of energy harvesters. A sum-throughput maximization problem is formulated and the optimization of IRS reflection coefficients, time and power allocation, transmit beamforming at the PS, and receive beamforming at the AP is studied. The efficiency of the proposed scheme is validated by conducting extensive numerical simulations. It is shown that the presented algorithm can be readily applied to the scenario where the IRS phase shifts are chosen from a finite set. We particularly show that a 2-bit resolution for the phase shift of IRS elements is sufficient for achieving the envisioned near-optimal performance.

Chapter 6 summarizes the findings of the thesis and provides potential research directions and open issues for extending and improving the schemes presented in this thesis.

The flowchart in Figure 1.2 depicts the structure of the thesis and summarizes the contents of each chapter.

1.6 Notations and Assumptions

In this thesis, scalars are denoted by italic letters, vectors and matrices are denoted by bold-face lower-case and upper-case letters, respectively. $(\cdot)^T$, $(\cdot)^H$, and $(\cdot)^{-1}$ denote transpose, Hermitian transpose, and matrix inversion operations, while $\mathrm{Tr}(\cdot)$ and $\mathrm{Rank}(\cdot)$ denote the matrix trace and rank, respectively. $\mathbb{C}^{a\times b}$ is the space of $a \times b$ complex-valued matrices. $\mathbb{E}[\cdot]$ stands for expectation and $\boldsymbol{I}_M$ denotes the identity matrix of size M. $\mathrm{Re}\{\cdot\}$, $|\cdot|$, $\arg(\cdot)$, and $\bar{(\cdot)}$ denote the real part, absolute value, angle, and conjugate of a complex number, respectively. $||\cdot||$ is the 2-norm of a vector and $[\cdot]_{i,j}$ indicates the element in the ith row and the jth column of a matrix. diag $(\boldsymbol{x})$ is a diagonal matrix where each diagonal element is the corresponding element in vector $\boldsymbol{x}$. The distribution of a circularly symmetric complex Gaussian (CSCG) random vector is denoted by $\mathcal{CN}(\boldsymbol{\mu}, \boldsymbol{\Sigma})$ with $\boldsymbol{\mu}$ being the mean vector and $\boldsymbol{\Sigma}$ representing the covariance matrix and $\sim$ stands for "distributed as".

We assume that all channels follow a quasi-static flat fading model, where all channel coefficients remain constant during each transmission block, but may vary from one block to the other. To characterize the gains brought by backscatter communication and IRS into WPCNs, we assume that channel state information (CSI) of all involved channels is available wherever needed; therefore, the obtained performance in each chapter can be regarded as an upper bound for the performance in practical

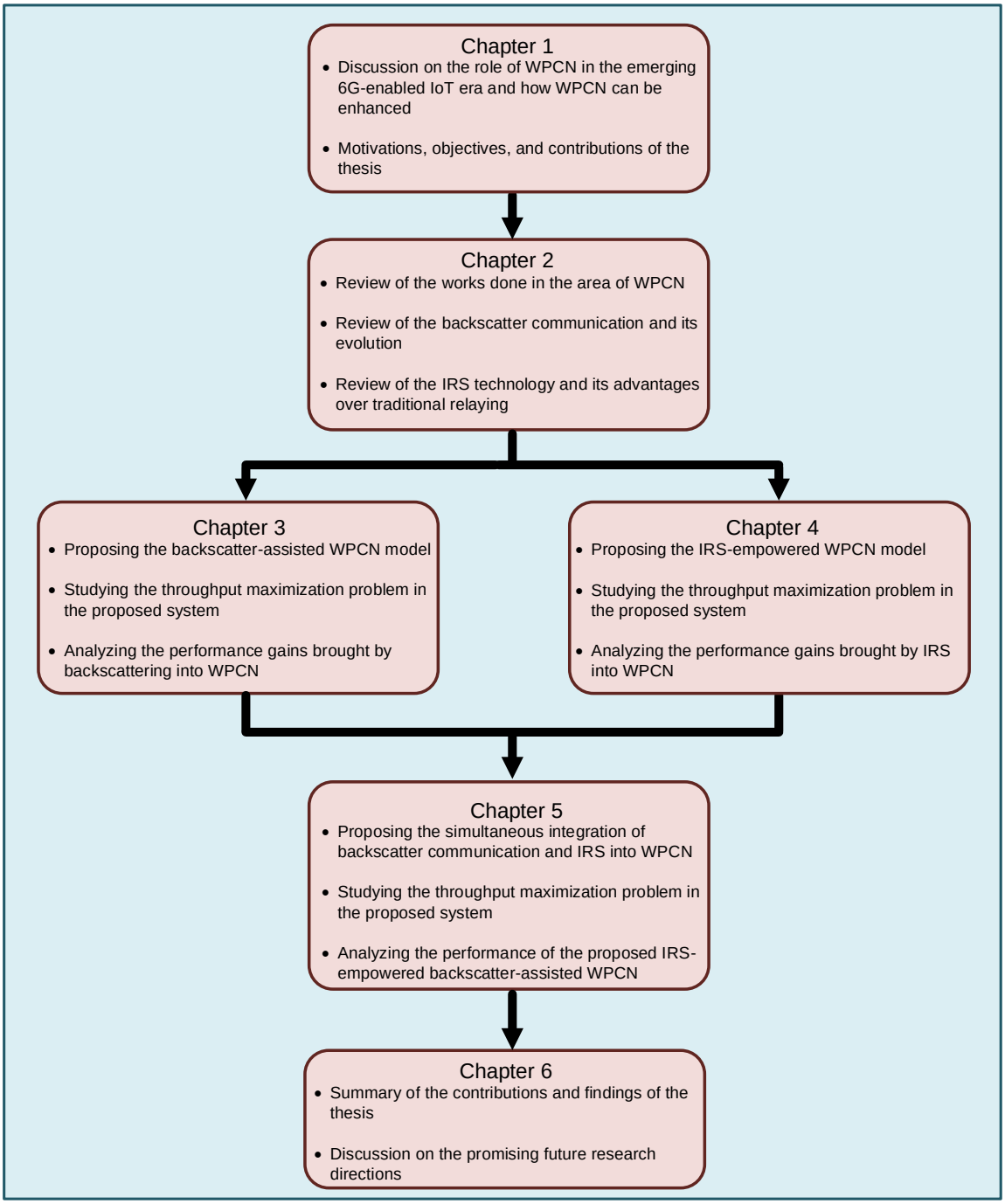

Figure 1.2: Thesis structure.

cases. CSI can be obtained based on the techniques and methods proposed in [71–75]. It is assumed that the power of the signals that are reflected by the IRS two or more

times is negligible and can be thus ignored. In all chapters, The AP serves as a central node which has the required resources in terms of energy and processing capacity for implementing the algorithms and performing all the necessary computations.

1.7 Chapter Summary

This chapter started by providing an overview on different generations of wireless communication networks from 1G to 5G, followed by presenting the requirements of the upcoming 6G systems. WPCN has been introduced as a key technology for realizing the self-sustainable communication in the 6G era and the integration of the innovative technologies of backscatter communication and IRS with WPCNs has been identified as an effective method for upgrading these networks. The motivations of conducting the works presented in this thesis have been explained along with a detailed discussion on the objectives and contributions of the thesis. Finally, the structure of the thesis has been explained and the notations and assumptions used in subsequent chapters have been presented.

Chapter 2

Background and Research Trends

In this chapter, we review the past and ongoing research in the areas of WPCN, backscatter communication, and IRS, with an emphasis on the history of WPCNs and how the two novel technologies of backscatter communication and IRS can help the progress of these networks. We begin by an introduction on WPCN and how the research community has endeavored to make WPCN more mature and practical. Followed by this, we look into the backscatter communication technology and its aptitude for being incorporated into the WPCN environment. We then proceed to review the IRS technology, its benefits over traditional relaying methods, and the promising outcomes of incorporating it into wireless networks. The chapter is closed by discussing the integration of IRS into WPCNs and presenting some preliminary studies on this integration. Our recent works on relay-based WPCN in [50] and [51] are reviewed in this chapter. Also, the contents of our Magazine paper in [28] have been partly used when introducing the IRS technology and its advantages over relaying techniques.

2.1 Wireless Powered Communication Networks

The emergence of WPCNs dates back to 2014, where a basic WPCN model operating based on the harvest-then-transmit (HTT) protocol was proposed [19]. In this work, the authors considered a multi-user network, with one central entity called the hybrid access point (HAP) taking the role of a conventional AP as well as acting as an energy transmitter for the users. The authors adopted the HTT protocol for the network operations such that the time frame has been divided into two phases, namely energy transfer and information transmission, where the former is dedicated to the downlink energy transfer from the HAP to the users and the latter is allocated for the users' uplink information transmission to the HAP. Studying the optimal time allocation for maximizing the total throughput, the authors disclosed a fundamental issue in their proposed WPCN, referred to as the doubly near-far problem. This problem stems from the unfair nature of throughput distribution when a co-located AP and PS, i.e. HAP, is used to serve the users. In specific, the users far from the HAP harvest less energy and yet they have to transmit with larger powers to achieve a comparable throughput with those closer to the HAP. The presented model and protocol, depicted in Figure 2.1, attracted notable interests from the research community and served as a baseline for later developments of WPCNs. Several extensions and enhancements have been proposed for WPCNs, some of which will be discussed in the following.

A lot of research endeavors have been made for enhancing the energy transfer efficiency in WPCNs by replacing the single-antennas HAP considered in [19] by a multi-antenna HAP so as to increase the harvested energy of the users. The conventional WPCN is extended in [30] by considering a multi-antenna HAP. Equipping the HAP with multiple antennas enables the energy beamforming and also lets users transmit their information in the uplink simultaneously via SDMA. To avoid the doubly near-far problem, the authors opt for a minimum throughput maximization

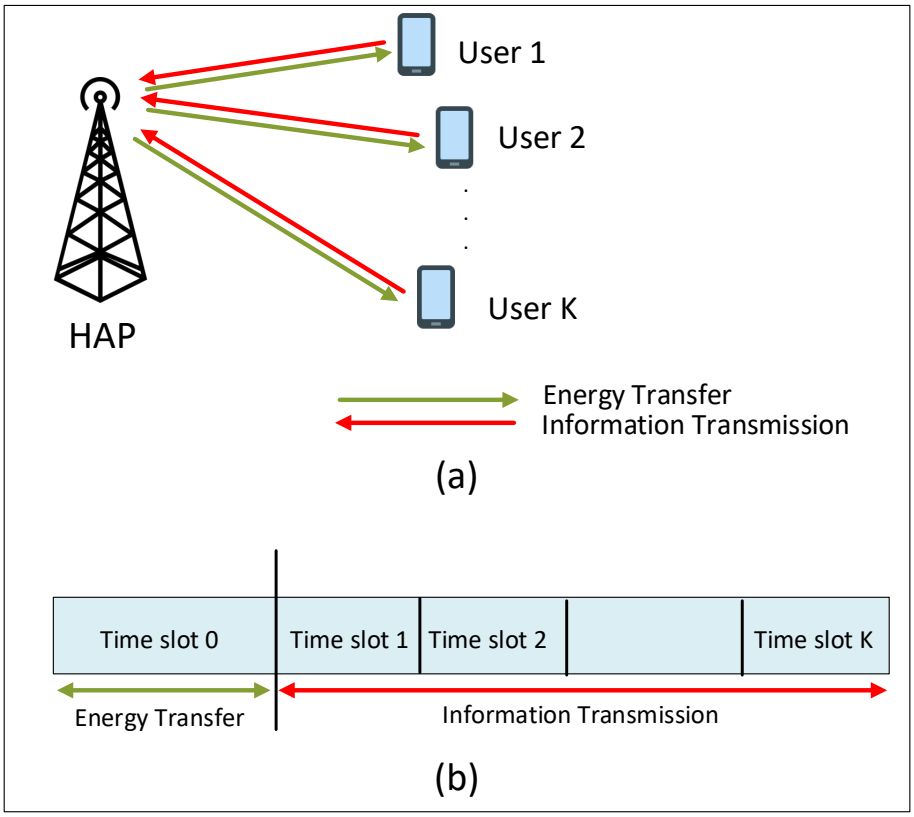

Figure 2.1: Wireless powered communication network (a) system model (b) harvest-then-transmit protocol.

problem instead of a total throughput maximization one, and optimize the time allocation, energy beamforming, users' power allocation, and receive beamforming. A WPCN with separate AP and PS is proposed in [29] with a multi-antenna PS serving several users by transferring a downlink energy signal. The users then utilize the energy collected from PS's energy signal to transmit their information to the AP in the uplink. This work provides several advantages over the baseline WPCN model in [19]. First, using separate AP and PS prevents the so-called doubly near-far problem and allows for a fairer throughput allocation. Furthermore, the multi-antenna PS adds another degree of freedom to the design as energy beamfoming vector can also be optimized in order to improve the WET efficiency. The authors also propose

a robust design for cases when only imperfect CSI is available. Reference [32] investigates the optimal energy harvesting time in a WPCN with a multi-antenna HAP and a number of multi-antenna users. The aim of this work is to minimize the total energy harvesting time, while ensuring that each user can collect enough energy in the specified time.

Enabling FD operation at the HAP is another strategy which has been widely used for improving the energy and spectral efficiency of WPCNs. In [33], Ju and Zhang extend their very first WPCN model by letting the HAP simultaneously transmit downlink energy and receive uplink information. It is shown that this full-duplex WPCN (FD-WPCN) can outperform its half-duplex (HD) counterpart if the self-interference at the HAP is effectively canceled. Reference [34] adopts an FD-WPCN model, where the HAP possesses two antennas for performing simultaneous energy transfer and information reception. The authors assume perfect isolation between the two antennas and ignore the self-interference effect at the HAP. Under this setup and by considering the energy causality constraint, sum-throughput maximization and total time minimization problems are investigated and the impact of user scheduling on the performance is examined. The authors of [35] study an FD-WPCN in which the users transmit their uplink information to the HAP based on orthogonal frequency division multiple access. Two cases are considered: perfect self-interference cancellation (SIC), where the HAP is able to completely remove the self-interference caused by its energy transfer and imperfect SIC, where residual self-interference is taken into account. The authors study the joint optimization of subcarrier scheduling and power allocation for maximizing the sum-rate in both scenarios. An FD-WPCN is studied in [36] in which the optimal allocation of power and time is investigated for maximizing the sum-rate. This work takes into consideration both the energy causality constraint and the imperfect SIC. The work in [37] studies an FD-WPCN,

where the FD HAP transfers energy and information in the downlink and at the same time receives information in the uplink. In addition to the legitimate users, multiple eavesdroppers are assumed to be present, overhearing the uplink and downlink communication between the users and the HAP. The problem of minimizing the system power is investigated under the energy harvesting constraint in downlink and security rate constraint in both uplink and downlink. Rezaei *et al.* consider an FD-WPCN where the HAP transfers downlink energy in all time-slots while simultaneously receiving users' information in the uplink [38]. In this work, the users which are not transmitting information to the HAP are considered as eavesdroppers. The authors first study the problem of sum secrecy throughput maximization where they optimize time durations and HAP beamforming vectors. Then, to address the fairness issue in their proposed FD-WPCN, they present max-min fair and proportional fair schemes. A robust beamforming and time allocation design for FD-WPCN is presented in reference [39], where the CSI uncertainty is assumed to be present due to the energy limitation of WPCN users which inhibits them from taking part in the channel estimation process. To solve the weighted sum rate maximization problem, the authors utilize the relationship between the weighted sum rate and the weighted sum of mean square error (MSE). [40] studies an FD-WPCN where the users are assigned to two different groups based on whether they are receiving energy from the HAP or transmitting information to the HAP. The optimization of time allocation, channel allocation, transmit and receive beamforming vectors is investigated for maximizing the total uplink throughput in both perfect and imperfect channel estimation scenarios. The authors in [41] propose a discrete rate-based FD-WPCN, where the transmission rate of the users is selected from a finite set of discrete rate levels. The minimization of the transmission completion time is studied, taking into account the traffic demand of the users.

As another way for improving the performance of WPCNs and alleviating the doubly near-far problem, cooperation strategies have been incorporated into WPCNs by letting the users which are closer to the HAP assist the information transmission of those being located far away. A user cooperation strategy is presented in [43] to tackle the doubly near-far problem in WPCN. A two-user WPCN is considered and the HTT protocol is adopted. The users harvest energy from the HAP's energy transfer in the downlink. In the uplink information transmission phase, the user with better a channel condition dedicates a part of its available energy and assigned transmission time to relay the information of the other user to the HAP. The authors in [44] consider a similar model to the one in [43] and study a three-node cooperative WPCN, where a relay cooperates with a user to transmit its information to the HAP. Both the relay and the user are assumed to be energy-constrained, powered by downlink energy transmission of the HAP. The authors then extend their study to a multi-relay scenario, where relay selection mechanisms are employed to select one relay for performing the cooperation task. The work in [45] extends [43] by assuming multiple antennas at the HAP and optimizing energy beamforming and power allocation, in addition to time assignment for energy and information transfer. The authors investigate two optimization problems, namely weighted sum-rate maximization and total transmission time minimization. Shin *et al.* propose a novel framework in [46] in which far users from the HAP overhear the uplink information transfer of the nearer users and harvest energy from their transmissions, in addition to scavenging energy from the HAP's downlink energy transfer. This mechanism eases the doubly near-far problem as it provides new energy collection opportunities for the users who experience harsh energy harvesting conditions.

Using additional PSs for transferring wireless energy has also been investigated for improving the energy harvesting of WPCN users. [47] proposes a power beacon-

assisted WPCN (PB-WPCN) which consists of a set of HAP-user pairs and a power beacon for providing additional energy to the energy-constrained users. The users are charged by energy transfer from the power beacon and their associated HAP, and transmit their information to their corresponding HAP. Two scenarios are investigated based on whether the power beacon cooperates with the HAPs or not. A sum-throughput maximization problem and an auction game are formulated for cooperative and non-cooperative cases, respectively. A water-filling-based solution is proposed for finding the optimal energy allocation of the PS and time allocation in the sum-throughput maximization problem. For the auction game, a distributed algorithm is presented for analyzing the interaction between the HAPs and the PS.

Optimizing the location of PS and AP is another useful way for performance improvement in WPCNs. In this regard, the placement optimization problem in WPCNs is studied in [20], where the authors consider the problem of minimizing the deployment cost, trying to use the minimum number of PSs and APs by searching for their optimal placement. This work studies two different scenarios, where the PSs and APs are assumed to be separately located in the first scenario, while each pair of PS and AP constitute a HAP in the second scenario.

Extension of the conventional WPCN model to more complicated scenarios has been an active area of research in the past years. Che *et al.* used stochastic geometry tools for analyzing the performance tradeoff between energy harvesting and information transmission in a large-scale WPCN [42]. A new HTT protocol is proposed where the time frame is partitioned into T time-slots, and the first N time-slots are assigned for energy transfer, with the remaining $T-N$ time-slots being allotted to the users' information transmission. The authors study the problem of spatial throughput maximization by optimizing the number of energy transfer time-slots and the users' transmit power, considering battery-free and battery-deployed wireless nodes.

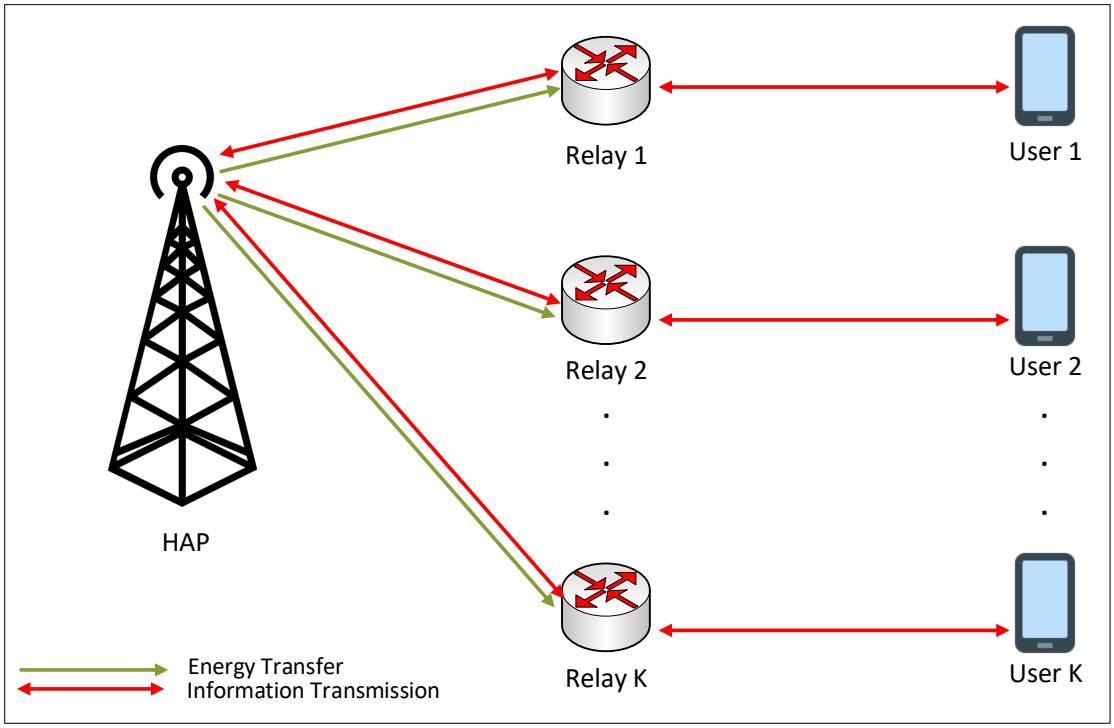

Figure 2.2: Dual-hop Wireless powered communication network.

Dedicated transmission of RF signals for powering WPCN users may be inefficient due to the high power loss of the signals over distance. Reference [48] investigates a WPCN where the users are enabled to harvest energy from environmental energy sources (e.g., solar energy). The authors then study the conditions under which dedicated WET needs to be activated. They then optimize the resource allocation policy for both cases of activated and non-activated WET.

There has also been much interest in the research community for integrating relay-based communication into WPCNs. A new dual-hop WPCN (DH-WPCN) model is studied in [22] which includes a HAP, a set of energy-stable users, and a number of energy-constrained relays. In this model, which is depicted in Figure 2.2, each user has its own dedicated relay for assisting its communication with the HAP. The HAP first transfers downlink energy to the relays; then, the information transmission

phase begins which is divided into time-slots, with each time-slot being allocated to a user-relay pair. The first half of each time-slot is used for the information transmission of a user to its corresponding relay and the second half is allocated to the relay to forward the information of its associated user to the HAP. In addition to uplink information transmission from the users to the HAP, the authors also study the downlink information transmission from the HAP to the users, where the concept of simultaneous wireless information and power transfer (SWIPT) is exploited to transmit both energy and information at the same time. Specifically, the relays are equipped with power splitters for splitting the downlink information signal of the HAP into two parts, one to be used for energy harvesting and the other to be forwarded to the corresponding user. The authors show that the doubly near-far problem exists in the uplink communication of the proposed DH-WPCN because the user whose relay is further from the HAP suffers from a very low throughput performance. Reference [23] studies fairness enhancement in the DH-WPCN proposed in [22], where a minimum throughput maximization problem is formulated and solved for ensuring that the maximum level of fairness is achieved in terms of users' individual throughputs. The authors' analysis reveals a trade-off between fairness and total throughput implying that the increased fairness is obtained at the cost of total throughput reduction. In [49], Lyu *et al.* extend the DH-WPCN in [22] by adding the FD functionality to the HAP to enable its concurrent energy transmission and information reception. As the HAP can transfer downlink energy to wireless powered relays while it is receiving uplink information signals, the relays can harvest energy during the whole time frame except for the duration in which they are involved in information forwarding. Reference [50] considers another dual-hop WPCN, where a single wireless powered amplify-and-forward (AF) relay assists the uplink information transmission of a set of users to the AP. The authors investigate the throughput

maximization problem by optimizing the time allocation for energy and information transfer as well as the relay's energy expenditure for assisting the communication of each user. [51] extends the work in [50] by studying a two-way relaying scenario, where both AF and decode-and-forward (DF) relaying modes are studied. This work considers a multi-antenna PS and a piece-wise linear energy conversion model and investigates the optimization of the time allocation, power allocation at the relay and the users, and PS beamforming vector.

The application of WPCN in cognitive radio networks has also attracted extensive research, where the transmission of primary users can be a useful source of energy for secondary users. Reference [52] studies a cognitive radio-enabled WPCN, where a WPCN shares spectrum with a primary network and the downlink energy transfer and uplink information transmission of WPCN users may interfere with the information transmission of the primary transmitter. The objective is to maximize the throughput of WPCN while keeping the quality of service of the primary network at the desired level. The proposed cognitive radio-enabled WPCN differs from conventional cognitive radio networks in that the interference to primary transmission can be more intense due to the additional energy transfer from the HAP to WPCN users. However, compared to simple WPCN, users in such a cognitive network have more opportunities for energy harvesting because they can collect energy from the information transmission of the primary transmitter. Kalamkar *et al.* study the integration of WPCN with a cooperative cognitive radio network in [53], where WPCN users, which are the secondary users of the proposed system, assist in information transmission of a primary user and in turn gain spectrum access for transmitting their own information. Sum throughput maximization of WPCN is investigated under the constraint of target primary rate and the authors find the optimal set of cooperative WPCN users, time and energy allocation. The work in [54] also studies a cognitive radio-enabled

WPCN and optimizes the power control for WET and time allocation under the maximum interference power constraint. In [55], a new cooperative protocol is presented for cognitive radio-based WPCNs, where WPCN as the secondary network coexists with a primary network which is facing security threats from multiple eavesdroppers. Under this setup, WPCN users help the primary network by sending signals to eavesdroppers in order to interfere with the primary signal received at the eavesdroppers and protect the primary transmission. The problem of maximizing the ergodic rate of WPCN is considered and the authors jointly optimize users' scheduling, time and power allocation.

2.2 Backscatter Communication

Backscatter communication is different from conventional wireless communication where the transmission of information requires active generation of RF signals on which the information can be carried. A backscatter transmitter does not possess any active RF components e.g., signal generator, analog-to-digital converter, power amplifier, etc. since it simply modulates and scatters back the impinging signal with no need for creating its own signal. Traditional backscatter systems, which are commercially used in radio frequency identification (RFID) applications on a wide scale, consist of two components: a carrier emitter referred to as reader and a backscatter transmitter called RFID tag. In this setup, referred to as monostatic backscatter configuration and illustrated in Figure 2.3, the reader initiates communication by transmitting an active RF signal to the tag; the tag uses a portion of the incident signal for energy harvesting, while it modulates the other part and reflects it back to the reader. Backscatter communication has also found applications in wireless sensor networks, where the sensors are integrated on RFID tags, making it possible to use

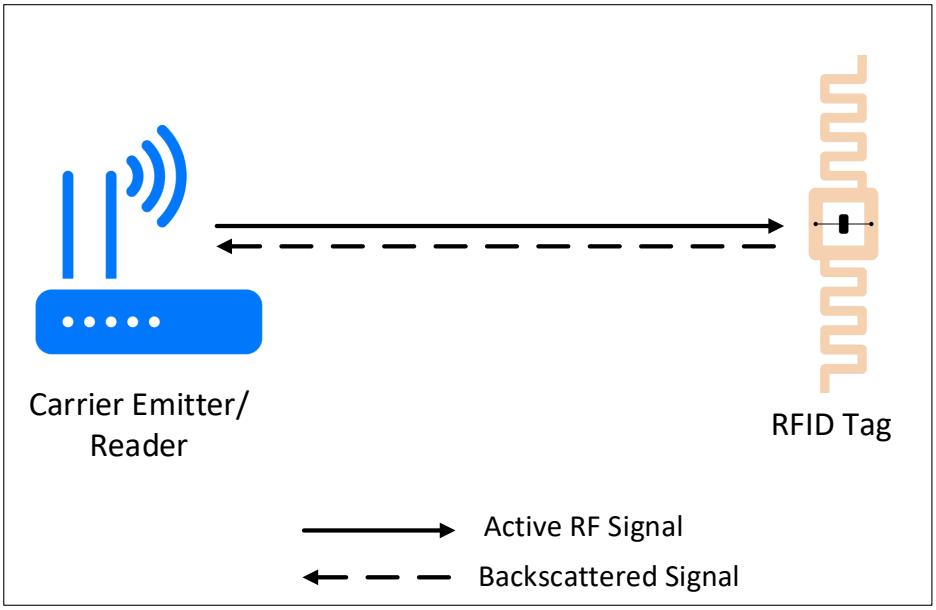

Figure 2.3: Monostatic backscatter configuration.

backscattering for the transmission of sensory data to the fusion center [76–79].

The monostatic backscatter system of Figure 2.3 suffers from low communication range due to the round-trip path loss which causes the signal to noise ratio (SNR) to fall with the fourth power of the tag-to-reader distance. To enable longer-range communication for wireless sensor networks, the work in [80] proposed a new model for backscsatter systems, in which the carrier emitter is detached from the reader, thus allowing for the flexible positioning of the carrier emitter and extending the transmission range. This bistatic backscatter model, therefore, has three components: a carrier emitter, a backscatter transmitter, and a reader. This configuration is shown in Figure 2.4.

There is also a third configuration for backscatter systems which resembles that of a bistatic backscatter system except that the dedicated carrier emitter is replaced by ambient RF sources [81–83]. This setup, depicted in Figure 2.5, admits lower cost and energy consumption compared to the other two configurations, but the performance of the system is highly dependent on the availability and strength of the ambient

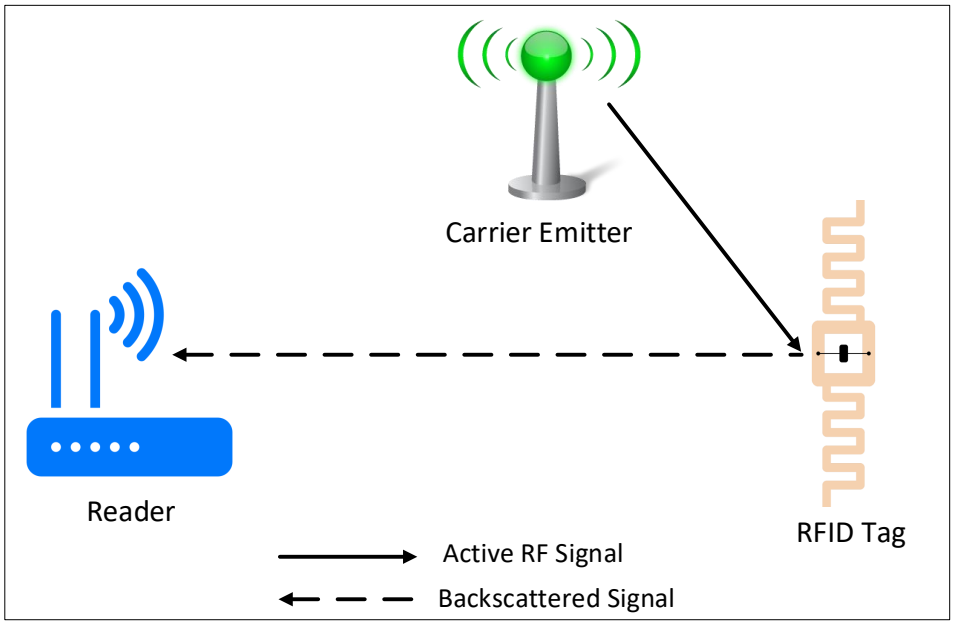

Figure 2.4: Bistatic backscatter configuration.

signals.

As both backscatter communication and wireless powered communication work based on recovering the existing RF signals for communication, special interest has been given to their integration from the research community.

Reference [84] studies a WPCN which is assisted by backscatter communication. The transmission block is split into three parts for energy harvesting, active information transmission, and backscatter transmission. Assuming that the HAP constantly transmits downlink signals, the authors investigate the sum-throughput maximization problem by finding the optimal time assignment policy.

The integration of wireless powered transmission and backscatter transmission is brought into cognitive radio networks in [85], where the secondary users can decide whether to use the primary signals for backscattering or to harvest energy from the signals and perform active transmission. The maximization of overall network throughput is investigated by optimizing the time sharing between energy harvest-

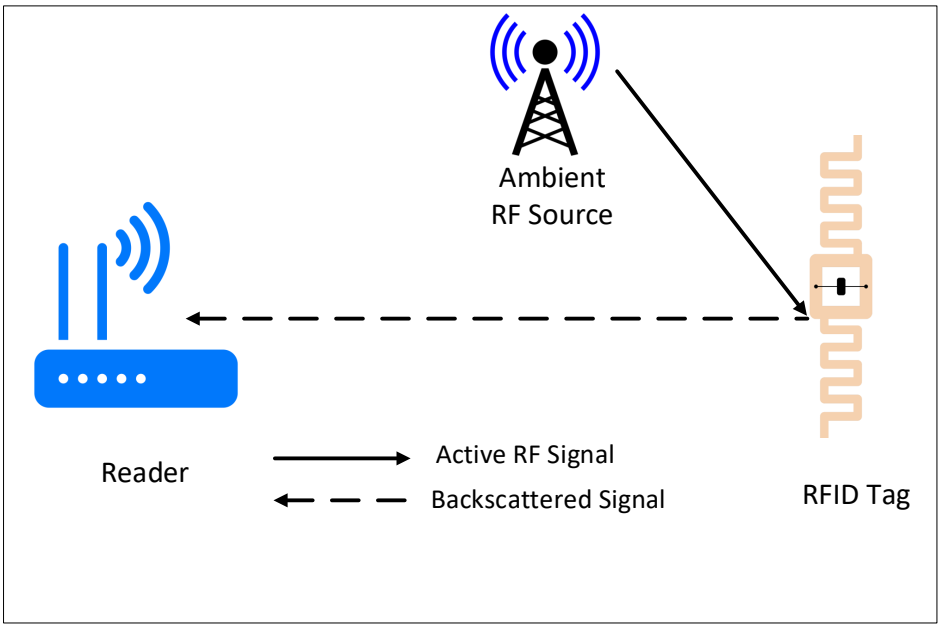

Figure 2.5: Ambient backscatter configuration.

ing, backscatter transmission, and active wireless powered transmission. This work is extended in [86] by considering the integration of active wireless powered and passive ambient backscatter transmissions in both underlay and overlay cognitive radio networks. Reference [87] studies a slightly different model than the one in [85], where a power beacon is added to the network to act as both a signal and an energy source for the secondary users when the primary transmitter is in the idle state.

The authors in [88] study the simultaneous integration of ambient and bistatic backscatter communication with wireless powered heterogeneous networks, where the conventional HTT-based transmission is adopted as the primary way of communication and the backscattering techniques are used as backup methods for information transmission when the harvested energy is not enough for performing active transmission. The optimal time allocation for different operation modes are found for maximizing the network throughput.

The work in [89] proposes a hybrid D2D communication system, where the trans-

mitter and the receiver are able to operate in two different modes: backscatter transmission mode and active transmission mode. The active transmission is performed based on the HTT protocol, where the transmitter device is wirelessly powered by the ambient RF sources before commencing its information transfer. Two mode selection protocols are presented which enable devices to toggle between the two modes. The idea of using dual-mode transmission is then incorporated into the relaying system in [90], where a hybrid relay assists the communication between a source-destination pair. Based on the mode selection protocols proposed by the authors, the relay can choose to work in either the active wireless powered mode or passive backscatter mode.

As confirmed by numerical evaluations in all the above works, the integration of backscatter communication and wireless powered communication can significantly outperform the scenarios based on either backscatter transmission or active wireless powered transmission. Hence, it is useful to further explore the performance gains stemmed from this integration. Our proposed model in Chapter 3 has similarities with [84–88]. However, these works only optimize time allocation while we also optimize the energy beamforming at the PS. Also, all these works assume a fixed backscatter transmission rate as a result of which the throughput only depends on the allocated transmission time. In our considered system, however, the backscatter throughput is also dependent on the reflected power from the backscatter transmitter, channel conditions, and noise power.

2.3 Intelligent Reflecting Surface

We traditionally know that an electromagnetic (EM) wave hitting a surface may be reflected, absorbed, refracted, etc. depending on the type of the surface and the

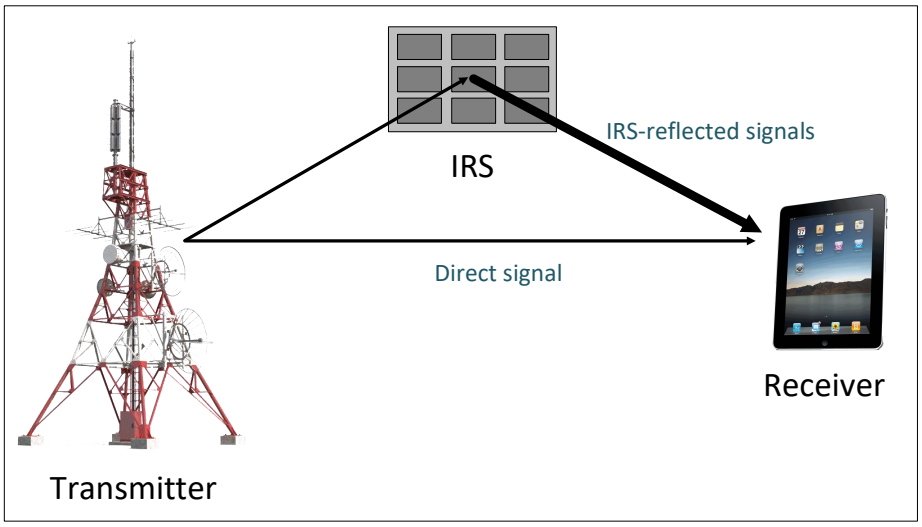

Figure 2.6: An IRS-aided communication system.

wavelength of the EM wave. The behavior of the surface is pre-determined and unalterable. The newly-emerged concept of IRS is a revolutionary paradigm which can change the way we view surfaces. The unique and unprecedented properties of IRS enable controllable and intelligent interaction with the EM signals and open a new dimension for improving the performance of wireless networks and applications [28].

IRS is a software-controlled metasurface, composed of a large number of passive elements which can be modified to shape the radio waves according to specific needs [91–93]. Thanks to the recent advancements in micro/nano electromechanical systems (MEMS/NEMS), IRS elements can be reconfigured dynamically and in real-time, allowing for instantaneous performance optimization of communication systems and catering to immediate changes of wireless networks. Reshaping the signals in the mid-way of communication, IRS makes it possible to optimize channel properties in addition to the optimization of transmission/reception schemes and fulfills the long-awaited dream of customizing the radio environment [28].

An example IRS-aided system is portrayed in Figure 2.6, where an IRS is deployed for aiding the communication between a transmitter-receiver pair. When the signal

sent by the transmitter impinges on the IRS, each element individually modifies and reflects the signal. This modification is performed in a unified manner such that the signals reflected by the IRS are constructively combined with those of the direct path, resulting in strengthened signal at the receiver, thereby improving the SNR and throughput.

The integration of IRS into conventional wireless networks can remarkably improve the performance of these networks in terms of spectral and energy efficiency, coverage, computation and communication latency, etc. A question, however, arises here: Why do we have to resort to IRS when traditional relays, which have already been thoroughly researched and tested, can be used for enhancing the performance of wireless networks [28]? A key point which has to be considered in answering this question is that future generations of wireless systems are not only about enhancing the performance by orders of magnitude; the expenses which must be put in for achieving the envisaged performance betterments need careful assessment as well. Note that, by expense we do not only mean financial spendings, but any kind of resource that is utilized for migrating from one generation of wireless networks to another. Traditional relaying technologies, although proved to be useful for performance enhancement of wireless networks, possess several handicaps which impede their seamless fitting into future 6G and beyond systems. In the following, we first present a qualitative overview of the limitations of the relaying techniques and how IRS can help mitigate those limitations. Having discussed the unmatched characteristics of IRS, we then briefly review the existing literature on IRS-assisted wireless systems.

2.3.1 Relays vs. IRS

Being active network elements, relays need sophisticated circuits to perform signal processing, information decoding and information forwarding tasks. Dedicated batteries are required at the relay in order to feed the energy-hungry components such as signal generator, power amplifier, digital-to-analog and analog-to-digital converters, RF filters, etc. This is undesirable as future network elements are expected to be ultra energy-efficient and preferably battery-free. During the past decade, energy harvesting has been raised as a solution to this problem, promising to make devices and networks self-sustainable. Specifically, wireless powered relays have emerged, able to collect their required energy from ambient and dedicated RF signals. This technique is not free of flaws either. As previously discussed, the severe attenuation of RF power over distance leads to very low efficiencies for RF-based energy harvesting, rendering only slight amounts of harvested power at the relays. This implies that relay nodes have to spend lengthy periods of time on collecting energy, causing considerable interruptions in their communication. Therefore, fully wireless powered relays are more imaginary than realistic considering the status quo of RF-based WET technologies. The HD functioning of the relays is also an issue because HD relays need additional resources in time or frequency, which leads to spectrum efficiency losses. FD relays can alleviate this issue by performing simultaneous transmission and reception on the same frequency band; however, as transmit and receive antennas are co-located at FD relays, the transmission of the relay interferes with its own reception, impelling FD relaying systems to implement analog and digital SIC techniques which further increase the complexity and cost of the system. What's more, the Tb/s data rate and massive connectivity requirements of 6G applications necessitate relays to be equipped with innumerable antennas, ending up in ultra-massive multiple-input multiple-output relaying networks and adding to hardware cost and energy consumption of the system.

In addition, different relaying strategies have their own shortcomings. A DF relay further raises the complexity and adds processing delay since the signal must be decoded and re-modulated at the relay. An AF relay simply amplifies and forwards the received signal without decoding; however, a strengthened version of the noise at the relay is also transmitted with the desired signal, which can severely impact the SNR at the destination.

The above concerns can be relieved if IRS is subbed for conventional relays. First of all, IRS elements are almost passive and do not require active chains for transmission and reception of signals. These passive elements consume much lower energy than conventional active relays, which makes ambient energy harvesting sufficient for the energy needs of IRS. Additionally, IRS is more spectrum-efficient than traditional relays as it essentially works in an FD manner, without requiring to implement the complex SIC techniques. IRS can also respond to the scalability demands of future wireless networks very well since the simple and low-complexity structure of IRS makes it possible to easily build IRSs with greater number of elements to achieve higher performance gains. Besides, to achieve high information rates, the number of needed IRS elements is less than the number of required antennas at the relay, which further justifies the supremacy of IRS over classic relaying techniques for the upcoming high-rate applications. Another merit of IRS is that it can be readily deployed and integrated into existing wireless communication networks with no need for manipulating the current network infrastructures and transceiver designs. Finally, compared to DF relays, IRS is more suitable for delay-sensitive applications since the processing delay due to decoding and re-encoding information signals does not exist in IRS-aided systems. Furthermore, IRS is a more proper choice than AF relays for throughput-sensitive scenarios because it does not add any thermal noise to the reflected signals.

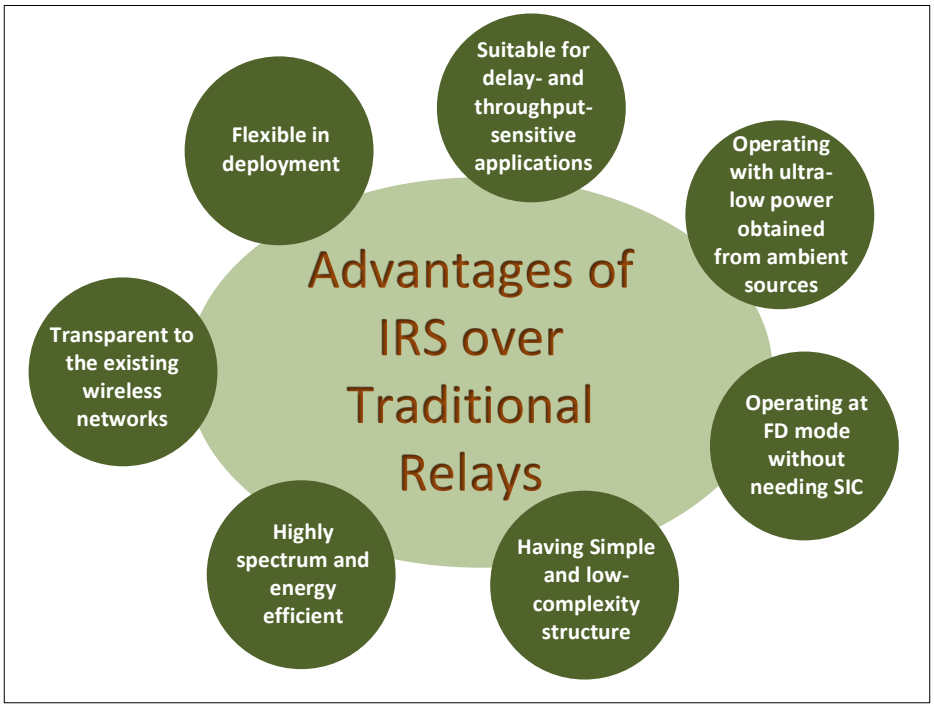

Figure 2.7: Advantages of IRS over relays.

Figure 2.7 provides a summary on the benefits of IRS over traditional relaying schemes.

Besides its clear advantages over traditional relays, IRS has more capabilities than what we have had with relaying strategies. For example, as will be overviewed in the next subsection, IRS elements can collaboratively adjust the incident signals in a way that the reflected signals cancel out the direct ones, thus substantially degrading the SNR at unintended receivers, e.g., eavesdroppers.

2.3.2 IRS-Assisted Wireless Networks

Due to its unparalleled properties, IRS has been considerably researched for improving the performance of wireless networks. Some of the pioneering works which investigated the performance enhancements achieved by the addition of IRS into existing wireless communication networks are overviewed in the following.

Reference [61] is one of the earliest works to study the potential of IRS for performance improvement in wireless networks. In this work, a downlink communication system has been considered where a base station communicates with multiple users through the IRS. The direct link is neglected in this paper due to poor propagating conditions between the base station and the users. The authors investigate the energy efficiency maximization problem by optimizing the base station transmit power and IRS phase shifts. A similar model to [61] is studied in [62] for minimizing the transmit power at the base station. In [62], the direct links are assumed to be present such that the base station can communicate with the users via both the direct link and the IRS-reflected links. Taking into account the minimum rate requirement of the users, transmit beamforming at the base station and phase shifts at the IRS are sub-optimally found. Secure IRS-aided communication is presented in [63], where an AP communicates with its intended user in the presence of an eavesdropper. With the help of IRS, the received signal at the legitimate user is boosted while the signal overheared by the eavesdropper is significantly reduced in power. Reference [64] considers a multi-cell environment and studies the performance of cell-edge users. An IRS is employed to assist the information transmission from each BS to its associated users and mitigate the unwanted inter-cell interference. References [65] and [66] study the application of IRS in SWIPT systems, where a base station serves two different sets of users: energy receivers and information receivers. The authors in [65] investigate the weighted sum power maximization at energy receivers subject to individual SNR requirements at information receivers. [66], on the other hand, studies the maximization of weighted sum rate for information receivers, while guaranteeing the energy harvesting requirements of energy receiving users. Reference [67] considers the application of IRS to two-way communication between two users where the users simultaneously transmit to each other. The authors analyze different metrics (e.g., outage probabil-

ity, spectral efficiency,etc.) for both reciprocal and non-reciprocal channels. Lin *et al.* study IRS-aided orthogonal frequency division multiplexing (OFDM) communication system in [68] and propose a novel transmission protocol in which channel estimation and passive IRS beamforming are performed concurrently. They also propose a technique for estimating the channel in which the CSI is progressively obtained. Reference [69] investigates a multi-IRS-assisted cognitive radio network, where a secondary transmitter-receiver pair coexists with a primary network. The objective is to maximize the achievable rate of the secondary transmission by optimizing the beamforming at the secondary transmitter and the reflection coefficients of each IRS.

It is worth mentioning that in practice, continuous phase shifts at IRS elements are challenging to implement and there exists a limited bit resolution for IRS phase shifters [70]. For example, with a 2-bit resolution phase shifter, the phase shifts of IRS elements can take only four discrete values, while eight discrete phase values are available at a 3-bit resolution IRS. This constraint, however, is usually ignored for simplifying the analysis and characterizing the performance bound.

IRS, has been verified to strikingly improve the performance of wireless communication systems. Its integration with WPCNs is therefore essential to study, where substantial performance enhancements can be envisioned for the two fundamental operations in WPCNs, i.e, downlink energy transfer and uplink information transmission. Some preliminary studies on the integration of IRS with WPCNs can be found in [94] and [95]. In [94], the authors study the application of IRS for WPCN performance improvement, where IRS elements assist in energy transfer from the HAP to the users and information transmission from users to the HAP. Reference [95] proposes a similar idea, where the user cooperation is also investigated for a two-user WPCN scenario. These works provide some insights on the performance enhancements offered by using IRS in WPCNs. However, this integration needs to be studied

more deeply in more complicated and realistic WPCN environments. In Chapter 4, we consider the incorporation of IRS into a WPCN with separate AP and PS, where the energy beamforming at the PS is also optimized for further improving the performance. We then present a novel IRS-empowered BS-WPCN in Chapter 5, where an IRS is deployed in a BS-WPCN for assisting backscatter and active information transmissions. In Chapter 5, the AP is considered to have multiple antennas and a practical piece-wise linear energy conversion model is also presented to further raise the practicality of the considered network.

2.4 Chapter Summary

This chapter reviewed the background on WPCN, backscatter communication, and IRS technologies. We first provided an overview on WPCNs, starting by the very basic model of these networks and discussing the improved models and schemes proposed for WPCNs in the literature. Then, backscatter communication was introduced and its integration with WPCN was surveyed. We finally presented the groundbreaking IRS technology and comprehensively discussed its superiority over relaying strategies. We also reviewed the works which studied the application of IRS for improving the performance of wireless networks, and explained the high potential of this ingenious technology for future WPCN developments.

Chapter 3

Backscatter-Assisted Wireless Powered Communication Network

This chapter studies a BS-WPCN, where a number of users communicate with an AP via backscatter and active wireless information transmissions. A PS is deployed to energize the energy-constrained users for their information transmission to the AP. The network operation consists of two phases; the first phase begins by PS transmitting an energy signal to the users in the downlink; the users utilize the transmitted signal of the PS for two purposes: energy harvesting and backscatter information transmission. In particular, each user is allocated a time-slot for backscattering operation in which the user modulates the energy signal of the PS with its own information and reflects it to the AP. Other users which are not scheduled for backscatter transmission harvest energy from the PS signal for their future active information transmission. In the second phase, each user is again assigned with a time-slot for information transmission in which the user uses the harvested energy in the first phase to generate an active information signal and transmit it to the AP. Under this setup, the aim of this chapter is to maximize the total network throughput including the throughput obtained from

both backscatter-based and active information transmission of the users. In light of this, we investigate the optimization of time allocation and PS beamforming vector, where the techniques of SDR and AO are exploited for finding a near-optimal solution to the throughput maximization problem. Numerical results are then provided at the end of this chapter for evaluating the performance of the proposed algorithm. The contents of this chapter have been taken from two of our papers [96] and [97].

3.1 System Model and Problem Formulation

As shown in Figure 3.1, we consider a BS-WPCN consisting of an AP, K users, and a PS. The PS is equipped with M antennas, while the AP and the users have one single antenna each. Figure 3.2 depicts the transmission block structure of the considered BS-WPCN, which is divided into two phases with each phase being further split into time-slots. We propose a harvest/backscatter-then-transmit protocol (HBTT) which enhances the traditional HTT protocol by incorporating backscatter transmission of the users into the first phase. Specifically, in the proposed protocol, the first phase is dedicated to the wireless power transmission from the PS to the users in the downlink and the users' backscatter transmission to the AP in the uplink. The active wireless information transmission of the users takes place in the second phase, where the users utilize the energy harvested in the first phase to actively transmit information signals to the AP. In what follows, the detailed operation of the two phases will be elaborated.

The first phase is divided into K time-slots for the backscatter transmission of the K users. During the ith time-slot of the first phase of duration $\tau_{1,i}$, the PS transmits a baseband energy signal given by $\hat{\boldsymbol{x}}_i = \boldsymbol{w}_i \hat{s}_i$, where $\boldsymbol{w}_i \in \mathbb{C}^{M\times 1}$ is the beamforming vector and $\hat{s}_i$ is the corresponding energy-carrying symbol with $\mathbb{E}\{|\hat{s}_i|^2\} = 1$. This signal is used by the ith user, denoted by U_i, as a carrier for backscatter information

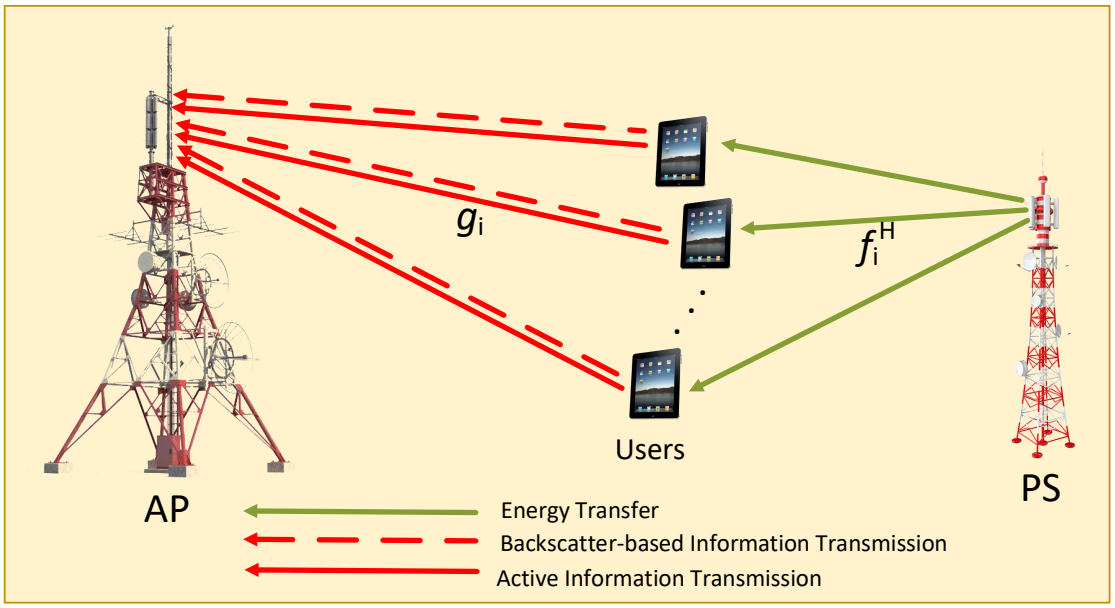

Figure 3.1: System model for backscatter-assisted wireless powered communication network.

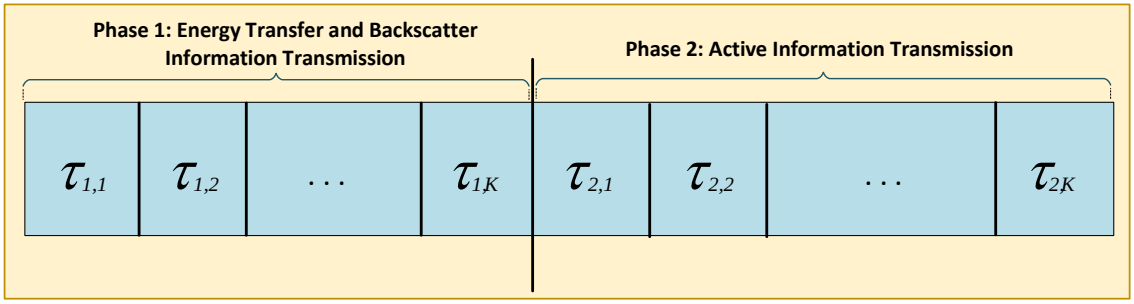

Figure 3.2: Transmission block for backscatter-assisted wireless powered communication network.

transmission to the AP, while other users utilize this signal for energy harvesting. Particularly, U_i backscatters a fraction β_i of the received power to transmit its information to the AP. The transmitted signal of U_i in the first phase can be expressed as

$$x_{1,i} = \sqrt{\beta_i}\boldsymbol{f}_i^H \hat{\boldsymbol{x}}_i s_{1,i} = \sqrt{\beta_i}\boldsymbol{f}_i^H(\boldsymbol{w}_i \hat{s}_i)s_{1,i}, \tag{3.1}$$

where $\boldsymbol{f}_i^H \in \mathbb{C}^{1\times M}$ is the equivalent baseband channel between the PS and U_i, and

$s_{1,i}$ is the information-bearing symbol of U_i in the first phase with $\mathbb{E}\{|s_{1,i}|^2\} = 1$. The signal received at the AP during $\tau_{1,i}$[1] is then given by

$$y_{1,i} = g_i x_{1,i} + n_A, \tag{3.2}$$

with g_i representing the channel between the AP and U_i, and $n_A \sim \mathcal{CN}(0, \sigma_A^2)$ being the overall additive noise at the AP due to the receiving antennas and RF band to baseband conversion.

The SNR and achievable throughput for U_i in the first phase can be written respectively as

$$\gamma_{1,i} = \frac{\beta_i |g_i|^2 |\boldsymbol{f}_i^H \boldsymbol{w}_i|^2}{\sigma_A^2} \tag{3.3}$$

$$R_{1,i} = \tau_{1,i} \log(1 + \gamma_{1,i}) = \tau_{1,i} \log\left(1 + \frac{\beta_i |g_i|^2 |\boldsymbol{f}_i^H \boldsymbol{w}_i|^2}{\sigma_A^2}\right). \tag{3.4}$$

Note: Throughout this thesis, we use the Shannon capacity formula for characterizing the throughput obtained in backscatter information transmission. We know, however, that the Shannon capacity is achievable with the Gaussian input while the multiplicative symbols, i.e., $\hat{s}_i s_{1,i}$'s, do not necessarily have Gaussian distribution. We can use a constant $\vartheta_i > 1$ to account for the SNR gap between Gaussian input and practical modulation and coding schemes such that the SNR in (3.3) is modified as $\gamma_{1,i} = \frac{\beta_i |g_i|^2 |\boldsymbol{f}_i^H \boldsymbol{w}_i|^2}{\vartheta_i \sigma_A^2}$. Nevertheless, this does not affect the solutions and algorithms developed in this thesis. We, therefore, set $\vartheta_i = 1,\ \forall i$, for notation simplicity.

Each user harvests energy from the transmitted signal of the PS in all time-slots of the first phase other than the one in which it is involved in backscatter transmission.

[1] In this thesis, we simply represent time-slots by their durations. For example, "during $\tau_{1,i}$" means during the ith time-slot of the first phase with duration $\tau_{1,i}$.

Therefore, the harvested energy of U_i can be calculated as

$$e_i = \eta_i \sum_{\substack{j=1 \\ j \neq i}}^{K} \tau_{1,j} |\boldsymbol{f}_i^H \boldsymbol{w}_j|^2, \tag{3.5}$$

where η_i is the energy conversion efficiency at U_i[2]. In the ith time-slot of the second phase with the duration of $\tau_{2,i}$, U_i uses up the previously harvested energy to actively transmit to the AP. The transmitted signal of U_i in this phase is given by $x_{2,i} = \sqrt{p_i} s_{2,i}$, where $s_{2,i}$ is the information-carrying symbol with $\mathbb{E}\{|s_{2,i}|^2\} = 1$ and p_i is the transmit power of U_i. Neglecting the circuit power consumption of U_i, the harvested energy of U_i will be fully used for its active information transfer and the transmit power is obtained as $p_i = \frac{e_i}{\tau_{2,i}} = \frac{\eta_i \sum_{j \neq i} \tau_{1,j} |\boldsymbol{f}_i^H \boldsymbol{w}_j|^2}{\tau_{2,i}}$. The signal received at the AP during $\tau_{2,i}$ is expressed as

$$y_{2,i} = g_i x_{2,i} + n_A. \tag{3.6}$$

The SNR and achievable throughput of U_i in this phase are respectively computed as

$$\gamma_{2,i} = \frac{\eta_i |g_i|^2}{\sigma_A^2} \frac{\sum_{j \neq i} \tau_{1,j} |\boldsymbol{f}_i^H \boldsymbol{w}_j|^2}{\tau_{2,i}} \tag{3.7}$$

$$R_{2,i} = \tau_{2,i} \log(1 + \gamma_{2,i}) = \tau_{2,i} \log\left(1 + \frac{\eta_i |g_i|^2}{\sigma_A^2} \frac{\sum_{j \neq i} \tau_{1,j} |\boldsymbol{f}_i^H \boldsymbol{w}_j|^2}{\tau_{2,i}}\right). \tag{3.8}$$

We aim to maximize the total throughput by optimizing the beamforming vector at the PS as well as the time allocation for energy harvesting, backscatter transmission, and active wireless powered transmission. The total throughput maximization

[2]The harvested power does not usually have a linear relationship with the received power. This will be discussed in detail in Chapter 5.

problem is formulated as follows:

$$\max_{\{\boldsymbol{w}_i\}_{i=1}^{K},\boldsymbol{\tau}_1,\boldsymbol{\tau}_2} \quad \sum_{i=1}^{K}(R_{1,i}+R_{2,i}) \tag{P3.1}$$

$$\text{s.t.} \quad \text{(C3.1)} \ ||\boldsymbol{w}_i||^2 \leq P_{max} \ \forall i,$$

$$\text{(C3.2)} \ \sum_{i=1}^{K}(\tau_{1,i}+\tau_{2,i}) \leq 1,$$

$$\text{(C3.3)} \ \tau_{1,i}, \tau_{2,i} \geq 0 \ \forall i,$$

where $\boldsymbol{\tau}_1 = [\tau_{1,1}, ..., \tau_{1,K}]$ and $\boldsymbol{\tau}_2 = [\tau_{2,1}, ..., \tau_{2,K}]$. (C3.1) is the maximum transmit power constraint at the PS, (C3.2) and (C3.3) are time constraints considering a normalized transmission block for the BS-WPCN.

Note: The above problem can be modified to a weighted total throughput maximization problem where different weights are assigned to different users and/or transmission modes. For instance, larger weights can be given to some users in order to prioritize them over the others. We can also give a higher priority to one of the transmission modes, e.g., backscatter transmission mode, by assigning a greater weight to the throughput obtained in the first phase. In such a case, the objective function of (P3.1) can be re-written as $\sum_{i=1}^{K}\varphi_i(\varrho_1 R_{1,i} + \varrho_2 R_{2,i})$ such that $\sum_{i=1}^{K}\varphi_i = 1$ and $\varrho_1 + \varrho_2 = 1$. The solutions presented in this thesis are readily applicable to the weighted total throughput maximization problem.

3.2 Total Throughput Maximization

Problem (P3.1) is not convex because the variables are coupled in the objective function. For solving this non-convex problem, we resort to the well-known AO method, where we first seek the optimal solution to the PS beamforming vectors having the

time allocation fixed and then, given the beamforming vectors at the PS, we optimize the time allocation for energy harvesting, backscatter transmission, and active transmission.

With fixed time allocation, we define new variables $\boldsymbol{W}_i = \boldsymbol{w}_i \boldsymbol{w}_i^H$, introduce auxiliary variables $t_{1,i}$ and $t_{2,i}$, $i = 1, ..., K$, and formulate the beamforming optimization problem as

$$\max_{\{\boldsymbol{W}\}_{i=1}^K, \boldsymbol{t}_1, \boldsymbol{t}_2} \quad \sum_{i=1}^{K} \Big(\tau_{1,i} \log(1 + a_{1,i} t_{1,i}) + \tau_{2,i} \log(1 + a_{2,i} t_{2,i}) \Big) \tag{P3.2}$$

$$\text{s.t.} \quad \text{(C3.4)} \; t_{1,i} \leq \text{Tr}(\boldsymbol{F}_i \boldsymbol{W}_i) \; \forall i,$$

$$\text{(C3.5)} \; t_{2,i} \leq \sum_{j=1}^{K} \tau_{1,j} \text{Tr}(\boldsymbol{F}_i \boldsymbol{W}_j) - \tau_{1,i} \text{Tr}(\boldsymbol{F}_i \boldsymbol{W}_i) \; \forall i,$$

$$\text{(C3.6)} \; \text{Tr}(\boldsymbol{W}_i) \leq P_{max} \; \forall i,$$

$$\text{(C3.7)} \; \boldsymbol{W}_i \geq 0 \; \forall i,$$

$$\text{(C3.8)} \; t_{1,i}, t_{2,i} \geq 0 \; \forall i,$$

$$\text{(C3.9)} \; \text{Rank}(\boldsymbol{W}_i) = 1 \; \forall i,$$

where $\boldsymbol{t}_1 = [t_{1,1}, ..., t_{1,K}]$, $\boldsymbol{t}_2 = [t_{2,1}, ..., t_{2,K}]$, $a_{1,i} = \frac{\beta_i |g_i|^2}{\sigma_A^2}$, $a_{2,i} = \frac{\eta_i |g_i|^2}{\sigma_A^2 \tau_{2,i}}$, and $\boldsymbol{F}_i = \boldsymbol{f}_i \boldsymbol{f}_i^H$.

The above problem is still non-convex due to the presence of rank-one constraint in (C3.9). SDR is a technique which deals with such issues. According to the SDR, the rank-one constraint is first relaxed to turn the problem into a semidefinite programming (SDP), which is a convex optimization problem; then, rank-one approximation techniques such as Eigen-decomposition and Gaussian randomization are used for extracting a feasible rank-one solution which can provide a near-optimal solution to the original problem [98]. In light of this, we relax the constraint (C3.9) to obtain a convex optimization problem. The resultant problem can be readily solved using convex optimization toolboxes such as CVX [60]. However, the solutions returned by CVX

for $\boldsymbol{W}_i$'s are not necessarily rank-one. Denoting the obtained solutions as $\boldsymbol{W}_i^\star$, $\forall i$, if the rank of $\boldsymbol{W}_i^\star$ is greater than one, we use Eigen-decomposition for approximating the solution with a rank-one matrix from which the corresponding near-optimal beamforming vector can be extracted. Specifically, we can write $\boldsymbol{W}_i^\star = \sum_{j=1}^{r_i} \lambda_{i,j} \boldsymbol{u}_{i,j} \boldsymbol{u}_{i,j}^H$, where $r_i = \text{Rank}(\boldsymbol{W}_i^\star)$, $\lambda_{i,1} \geq \lambda_{i,2} ... \geq \lambda_{i,r_i} > 0$ are the positive eigen-values of $\boldsymbol{W}_i^\star$ and $\boldsymbol{u}_{i,j}$'s are the corresponding eigen-vectors. Then, $\hat{\boldsymbol{W}}_i = \lambda_{i,1} \boldsymbol{u}_{i,1} \boldsymbol{u}_{i,1}^H$ is a rank-one approximation of $\boldsymbol{W}_i^\star$ and $\boldsymbol{w}_i^\star = \sqrt{\lambda_{i,1}} \boldsymbol{u}_{i,1}$ is the near-optimal beamforming vector extracted from $\boldsymbol{W}_i^\star$.

Subsequently, we optimize the time allocation given the PS beamforming vectors. Setting $c_{i,j} = |\boldsymbol{f}_i^H \boldsymbol{w}_j|^2$ and $\Gamma_i = \sum_{j=1}^K c_{i,j} \tau_{1,j}$, the time allocation optimization problem can be written as

$$\max_{\boldsymbol{\Gamma}, \boldsymbol{\tau}_1, \boldsymbol{\tau}_2} \quad \sum_{i=1}^K (\tau_{1,i} \log(1 + \frac{c_{i,i} \beta_i |g_i|^2}{\sigma_A^2}) + \tau_{2,i} \log(1 + \frac{\eta_i |g_i|^2}{\sigma_A^2} \frac{\Gamma_i - c_{i,i} \tau_{1,i}}{\tau_{2,i}})) \qquad \text{(P3.3)}$$

$$\text{s.t.} \quad \text{(C3.2) and (C3.3)}$$

$$\text{(C3.10)} \ \Gamma_i \leq \sum_{j=1}^K c_{i,j} \tau_{1,j} \ \forall i,$$

$$\text{(C3.11)} \ \Gamma_i \geq 0 \ \forall i,$$

with $\boldsymbol{\Gamma} = [\Gamma_1, ..., \Gamma_K]$.

It is easy to show that (P3.3) is a convex optimization problem which can be solved either analytically by convex optimization methods (e.g., Lagrange duality method) or using the CVX toolbox.

Using an iterative approach, we alternately optimize beamforming vectors of the PS and time allocation until a satisfactory convergence is achieved. Algorithm 1 summarizes the procedure for solving the total throughput maximization problem in (P3.1).

Algorithm 1 Total Throughput Maximization Algorithm for Solving (P3.1)

1: Initialize time allocation $\boldsymbol{\tau}_1^{\star(0)}$ and $\boldsymbol{\tau}_2^{\star(0)}$. Set $R^{(0)} = 0$ and $l = 0$;

2: **Repeat**

3: Update iteration index $l = l + 1$.

4: Given $\boldsymbol{\tau}_1^{\star(l-1)}$ and $\boldsymbol{\tau}_2^{\star(l-1)}$, solve the relaxed version of (P3.2) using the CVX toolbox and obtain $\boldsymbol{W}_i^{\star(l)}$.

a) **If** $\boldsymbol{W}_i^{\star(l)}$ is rank-one, $\boldsymbol{w}_i^{\star(l)}$ is the desired beamforming vector where $\boldsymbol{W}_i^{\star(l)} = \boldsymbol{w}_i^{\star(l)}\boldsymbol{w}_i^{\star(l)H}$.

b) **Else if** the rank of $\boldsymbol{W}_i^{\star(l)}$ is larger than one, use Gaussian randomization or Eigen-decomposition to extract a near-optimal beamforming vector $\boldsymbol{w}_i^{\star(l)}$ from $\boldsymbol{W}_i^{\star(l)}$.

5: Given the beamforming vectors $\boldsymbol{w}_i^{\star(l)}$'s, solve (P3.3) by Lagrange duality method or using the CVX toolbox and obtain the optimal time allocation $\boldsymbol{\tau}_1^{\star(l)}$ and $\boldsymbol{\tau}_2^{\star(l)}$.

6: Compute $R^{(l)} = \sum_{i=1}^{K}(R_{1,i}^{(l)} + R_{2,i}^{(l)})$.

7: **Until** $|R^{(l)} - R^{(l-1)}| < \epsilon$.

8: $R_{\max} = R^{(l)}$, $\boldsymbol{w}_i^{\text{opt}} = \boldsymbol{w}_i^{\star(l)}$, $\boldsymbol{\tau}_1^{\text{opt}} = \boldsymbol{\tau}_1^{\star(l)}$, and $\boldsymbol{\tau}_2^{\text{opt}} = \boldsymbol{\tau}_2^{\star(l)}$.

3.3 Performance Evaluation

In this section, we evaluate the performance of the HBTT protocol presented in this chapter by comparing it with two benchmark schemes. One of the benchmarks is the conventional HTT protocol, where the users harvest energy from the PS and transmit their information to the AP via active wireless powered transmission. The second benchmark, which is labeled as "BS" on the figures is the scheme in which the users communicate with the AP only via passive backscatter transmission, where they modulate their information onto the signal sent by the PS and reflect the signal

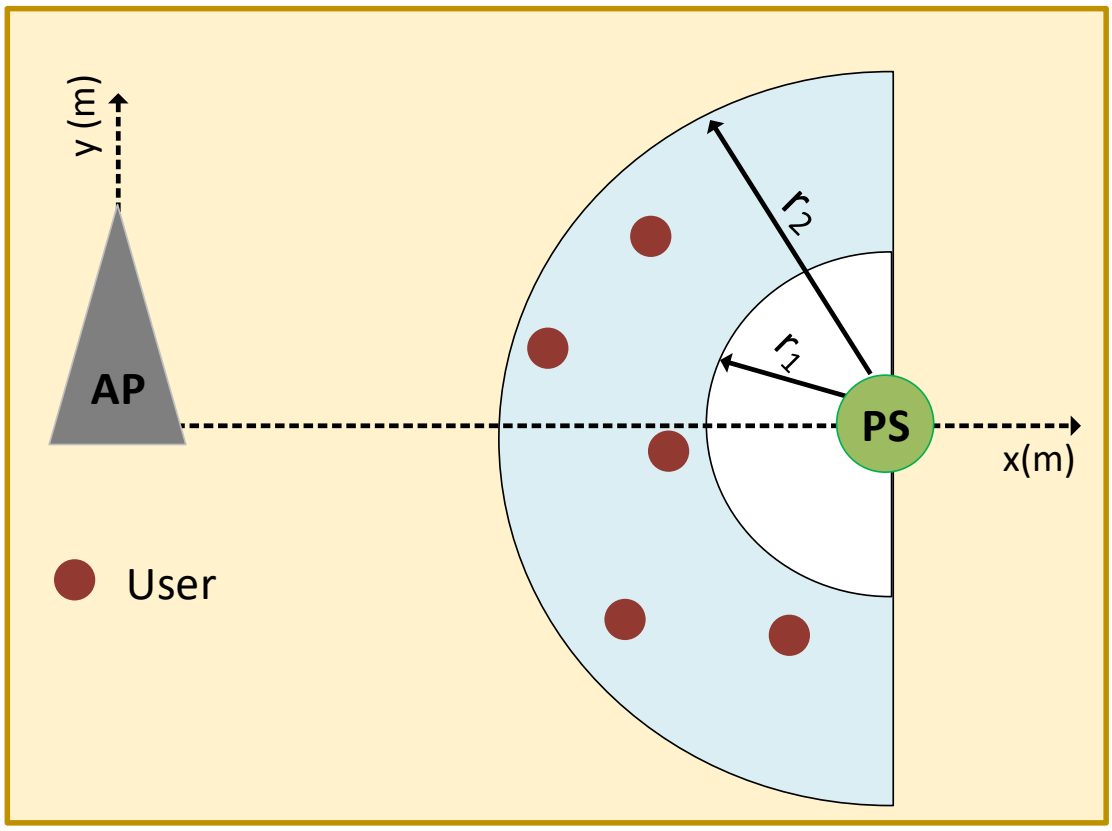

Figure 3.3: Simulation setup.

towards the AP.

3.3.1 Simulation Setup

The simulation setup is depicted in Figure 3.3, where an $x-y$ coordinate system is considered with the AP being positioned at the origin, the PS being located at $(x_{PS}, 0)$, and K users being randomly placed on the left side of the PS with a minimum distance of r_1 and a maximum distance of r_2 from the PS. The Rician fading channel model is used for all channels. Specifically, $\boldsymbol{f}_i$ and g_i are modeled as

$$\boldsymbol{f}_i^H = \sqrt{\frac{\kappa_{f,i}}{\kappa_{f,i}+1}}\boldsymbol{f}_i^{H(\text{LoS})} + \sqrt{\frac{1}{\kappa_{f,i}+1}}\boldsymbol{f}_i^{H(\text{NLoS})}, \ \forall i, \tag{3.9}$$

$$g_i = \sqrt{\frac{\kappa_{g,i}}{\kappa_{g,i}+1}} g_i^{\text{LoS}} + \sqrt{\frac{1}{\kappa_{g,i}+1}} g_i^{\text{NLoS}}, \ \forall i, \tag{3.10}$$

respectively, where $\kappa_{f,i}$ and $\kappa_{g,i}$ are the Rician factors of the corresponding channels. $\boldsymbol{f}_i^{H(\text{LoS})} \in \mathbb{C}^{1\times M}$ and $\boldsymbol{f}_i^{H(\text{NLoS})} \in \mathbb{C}^{1\times M}$ are the line-of-sight (LoS) and non-line-of-sight (NLoS) components of $\boldsymbol{f}_i^H$ and the same is true for g_i. We have $\boldsymbol{f}_i^{H(\text{LoS})} = [1 \ e^{j\pi\sin(\varphi)} \ e^{j2\pi\sin(\varphi)} ... e^{j(M-1)\pi\sin(\varphi)}]$ where φ is the angle of departure from the PS and $g_i^{\text{LoS}} = 1$. g_i^{NLoS} and the elements of $\boldsymbol{f}_i^{\text{NLoS}}$ follow the standard Rayleigh fading. $\boldsymbol{f}_i$ and g_i are then multiplied by $\sqrt{C_0(\frac{d_{f,i}}{d_0})^{-\rho_f}}$ and $\sqrt{C_0(\frac{d_{g,i}}{d_0})^{-\rho_g}}$, respectively, where $d_{f,i}$ is the distance between the PS and U_i, $d_{g,i}$ is the distance between U_i and the AP, ρ_f and ρ_g are the path-loss exponents of the corresponding channels. $C_0 = -20$ dB is the path-loss at the reference distance of $d_0 = 1$ m.

Unless otherwise stated, the following set of parameters are used for the simulations: $K = 10$, $M = 4$, $\beta_i = 0.6, \forall i$, $\eta_i = 0.5, \forall i$. The maximum PS transmit power is set as $P_{max} = 30$ dBm and the channel-related parameters are $\kappa_{f,i} = \kappa_f = 3, \forall i$, $\kappa_{g,i} = \kappa_g = 3, \forall i$, $\rho_f = \rho_g = 2.8$. The x-coordinate of the PS is set as $x_{PS} = 40$ m; also, $r_1 = 10$ m and $r_2 = 25$ m. The noise power spectral density at the AP is set as -160 dBm/Hz, the bandwidth is 1 MHz, and the convergence threshold in Algorithm 1 is chosen to be $\epsilon = 0.01$. The results are based on the average of 1000 different channel realizations. Table 3.1 lists the parameter values we used in the simulations of this chapter.

3.3.2 Numerical Results

Figure 3.4 depicts the total network throughput as a function of the maximum PS transmit power. As expected, the throughputs improve with increasing the PS transmit power because on the one hand, the power of the backscattered signals to the AP increases and on the other hand, the users can accumulate more energy which

Table 3.1: Simulation parameters for BS-WPCN.

Parameter	**Description**	**Setting**
K	Number of users	10
M	Number of PS antennas	4
P_{max}	Maximum PS transmit power	30 dBm
x_{PS}	X-coordinate of the PS	40 m
r_1	Minimum distance between PS and users	10 m
r_2	Maximum distance between PS and users	25 m
$\beta_i,\ \forall i$	Backscatter coefficient of all users	0.6
$\eta_i,\ \forall i$	Energy conversion efficiency of all users	0.5
κ_f	Rician factor for the channel between PS and users	3
κ_g	Rician factor for the channel between users and AP	3
ρ_f	Path-loss exponent for the channel between PS and users	2.8
ρ_g	Path-loss exponent for the channel between users and AP	2.8
d_0	Reference distance	1 m
C_0	Path-loss at the reference distance	-20 dBm
σ_A^2	Noise power at the AP	-100 dBm
ϵ	Convergence threshold for Algorithm 1	0.01

increases the power of their active transmitted signal to the AP. Therefore, the SNR and the achievable throughput for both backscatter transmission and wireless powered transmission increases. It can be observed that the proposed HBTT protocol which uses a hybrid of backscatter and active wireless transmissions outperforms the other two schemes which utilize only one of the transmission modes.

Figure 3.5 shows the throughput versus the number of PS antennas. As can be seen in the figure, with more antennas at the PS, the throughput improves for all schemes. That's because increasing the antennas increases the degrees of freedom and results in more effective beamforming at the PS. Therefore, the power of the received signal at the users increases which leads to throughput enhancement for both backscatter and active transmissions. The superiority of our proposed scheme over the benchmarks is clear in the figure which confirms the effectiveness of integrating backscatter communication into the traditional WPCN model.

Next, we investigate the impact of PS location on the total throughput. Figure 3.6

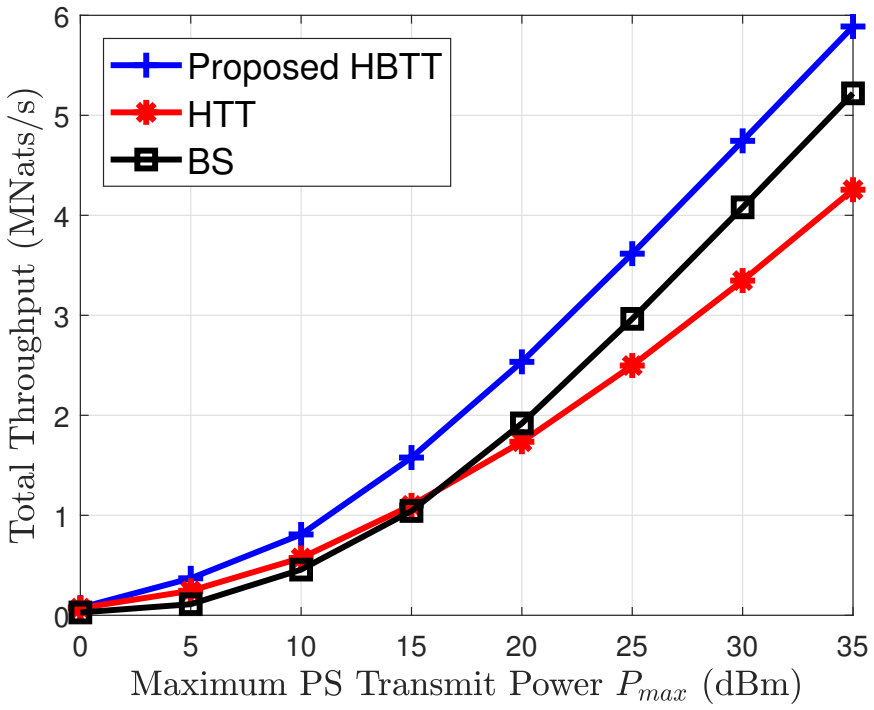

Figure 3.4: Total throughput vs. maximum transmit power of the PS.

illustrates the throughput performance as a function of x-coordinate of the PS, while the y-coordinate of the PS is fixed at $y_{PS} = 0$ and the distance from the users to the PS also remains unchanged. As is clear from the figure, increasing the x-coordinate of the PS degrades the throughput because when the PS gets further away from the AP, the distance from the users to the AP also increases (since we assumed that the distance from the users to the PS does not change) which decreases the power of the received signal from the users at the AP and reduces the throughput. It can also be seen that when the PS and the users are closer to the AP, the difference between the HBTT protocol and the scheme with only backscatter transmission is small. The reason for this observation is that when users are close to the AP, they are more willing to communicate with the AP via backscatter transmission; thus, a large portion of the transmission block is allocated for users' backscatter transmission. Therefore, most of the total throughput belongs to the throughput obtained in the

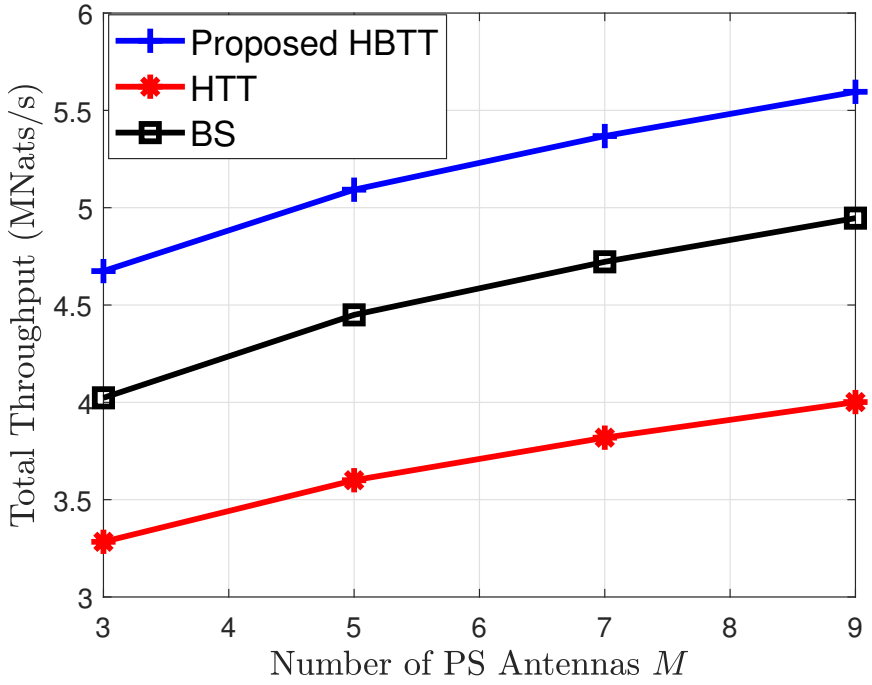

Figure 3.5: Total throughput vs. number of antennas at the PS.

backscatter transmission phase. When the distance from the PS and the users to the AP increases, the users tend to accumulate energy and transmit their information to the AP via active wireless powered transmission.

Figure 3.7 studies the impact of channel conditions on the network throughput. In Figure 3.7(a), the total throughput is plotted as a function of ρ_f. It is observed that greater values for ρ_f result in lower throughputs. That is because with larger ρ_f values, the signal that is sent from the PS to the users gets more attenuated; therefore, the power of the reflected signal from the users and their harvested energy decrease which leads to throughput reduction in both backscatter and active information transfer. Figure 3.7(b) shows the effect of the Rician factor of the users-AP channel (κ_g) on the throughput. Increasing κ_g increases the chance of LoS links between the users and the AP which in turn improves the quality of the received signals at the AP and the throughput. To avoid repetition, we have only shown the throughput performance as a function of ρ_f and κ_g since similar observations as Figure 3.7(a) and Figure 3.7(b)

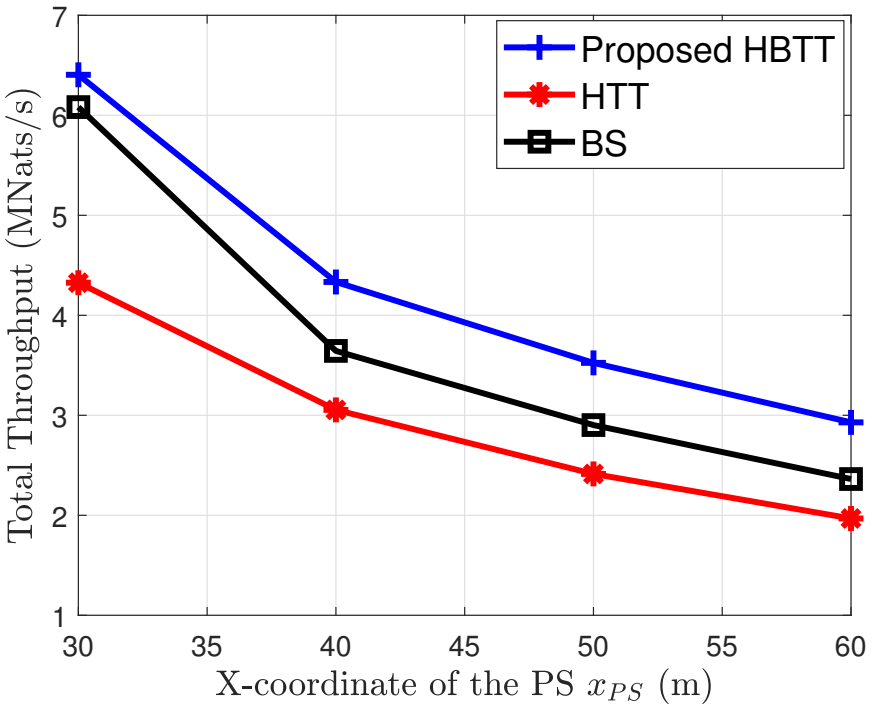

Figure 3.6: Total throughput vs. PS location.

are expected for throughput versus ρ_g and κ_f, respectively. The superiority of our proposed scheme over the benchmarks is once again acknowledged in Figure 3.7.

At the end, it is useful to see the contribution of backscatter communication and active wireless powered communication to the total throughput. Figure 3.8 shows the normalized throughput of backscatter and wireless powered transmissions versus the maximum transmit power of the PS. It is observed that in low PS transmit powers, a large portion of the total throughput belongs to wireless powered transmission while the share of backscatter transmission increases with increasing $P_{\max}$. From this observation, it can be inferred that the users are more willing to actively transmit their information to the AP when their received power from the PS is very low. Therefore, they prefer to spend more time on energy accumulation in the first phase so that they can collect enough energy for their active transmission. When PS uses more transmit power, the part of the throughput which belongs to backscattering

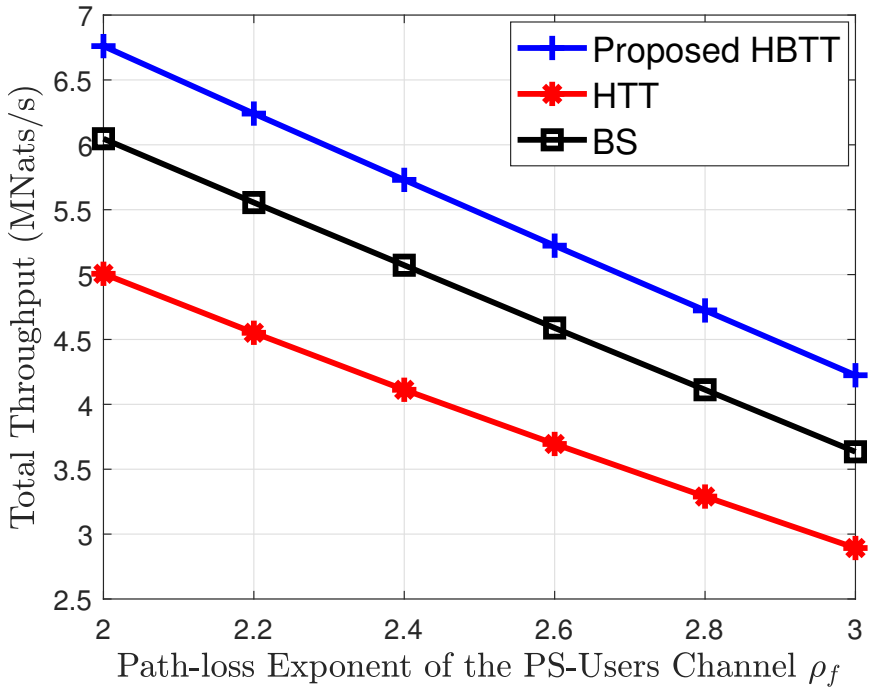

(a)

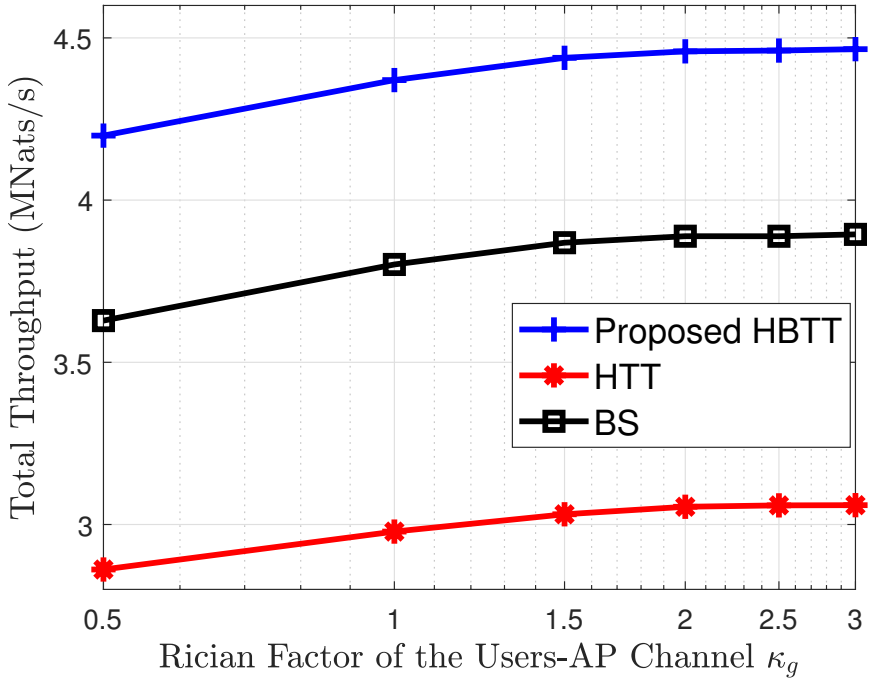

(b)

Figure 3.7: Impact of channel conditions on total throughput (a) throughput vs. path-loss exponent of the PS-users channel (b) throughput vs. Rician factor of the users-AP channel.

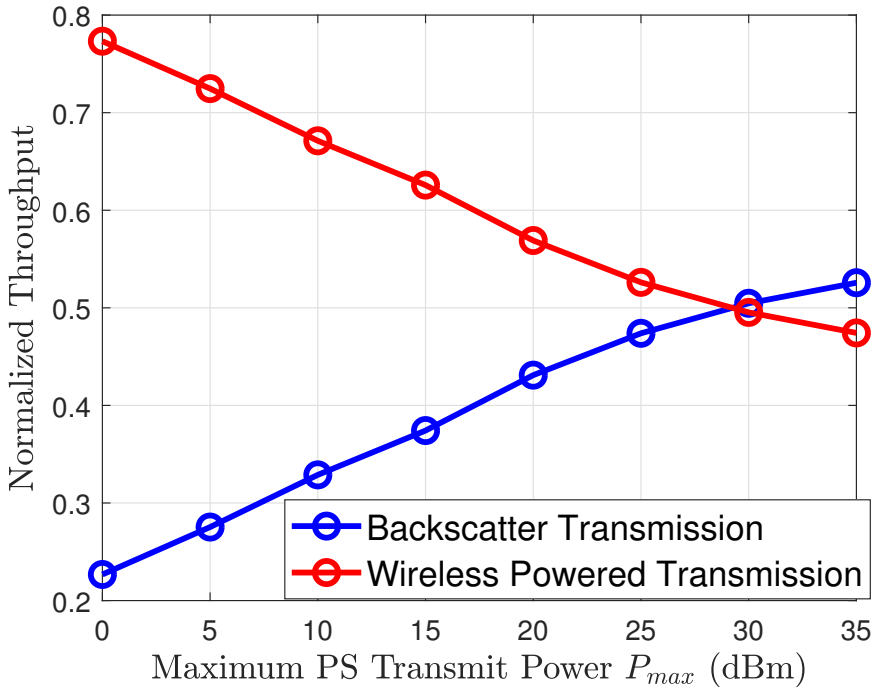

Figure 3.8: Normalized throughput of backscatter and wireless powered transmissions in the proposed HBTT protocol.

increases, owing to the enhanced received power at the users which in turn boosts the received power at the AP.

3.4 Conclusion

This chapter studied a BS-WPCN, where a number of energy-constrained users transmit their information to an AP via passive backscatter and active wireless powered communication. A PS is employed to act as both a signal source and an energy source for the users. Particularly, the PS transmits a downlink wireless signal to the users; this signal is utilized by the users for both backscatter transmission and energy harvesting. A two-phase HBTT protocol is proposed, where both phases are divided into K time-slots. In the first phase, the ith time-slot is allocated for U_i's backscatter transmission, while all other users perform energy collection in this time-slot. The

ith time-slot of the second phase is dedicated to U_i's active information transmission where U_i uses the energy harvested in the first phase to actively communicate with the AP. The total throughput maximization problem is then investigated and an AO-based solution is presented for optimizing the PS beamforming vector and network time allocation. The performance of the proposed scheme is evaluated through numerical simulations, where it is confirmed that the integration of backscatter communication into WPCN is beneficial for improving the network performance because the network can take advantage of the potentials of both backscatter and wireless powered transmissions.

Chapter 4

Intelligent Reflecting Surface-Empowered Wireless Powered Communication Network

This chapter studies an IRS-empowered WPCN, where an IRS is deployed to assist the downlink energy transfer from the PS to the users and the uplink information transmission from the users to the AP by inducing amplitude changes and phase shifts to the signals incident on the surface and reflecting them towards the desired direction. The network operations are divided into two phases, where similar to the traditional WPCN model, the first phase is dedicated to energy transfer from the PS to the users and the second phase is used for information transmission from the users to the AP. Particularly, the PS transmits a wireless energy signal to the users in the downlink during the first phase and the energy transmission of the PS is empowered by IRS elements which apply modifications to the PS signal and reflect them towards the users, thus boosting the received signal power at the users. The second phase is dedicated to information transfer, where the users transmit their information to

the AP using the energy harvested in the first phase, with their transmission being aided by IRS elements. With this setup, we are interested in maximizing the total network throughout by optimizing IRS reflection coefficients for assisting energy and information transmissions, time and power allocation, and PS beamforming vector. To this end, we devise a two-stage algorithm, where the optimal IRS reflection coefficients in the second phase are obtained in closed-form in the first stage, and the techniques of SDR, SCA, and AO are utilized for optimizing other variables in the second stage. Numerical results are finally presented to assess the performance of the proposed algorithm and validate its superiority over benchmark schemes. We also numerically evaluate the performance of the IRS-empowered WPCN when IRS itself is assumed to be energy-constrained, needing to harvest energy from the PS before assisting in information and energy transfer of the WPCN. This evaluation shows that the usefulness of an energy harvesting IRS for aiding network operations largely depends on the power consumption of IRS elements. The contributions of this chapter are partly taken from the work in [99] with some modifications.

4.1 System Model and Problem Formulation

The system model for IRS-empowered WPCN is depicted in Figure 4.1. The model is similar to the traditional WPCN model except for the addition of IRS which is deployed to assist both the downlink energy transfer and the uplink information transmission. The IRS has N reflecting elements and the PS has M antennas. The AP and each of the K users are equipped with one single antenna. The network operates in two phases with the first phase being dedicated to the users' energy harvesting, and the second phase being devoted to the users' information transmission[1]. The

[1]In this chapter, we do not consider the backscatter transmission and focus on the IRS-aided energy transfer and active information transmission. The next chapter extends this model by combining the models considered in this chapter and Chapter 3.

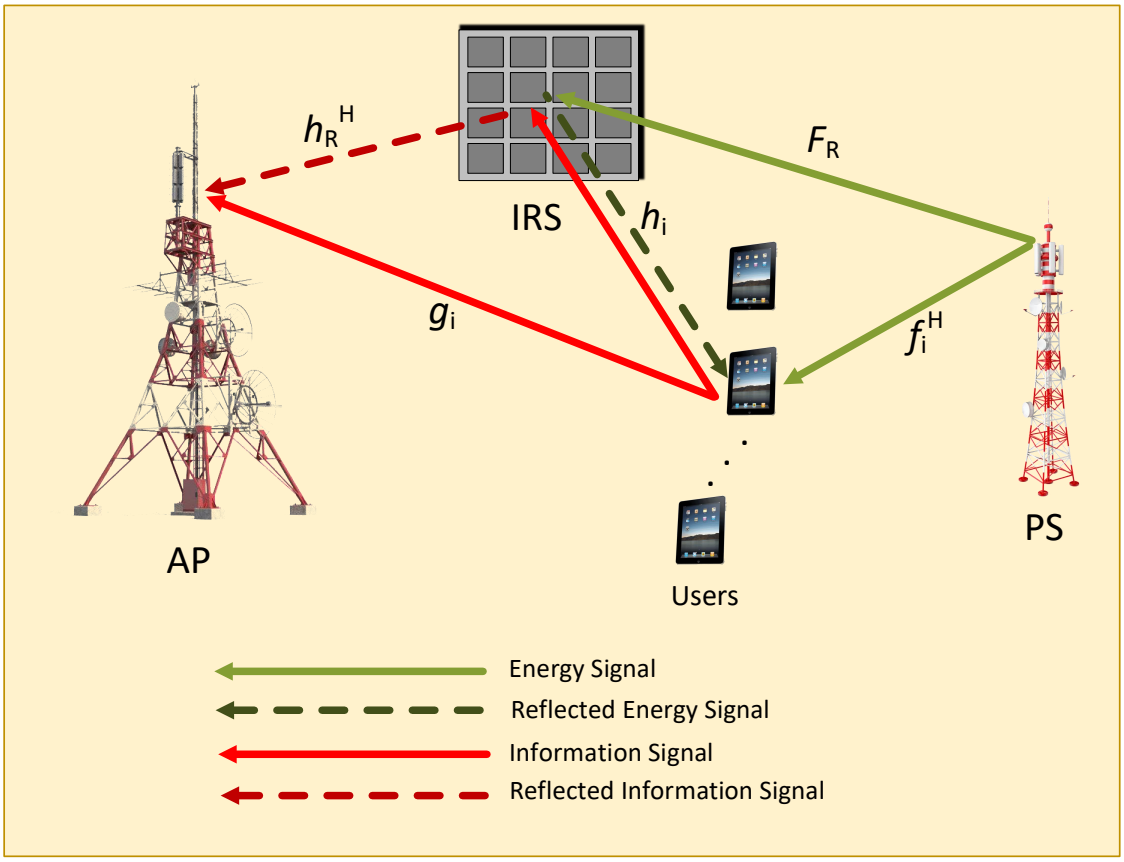

Figure 4.1: System model for IRS-empowered wireless powered communication network.

transmission block for the considered system is illustrated in Figure 4.2. In the first τ_1 fraction of time, users harvest energy from the energy signal sent by the PS, while IRS assists in the energy transfer process by enhancing the received signal power at the users. The second phase is divided into K time-slots and each time-slot is allocated to one of the K users for performing active information transmission to the AP using the previously harvested energy. The IRS again assists the network by empowering the users' information transmission and enhancing the received signal power at the AP.

The transmitted baseband signal of the PS during τ_1 is given by $\hat{\boldsymbol{x}} = \boldsymbol{w}\hat{s}$, where $\boldsymbol{w} \in \mathbb{C}^{M\times 1}$ is the beamforming vector and $\hat{s}$ is the energy-carrying symbol with $\mathbb{E}\{|\hat{s}|^2\} = 1$. This signal is used by the users for energy accumulation, while IRS

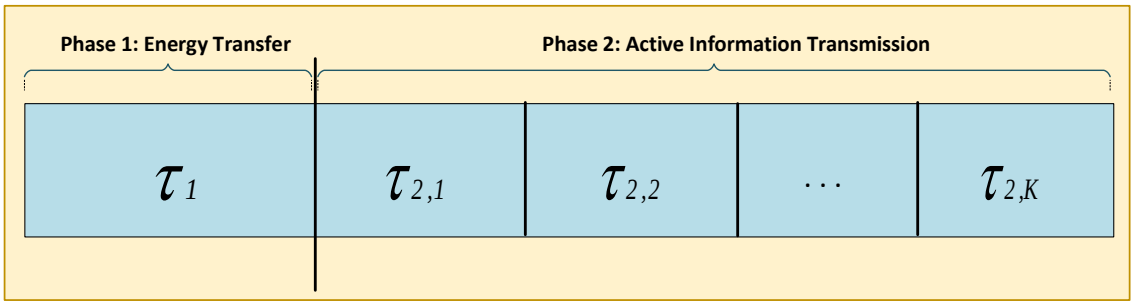

Figure 4.2: Transmission block for IRS-empowered wireless powered communication network.

assists the energy transfer from the PS to the users. The reflection matrix of IRS during τ_1 is given by $\boldsymbol{\Theta}_1 = \text{diag}(\alpha_{1,1}e^{j\theta_{1,1}}, ..., \alpha_{1,N}e^{j\theta_{1,N}})$, where $\alpha_{1,n}$ and $\theta_{1,n}$ are the amplitude reflection and phase shift applied by the nth IRS element to the incident energy signal. The real-time amplitude and phase adjustment of IRS elements are performed by a smart controller which is powered by a stable energy source (e.g., battery or grid). The harvested energy of U_i is obtained as

$$e_i = \tau_1 \eta_i |(\boldsymbol{h}_i^T \boldsymbol{\Theta}_1 \boldsymbol{F}_R + \boldsymbol{f}_i^H)\boldsymbol{w}|^2, \tag{4.1}$$

where η_i is the energy conversion efficiency of the energy harvesting circuit at U_i, $\boldsymbol{F}_R \in \mathbb{C}^{N\times M}$, $\boldsymbol{f}_i^H \in \mathbb{C}^{1\times M}$, and $\boldsymbol{h}_i \in \mathbb{C}^{N\times 1}$ respectively represent the channels between the PS and IRS, between the PS and U_i, and between the U_i and IRS[2].

In the second phase which is the information transmission phase, each user utilizes the harvested energy to transmit information to the AP in its assigned time-slot. Particularly, the ith time-slot of the information transmission phase, having a duration of $\tau_{2,i}$, is allocated to U_i for communicating to the AP. IRS elements assist the transmission of each user by modifying the incident signal to make a constructive combination of the signals from different paths at the AP. The reflection matrix of

[2]The channel reciprocity is assumed to be held for the channels between users and IRS such that the channels in forward and reverse directions are the transpose of each other.

IRS during $\tau_{2,i}$ is expressed as $\boldsymbol{\Theta}_{2,i} = \text{diag}(\alpha_{2,i,1}e^{j\theta_{2,i,1}}, ..., \alpha_{2,i,N}e^{j\theta_{2,i,N}})$, where $\alpha_{2,i,n}$ and $\theta_{2,i,n}$ are the amplitude reflection and phase shift induced by the nth IRS element. $x_i = \sqrt{p_i}s_i$ is the transmitted signal of U_i, where p_i is the transmit power and s_i is the information-bearing symbol with $\mathbb{E}\{|s_i|^2\} = 1$. The received signal at the AP is expressed as

$$y_i = (\boldsymbol{h}_R^H \boldsymbol{\Theta}_{2,i} \boldsymbol{h}_i + g_i)x_i + n_A, \tag{4.2}$$

where $\boldsymbol{h}_R^H \in \mathbb{C}^{1\times N}$ is the channel between the AP and IRS. g_i and n_R specify the U_i-AP channel and the additive noise at the AP, respectively, with $n_A \sim \mathcal{CN}(0, \sigma_A^2)$. The SNR and achievable throughput for U_i are then obtained as

$$\gamma_i = \frac{p_i|(\boldsymbol{h}_R^H \boldsymbol{\Theta}_{2,i} \boldsymbol{h}_i) + g_i|^2}{\sigma_A^2}, \tag{4.3}$$

$$R_i = \tau_{2,i}\log(1+\gamma_i) = \tau_{2,i}\log(1 + \frac{p_i|(\boldsymbol{h}_R^H \boldsymbol{\Theta}_{2,i} \boldsymbol{h}_i) + g_i|^2}{\sigma_A^2}). \tag{4.4}$$

The objective of this chapter is to maximize the total throughput by optimizing the IRS reflection coefficients in both energy transfer and information transmission phases, PS beamforming vector, power allocation at the users, and time allocation. The formulated problem is expressed as follows:

$$\max_{\substack{\boldsymbol{\Theta}_1, \{\boldsymbol{\Theta}_{2,i}\}_{i=1}^K \boldsymbol{w}, \\ \boldsymbol{p}, \tau_1, \boldsymbol{\tau}_2}} \quad \sum_{i=1}^{K} R_i \tag{P4.1}$$

$$\text{s.t.} \quad \text{(C4.1)}\ p_i\tau_{2,i} + p_i'\tau_{2,i} \le e_i,\ \forall i,$$

$$\text{(C4.2)}\ ||\boldsymbol{w}||^2 \le P_{max},$$

$$\text{(C4.3)}\ \tau_1 + \sum_{i=1}^{K} \tau_{2,i} \le 1,$$

$$\text{(C4.4)}\ \tau_1 \ge 0, \tau_{2,i} \ge 0\ \forall i,$$

$$\text{(C4.5)}\ p_i \ge 0\ \forall i,$$

$$\text{(C4.6)}\ 0 \leq \alpha_{1,n} \leq 1\ \forall n,\ 0 \leq \alpha_{2,i,n} \leq 1\ \forall i, n,$$

$$\text{(C4.7)}\ 0 \leq \theta_{1,n} < 2\pi\ \forall n,\ 0 \leq \theta_{2,i,n} < 2\pi\ \forall i, n,$$

where $\boldsymbol{p} = [p_1, ..., p_K]$, $\boldsymbol{\tau}_2 = [\tau_{2,1}, ..., \tau_{2,K}]$ and p_i' represents the circuit power consumption of U_i. Constraints (C4.1) is the energy-causality constraint indicating that the energy consumed by the users cannot exceed their harvested energy. Constraint (C4.2) sets a limit for the maximum transmit power of the PS, (C4.3) and (C4.4) are the constraints on time allocation assuming a normalized transmission block, (C4.5) indicates that the transmit power must be non-negative, (C4.6) and (C4.7) specify the range of amplitude reflection coefficient and phase shift for IRS elements.

4.2 Total Throughput Maximization

Problem (P4.1) is clearly non-convex because the objective function is not concave and the variables are coupled in the objective function and the constraints. Therefore, convex optimization techniques cannot be readily applied for finding the solution to (P4.1). For solving this problem, we propose a two-stage algorithm in which the optimal solution for the IRS reflection coefficients in the information transfer phase is obtained in the first stage, while the AO method is exploited for finding the near-optimal solution to other variables in the second stage.

4.2.1 Optimization of IRS Reflection Coefficients in the Information Transfer Phase

In problem (P4.1), the reflection matrices in different time-slots of the information transmission phase are independent from each other and also from other optimization variables. Therefore, the problem for optimizing the IRS amplitude reflection

coefficients and phase shifts in the information transmission phase can be decoupled into K separate sub-problems, each having a closed-form solution for the reflection coefficients of IRS elements. Specifically, the ith sub-problem is formulated as

$$\begin{aligned} \max_{\boldsymbol{\Theta}_{2,i}} \quad & |(\boldsymbol{h}_R^H \boldsymbol{\Theta}_{2,i} \boldsymbol{h}_i) + g_i|^2 \\ \text{s.t.} \quad & \text{(C4.8)}\ 0 \le \alpha_{2,i,n} \le 1\ \forall n, \quad 0 \le \theta_{2,i,n} < 2\pi\ \forall n. \end{aligned} \tag{P4.2}$$

Problem (P4.2) is equivalent to the following problem:

$$\begin{aligned} \max_{\{\alpha_{2,i,n}\}_{n=1}^N, \{\theta_{2,i,n}\}_{n=1}^N} \quad & |\sum_{n=1}^{N} \alpha_{2,i,n} h_{R,n} h_{i,n} e^{j\theta_{2,i,n}} + g_i| \\ \text{s.t.} \quad & \text{(C4.8)}, \end{aligned} \tag{P4.3}$$

where $h_{R,n}$ and $h_{i,n}$ are the nth elements of $\boldsymbol{h}_R^H$ and $\boldsymbol{h}_i$, respectively. Applying the triangle inequality, we have

$$\begin{aligned} |\sum_{n=1}^{N} \alpha_{2,i,n} h_{R,n} h_{i,n} e^{j\theta_{2,i,n}} + g_i| &\le |\sum_{n=1}^{N} \alpha_{2,i,n} h_{R,n} h_{i,n} e^{j\theta_{2,i,n}}| + |g_i| \\ &\le \sum_{n=1}^{N} |\alpha_{2,i,n} h_{R,n} h_{i,n} e^{j\theta_{2,i,n}}| + |g_i|. \end{aligned} \tag{4.5}$$

Therefore, the objective function in (P4.3) is maximized when the amplitude reflection coefficients of all N elements are equal to 1 and all the $N+1$ channels (i.e., the direct channel and the N reflective channels) are phase-aligned. The optimal solution to (P4.3) can be hence obtained as

$$\alpha_{2,i,n}^{\text{opt}} = 1,\ \forall n = 1, .., N, \tag{4.6}$$

$$\theta_{2,i,n}^{\text{opt}} = \arg(g_i) - \arg(h_{R,n}) - \arg(h_{i,n}),\ \forall n = 1, ..., N. \tag{4.7}$$

4.2.2 Optimization of Other Variables

Having the optimal solution for the IRS reflection coefficients in the information transmission phase and setting $E_i = p_i\tau_{2,i}\ \forall i$, $\tilde{\boldsymbol{W}} = \tau_1 \boldsymbol{w}\boldsymbol{w}^H$, the second-stage optimization problem is formulated as

$$\max_{\substack{\boldsymbol{\Theta}_1, \tilde{\boldsymbol{W}}, \\ \boldsymbol{E}, \tau_1, \boldsymbol{\tau}_2}} \quad \sum_{i=1}^{K} \tau_{2,i} \log(1 + a_i \frac{E_i}{\tau_{2,i}}) \tag{P4.4}$$

$$\text{s.t.} \quad \text{(C4.3) and (C4.4)},$$

$$\text{(C4.9)}\ E_i + p_i' \tau_{2,i} \leq \eta_i \mathrm{Tr}(\tilde{\boldsymbol{W}} \boldsymbol{F}_i'(\boldsymbol{\Theta}_1)),\ \forall i,$$

$$\text{(C4.10)}\ \mathrm{Tr}(\tilde{\boldsymbol{W}}) \leq P_{max}\tau_1,$$

$$\text{(C4.11)}\ E_i \geq 0\ \forall i,$$

$$\text{(C4.12)}\ 0 \leq \alpha_{1,n} \leq 1\ \forall n, \quad 0 \leq \theta_{1,n} < 2\pi\ \forall n,$$

$$\text{(C4.13)}\ \tilde{\boldsymbol{W}} \succeq \boldsymbol{0},$$

$$\text{(C4.14)}\ \mathrm{Rank}(\tilde{\boldsymbol{W}}) \leq 1,$$

where $\boldsymbol{E} = [E_1, ..., E_K]$, $a_i = \frac{|(\boldsymbol{h}_R^H \boldsymbol{\Theta}_{2,i}^{\mathrm{opt}} \boldsymbol{h}_i) + g_i|^2}{\sigma_A^2}$, and $\boldsymbol{F}_i'(\boldsymbol{\Theta}_1) = \boldsymbol{f}_i'(\boldsymbol{\Theta}_1)\boldsymbol{f}_i'^H(\boldsymbol{\Theta}_1)$ where $\boldsymbol{f}_i'^H(\boldsymbol{\Theta}_1) = \boldsymbol{h}_i^T \boldsymbol{\Theta}_1 \boldsymbol{F}_R + \boldsymbol{f}_i^H$. Problem (P4.4) is non-convex due to the coupling of $\boldsymbol{\Theta}_1$ and $\tilde{\boldsymbol{W}}$ in (C4.9) and the rank constraints in (C4.14). Hence, the above problem cannot be directly solved by convex optimization techniques. To deal with the first source of non-convexity which is constraint (C4.9), we use the AO method; we first maximize the throughput in (P4.4) with fixed $\boldsymbol{\Theta}_1$ and then optimize $\boldsymbol{\Theta}_1$ for further improving the throughput. Also, similar to the approach we took in Chapter 3, we use the SDR technique followed by Eigen-decomposition for finding a near-optimal solution for the beamforming vector.

Fixing the reflection matrix $\boldsymbol{\Theta}_1$ and relaxing constraint (C4.14), (P4.4) will turn into a convex optimization problem which can be solved by the CVX toolbox [60] or

other convex optimization toolboxes. Then, using the Eigen-decomposition technique, the near-optimal solution for $\boldsymbol{w}$ is obtained. Particularly, assume that $\tilde{\boldsymbol{W}}^{\star}$ is the optimal solution for $\tilde{\boldsymbol{W}}$ with rank greater than one. Then, $\boldsymbol{w}^{\star} = \sqrt{\frac{\lambda_1}{\tau_1^{\star}}}\boldsymbol{u}_1$ is the near-optimal beamforming vector, where λ_1 is the largest eigen-value of $\tilde{\boldsymbol{W}}^{\star}$ and $\boldsymbol{u}_1$ is the corresponding eigen-vector. $\tau_1^{\star}$ is the optimal time duration for energy transfer, while the optimal time allocation for users' information transmission is denoted by $\boldsymbol{\tau}_2^{\star} = [\tau_{2,1}^{\star}, ..., \tau_{2,K}^{\star}]$.

Next, we seek the optimal IRS reflection coefficient design in the energy transfer phase by considering the following problem:

$$\begin{aligned} \max_{\boldsymbol{E},\boldsymbol{\Theta}_1} \quad & \sum_{i=1}^{K} \tau_{2,i}^{\star} \log(1 + a_i \frac{E_i}{\tau_{2,i}^{\star}}) \\ \text{s.t.} \quad & \text{(C4.11) and (C4.12)}, \\ & \text{(C4.15) } E_i + p_i' \tau_{2,i}^{\star} \leq \tau_1^{\star} \eta_i |(\boldsymbol{h}_i^T \boldsymbol{\Theta}_1 \boldsymbol{F}_R + \boldsymbol{f}_i^H) \boldsymbol{w}^{\star}|^2. \end{aligned} \tag{P4.5}$$

We define $v_n = \alpha_{1,n} e^{j\theta_{1,n}}\ \forall n$, $\boldsymbol{v}^H = [v_1, ..., v_N]$, and $\boldsymbol{\phi}_i = \text{diag}(\boldsymbol{h}_i^T)\boldsymbol{F}_R \boldsymbol{w}^{\star}$. Constraint (C4.15) can then be re-written as

$$E_i + p_i' \tau_{2,i}^{\star} \leq \tau_1^{\star} \eta_i |\boldsymbol{v}^H \boldsymbol{\phi}_i + \boldsymbol{f}_i^H \boldsymbol{w}^{\star}|^2. \tag{4.8}$$

The right hand side of (4.8) makes the constraint non-convex. To deal with this, we use the SCA technique and approximate $|\boldsymbol{v}^H \boldsymbol{\phi}_i + \boldsymbol{f}_i^H \boldsymbol{w}^{\star}|^2$ by its lower-bound, using the first-order Taylor series expansion. Then, we need to iteratively update the lower-bound until an acceptable convergence is achieved. Specifically, we have

$$|\boldsymbol{v}^H \boldsymbol{\phi}_i + \boldsymbol{f}_i^H \boldsymbol{w}^{\star}|^2 = \boldsymbol{v}^H \boldsymbol{\Phi}_i \boldsymbol{v} + 2\text{Re}\{\bar{c}_i \boldsymbol{v}_i^H \boldsymbol{\phi}\} + |c_i|^2, \tag{4.9}$$

where $\boldsymbol{\Phi}_i = \boldsymbol{\phi}_i \boldsymbol{\phi}_i^H$ and $c_i = \boldsymbol{f}_i^H \boldsymbol{w}^{\star}$. Now, using the first-order Taylor series expansion,

at any feasible point $\boldsymbol{v}^{(0)}$, the convex term $\boldsymbol{v}^H \boldsymbol{\Phi}_i \boldsymbol{v}$ is lower-bounded as

$$\boldsymbol{v}^H \boldsymbol{\Phi}_i \boldsymbol{v} \geq -\boldsymbol{v}^{(0)H} \boldsymbol{\Phi}_i \boldsymbol{v}^{(0)} + 2\mathrm{Re}\{\boldsymbol{v}^H \boldsymbol{\Phi}_i \boldsymbol{v}^{(0)}\}. \tag{4.10}$$

We thus have to replace the right hand side of (C4.15) by its concave lower bound in (4.10) and iteratively solve the problem for optimizing the IRS reflection coefficients in the energy transfer phase until convergence. The problem for the lth iteration can be expressed as

$$\begin{aligned} \max_{\boldsymbol{E},\boldsymbol{v}} \quad & \sum_{i=1}^{K} \tau_{2,i}^{\star} \log(1 + a_i \frac{E_i}{\tau_{2,i}^{\star}}) \qquad \text{(P4.6)} \\ \text{s.t.} \quad & \text{(C4.11)}, \\ & \text{(C4.16)} \ |v_n| \leq 1, \ \forall n \\ & \text{(C4.17)} \ E_i \leq 2\tau_1^{\star} \eta_i \mathrm{Re}\{\boldsymbol{v}^H (\bar{c}_i \boldsymbol{\phi}_i + \boldsymbol{\Phi}_i \boldsymbol{v}^{(l-1)})\} + c_i^{\prime(l-1)}, \ \forall i, \end{aligned}$$

with $\boldsymbol{v}^{(l-1)}$ being the solution obtained in the $(l-1)$th iteration and

$$c_i^{\prime(l-1)} = |c_i|^2 - p_i' \tau_{2,i}^{\star} - \boldsymbol{v}^{(l-1)H} \boldsymbol{\Phi}_i \boldsymbol{v}^{(l-1)}. \tag{4.11}$$

4.2.3 Overall Throughput Maximization Algorithm

The overall two-stage algorithm for maximizing the network throughput is given in Algorithm 2, where the first stage finds the closed-form IRS reflection coefficients in the information transmission phase and the second stage finds a near-optimal solution to the remaining optimization variables through the techniques of AO, SDR and SCA.

Algorithm 2 Total Throughput Maximization Algorithm for Solving (P4.1)

1: **For** $i = 1 : K$ do

Find the optimal IRS amplitude reflection coefficients and phase shifts in the K time-slots of the information transmission phase (i.e., $\alpha_{2,i,n}^{\text{opt}}$ and $\theta_{2,i,n}^{\text{opt}}$ $\forall i, n$) using (4.6) and (4.7), and obtain the optimal reflection matrices $\boldsymbol{\Theta}_{2,i}^{\text{opt}}$, $\forall i$.

2: Initialize $\alpha_{1,n}^{\star(0)}$ and $\theta_{1,n}^{\star(0)}$ $\forall n$. Set $R^{(0)} = 0$ and $l_1 = 0$;

3: **Repeat**

Update iteration index $l_1 = l_1 + 1$.

With given $\boldsymbol{\Theta}_1^{\star(l_1-1)}$, solve the relaxed version of (P4.4) using the CVX toolbox and obtain $\tilde{\boldsymbol{W}}^{\star(l_1)}$, $\tau_1^{\star(l_1)}$, $\boldsymbol{\tau}_2^{\star(l_1)}$.

If $\tilde{\boldsymbol{W}}^{\star(l_1)}$ does not satisfy the rank-one constraint, use Gaussian randomization or Eigen-decomposition to extract $\boldsymbol{w}^{\star(l_1)}$.

Set $\boldsymbol{v}^{(0)H} = [v_1^{(0)}, ..., v_N^{(0)}]$, where $v_n^{(0)} = \alpha_{1,n}^{\star(0)} e^{j\theta_{1,n}^{\star(0)}}$. Set $l_2 = 0$.

Repeat

Update iteration index $l_2 = l_2 + 1$.

Compute $c_i'^{(l_2-1)}$.

Solve (P4.6) and obtain $\boldsymbol{v}^{(l_2)}$.

Until $||\boldsymbol{v}^{(l_2)} - \boldsymbol{v}^{(l_2-1)}|| \leq \epsilon_2$.

Return $\boldsymbol{E}^{\star(l_1)}$, $\alpha_{1,n}^{\star(l_1)} = |v_n^{(l_2)}|$ $\forall n$, $\theta_{1,n}^{\star(l_1)} = \arg(v_n^{(l_2)})$ $\forall n$.

Compute $R^{(l_1)} = \sum_{i=1}^{K} R_i^{(l_1)}$.

4: **Until** $|R^{(l_1)} - R^{(l_1-1)}| < \epsilon_1$.

5: $R_{\max} = R^{(l_1)}$, $\boldsymbol{w}^{\text{opt}} = \boldsymbol{w}^{\star(l_1)}$, $\tau_0^{\text{opt}} = \tau_0^{\star(l_1)}$, $\tau_1^{\text{opt}} = \tau_1^{\star(l_1)}$, $\boldsymbol{\tau}_2^{\text{opt}} = \boldsymbol{\tau}_2^{\star(l_1)}$, $\boldsymbol{E}^{\text{opt}} = \boldsymbol{E}^{\star(l_1)}$, $\boldsymbol{\Theta}_1^{\text{opt}} = \boldsymbol{\Theta}_1^{\star(l_1)}$.

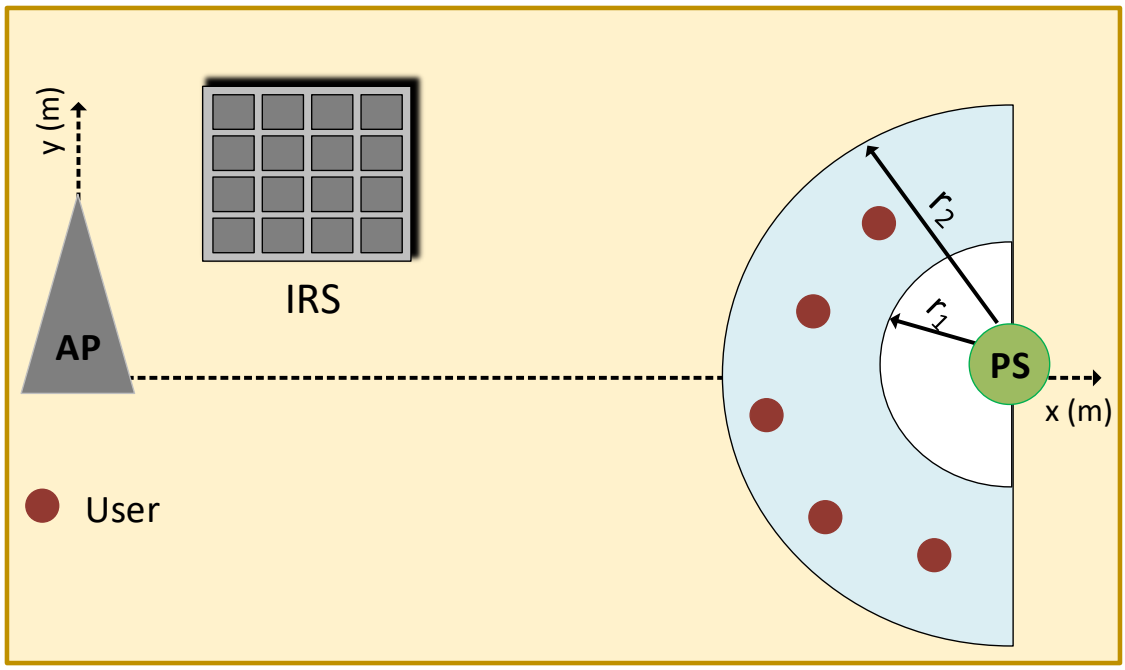

Figure 4.3: Simulation setup.

4.3 Performance Evaluation

In this section, we assess the performance of the presented IRS-empowered WPCN by comparing it to two benchmarks in different network settings. The first benchmark is an IRS-empowered WPCN where the phase shifts of IRS elements in all time-slots are randomly chosen from the interval $[0, 2\pi)$ and all other variables are optimized based on the methods proposed in this chapter. This benchmark scheme is labeled as "IRS-empowered WPCN: Random" on the figures. The second benchmark represents the conventional WPCN without IRS and is denoted as "WPCN without IRS" on the figures.

4.3.1 Simulation Setup

As illustrated in Figure 4.3, an $x - y$ coordinate system is considered, where the AP is located at the origin, the reference element of the IRS is placed at (x_{IRS}, y_{IRS}),

and the PS is posited at $(x_{PS}, 0)$. K user are randomly placed on the left side of the PS with a minimum distance of r_1 and a maximum distance of r_2 from the PS. For small-scale fading, channels are modeled based on the Rician fading model. For instance, $\boldsymbol{F}_R$ is given by

$$\boldsymbol{F}_R = \sqrt{\frac{\kappa_{f,r}}{\kappa_{f,r}+1}}\boldsymbol{F}_R^{\text{LoS}} + \sqrt{\frac{1}{\kappa_{f,r}+1}}\boldsymbol{F}_R^{\text{NLoS}}, \tag{4.12}$$

where $\kappa_{f,r}$ denotes the Rician factor, $\boldsymbol{F}_R^{\text{LoS}} \in \mathbb{C}^{N\times M}$ and $\boldsymbol{F}_R^{\text{NLoS}} \in \mathbb{C}^{N\times M}$ are the LoS and NLoS components of $\boldsymbol{F}_R$. The LoS channel matrix is modeled as $\boldsymbol{F}_R^{\text{LoS}} = \hat{\boldsymbol{f}}_R^{(N)}(\varphi_{\text{AoA}})\hat{\boldsymbol{f}}_R^{(M)H}(\varphi_{\text{AoD}})$, where φ_{AoA} and φ_{AoD} denote the angle of arrival and angle of departure, respectively, and $\hat{\boldsymbol{f}}_R^{(X)}(\varphi) = [1, e^{j\pi\sin(\varphi)}, e^{j2\pi\sin(\varphi)}, ..., e^{j(X-1)\pi\sin(\varphi)}]^T$. The elements of the NLoS channel matrix $\boldsymbol{F}_R^{\text{NLoS}}$ follow the standard Rayleigh fading. (4.12) is then multiplied by the large-scale fading, given by $\sqrt{C_0(d_{f,r}/d_0)^{-\rho_{f,r}}}$, where C_0 is the path-loss at the reference distance of $d_0 = 1$ meter (m), set as $C_0 = -20$ dB, $d_{f,r}$ represents the distance between IRS and PS, and $\rho_{f,r}$ is the path-loss exponent of the channel between IRS and PS. Channels $\boldsymbol{f}_i^H$, $\forall i$, $\boldsymbol{h}_R^H$, $\boldsymbol{h}_i$, $\forall i$, and g_i, $\forall i$ are modeled in a similar way with κ_f, $\kappa_{h,r}$, κ_h, and κ_g denoting their Rician factors and ρ_f, $\rho_{h,r}$, ρ_h, and ρ_g being the corresponding path-loss exponents.

Unless otherwise specified, the following set of parameters are used throughout the simulations: $K = 10$, $M = 5$, and $N = 40$. The channel-related parameters are set as $\rho_f = 2$, $\rho_g = 3.5$, $\rho_h = 2.5$, $\rho_{h,r} = 2$, $\rho_{f,r} = 2.5$, $\kappa_f = \infty$, $\kappa_g = 0$, $\kappa_h = 3$, $\kappa_{h,r} = \infty$, $\kappa_{f,r} = 3$. The x-coordinate of the PS is $x_{PS} = 30$ m and the reference element of IRS is assumed to be located at (5 m, 5 m). Also, $r_1 = 5$ m and $r_2 = 15$ m. $P_{max} = 30$ dBm and $\eta_i = 0.5$, $\forall i$. The circuit power consumption is assumed to be $p_i' = 1$ mW, $\forall i$. The noise power spectral density at the AP is set as -160 dBm/Hz, the bandwidth is 1 MHz, and the convergence threshold in Algorithm 2 is chosen to be $\epsilon = 0.01$. The results are based on the average of 1000 different channel

realizations. Table 4.1 summarizes the parameter settings for the simulations of this chapter.

Table 4.1: Simulation parameters for IRS-empowered WPCN.

Parameter	**Description**	**Setting**
K	Number of users	10
M	Number of PS antennas	5
N	Number of IRS elements	40
P_{max}	Maximum PS transmit power	30 dBm
x_{PS}	X-coordinate of the PS	30 m
x_{IRS}	X-coordinate of the reference element of IRS	5 m
y_{IRS}	Y-coordinate of the reference element of IRS	5 m
r_1	Minimum distance between PS and users	5 m
r_2	Maximum distance between PS and users	15 m
$p'_i,\ \forall i$	Circuit power consumption of all users	1 mW
$\eta_i,\ \forall i$	Energy conversion efficiency of all users	0.5
κ_f	Rician factor for the channel between PS and users	∞
κ_g	Rician factor for the channel between users and AP	0
κ_h	Rician factor for the channel between IRS and users	3
$\kappa_{h,r}$	Rician factor for the channel between IRS and AP	∞
$\kappa_{f,r}$	Rician factor for the channel between IRS and PS	3
ρ_f	Path-loss exponent for the channel between PS and users	2
ρ_g	Path-loss exponent for the channel between users and AP	3.5
ρ_h	Path-loss exponent for the channel between IRS and users	2.5
$\rho_{h,r}$	Path-loss exponent for the channel between IRS and AP	2
$\rho_{f,r}$	Path-loss exponent for the channel between IRS and PS	2.5
d_0	Reference distance	1 m
C_0	Path-loss at the reference distance	-20 dBm
σ_A^2	Noise power at the AP	-100 dBm
ϵ	Convergence threshold for Algorithm 2	0.01

4.3.2 Numerical Results

Figure 4.4 shows the total throughput as a function of the maximum transmit power of the PS. The throughput of all schemes improves with increasing the PS transmit power because increasing P_{max} improves the users' harvested energy, transmit power, and consequently their SNR at the AP. As can be seen in the figure, the proposed

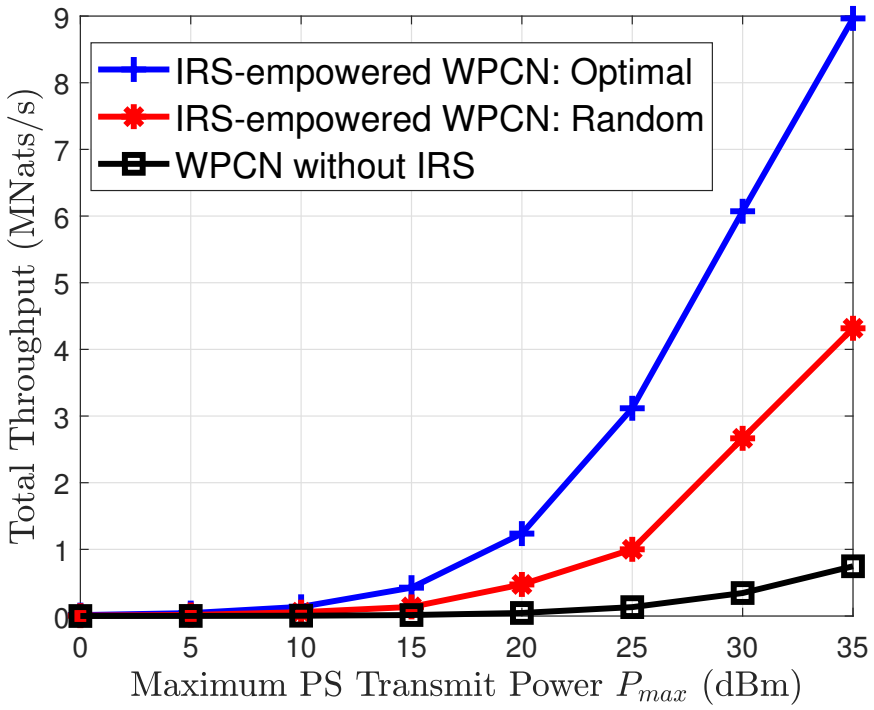

Figure 4.4: Total throughput vs. maximum transmit power of the PS.

scheme outperforms the two benchmarks and the gap between the proposed scheme and the benchmark schemes increases with increasing the PS transmit power. The large difference between the throughputs achieved in traditional WPCN and IRS-empowered WPCN shows the remarkable advantage of integrating IRS with WPCN. The red curve which corresponds to the IRS-empowered WPCN with non-optimized phase shifts also significantly outperforms WPCN without IRS, which indicates that using IRS even without optimizing its phase shift values can be beneficial for performance enhancement. However, the gap between the IRS-empowered WPCN with optimized phase shifts and the one with non-optimized phase shifts shows that optimizing the phase shift values of IRS elements can be very helpful for further performance improvement of WPCNs.

Figure 4.5 depicts the throughput performance versus the number of elements at the IRS. The figure shows that using more elements at the IRS improves the perfor-

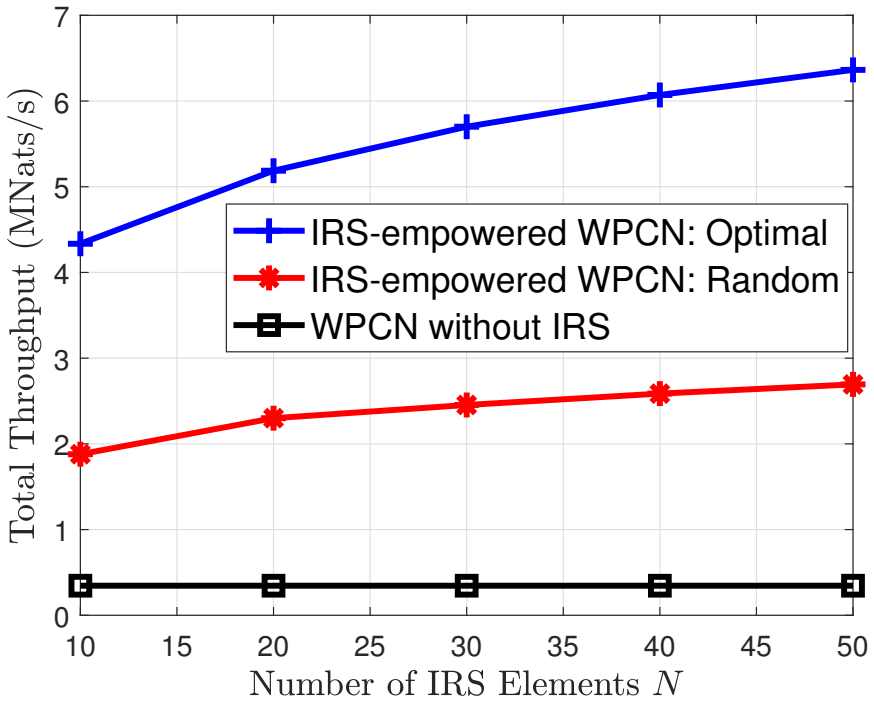

Figure 4.5: Total throughput vs. number of IRS elements.

mance, especially when the phase shifts of IRS elements have been optimized. That's because increasing IRS elements adds new degrees of freedom for further performance improvements. The large difference between the performance of the presented scheme and the two benchmarks confirms the effectiveness of the proposed scheme for improving the performance of conventional WPCNs and making them more suitable for being incorporated into the 6G ecosystem. As an example, when 30 elements are employed at the IRS, the throughput of the proposed scheme outperforms the throughputs of IRS-empowered WPCN with non-optimized phase shifts and WPCN without IRS by 136% and 1700%, respectively.

In Figure 4.6, we have plotted the throughput as a function of the users' circuit power consumption. According to the figure, increasing the users' circuit power consumption degrades the throughput. That's because when the circuit power increases, the users have to expend more energy for powering their circuit operations, which reduces the amount of energy remained for information transmission. The users thus

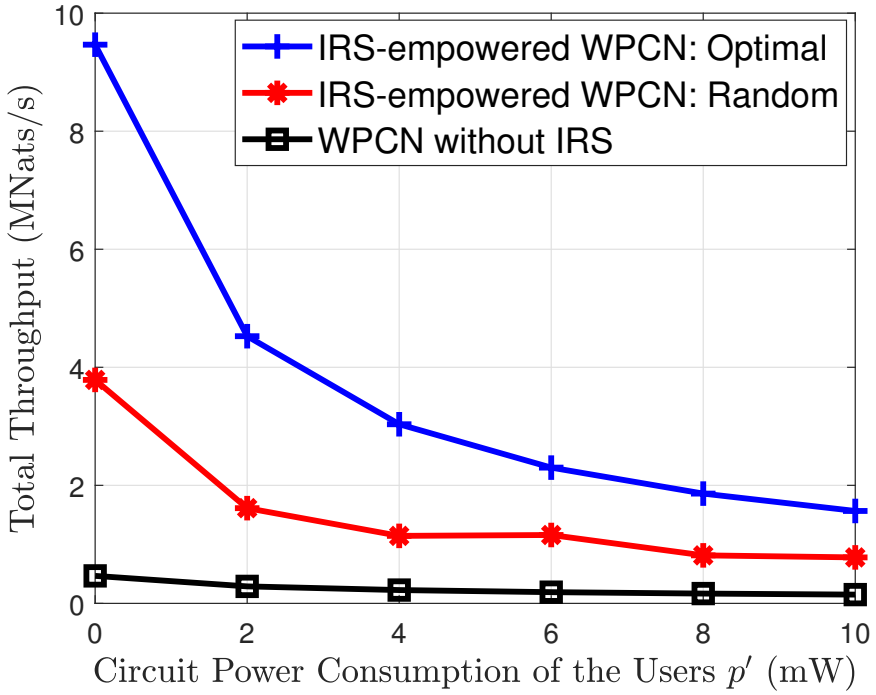

Figure 4.6: Total throughput vs. users' circuit power consumption.

have to use less power for transmitting their information which decreases their SNR and throughput.

Next, we investigate the impact of channel conditions on the throughput performance. Figure 4.7 shows the total throughput versus the path-loss exponent of the channels between IRS and users (i.e., $\boldsymbol{h}_i$'s) and the channel between PS and IRS (i.e, $\boldsymbol{F}_R$). As expected, the throughput of the IRS-empowered WPCN schemes generally decrease with larger path-loss exponent, which is due to the fact that the energy signals from the PS to the IRS and from the IRS to the users as well as the information signals from the users to the IRS get weaker. We can observe from Figure 4.7 that the benchmark scheme with non-optimized IRS phase shifts shows some irregularities. Specifically, when the path-loss exponents increase from 2 to 2.2, the throughput of this scheme increases. The reason for this observation is the randomness of the phase shifts chosen for IRS elements in this scheme. To elaborate more, since phase shift values in all time-slots are randomly selected, it is not guaranteed that they will be

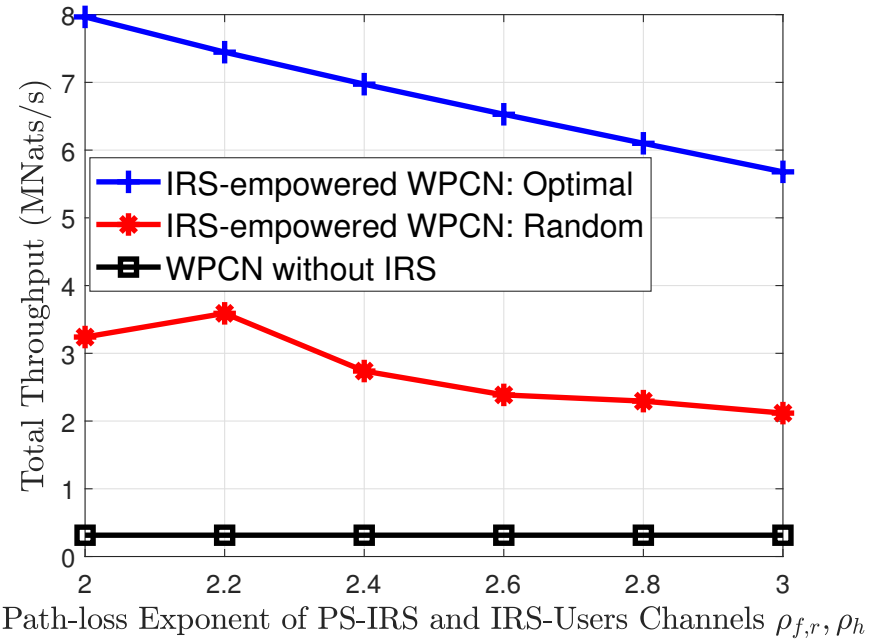

Figure 4.7: Total throughput vs. PS-IRS and IRS-users path-loss.

constructively combined at the designated receiver(s). In other words, some phase shifts may be constructively combined, while others cancel out each other and the level of constructiveness and destructiveness depends on the selected random phase shifts. The performance of the WPCN without IRS is the lowest of all schemes and is unaffected by the value of the path-loss exponents. This figure once again shows the supremacy of the proposed scheme and endorses the effectiveness of IRS for improving the performance of WPCNs.

The effect of the path-loss exponent of the channel between users and AP is investigated in Figure 4.8. We can clearly see that the path-loss exponent between the users and the AP has minimal impact on the performance of IRS-empowered WPCN schemes. Particularly, the throughput of our presented scheme decreases only by 0.58% from 6.0488 MNats/s to 6.0135 MNats/s when the path-loss exponent is increased from 2.5 to 4.5. This is while the throughput of the benchmark without IRS decreases by almost 97% from 1.1998 MNats/s to 0.0397 MNats/s. This observation

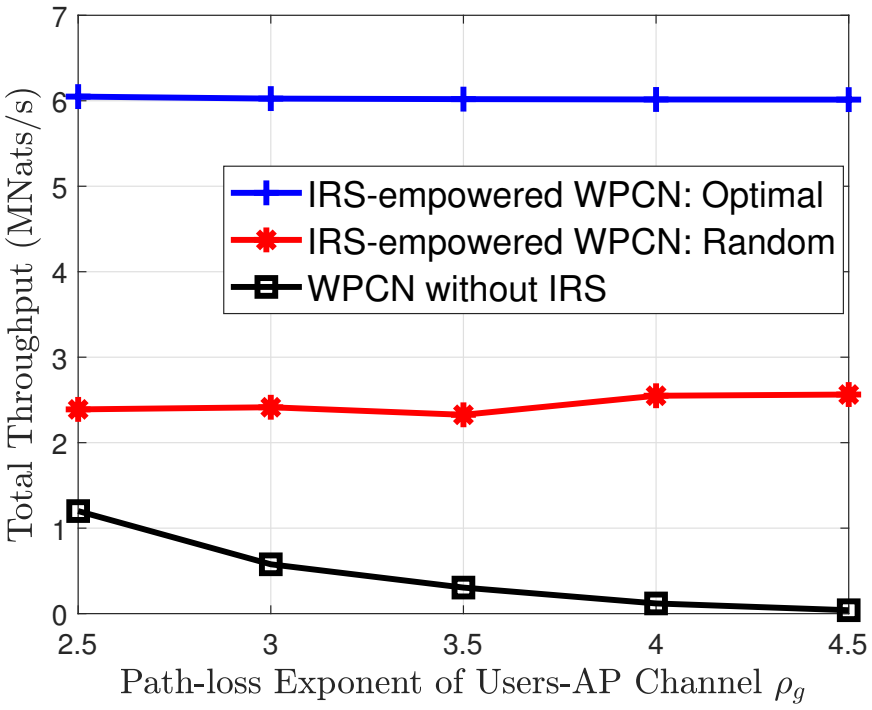

Figure 4.8: Total throughput vs. users-AP path-loss.

demonstrates the robustness of the IRS-empowered WPCN against the conditions of the direct channel between the users and the AP and shows that the IRS can be helpful for guaranteeing the performance of WPCNs even if there exists blockages between the users and the AP.

So far, we have assumed that the energy needed for the operation of IRS elements is provided by stable energy sources, e.g., battery. To achieve a completely self-sustainable network environment, IRS may be equipped with energy harvesting modules so that, similar to WPCN users, it can harvest its required energy from the signals transmitted by RF sources. Here, we want to study the case where IRS needs to harvest energy from the signals transmitted by the PS and see whether IRS can still be useful for performance enhancement in WPCN if it has to spend some time for collecting sufficient energy before being able to assist the network. To this end, we denote the power consumption of each IRS elements by p_R and assume that a

time-slot of duration τ_0 at the beginning of the transmission block is used for energy harvesting of IRS. Specifically, we assume that during τ_0, the PS transmits the signal $\boldsymbol{w}_0\hat{s}_0$ in the downlink and IRS and users independently harvest energy from this signal. Then, the remaining transmission block is allocated for energy and information transfer based on the model described earlier, i.e., the PS transmits another energy signal during τ_1 to power users and the IRS assists in the energy transfer using its previously harvested energy. Then, the active information transmission of the users takes place exactly as explained before. We thus have new variables τ_0 and $\boldsymbol{w}_0$ to optimize and the following constraints are added to problem (P4.1):

$$Np_R(\tau_1 + \sum_{i=1}^{K} \tau_{2,i}) \leq \eta_R \tau_0 ||\boldsymbol{F}_R \boldsymbol{w}_0||^2, \tag{4.13}$$

$$||\boldsymbol{w}_0||^2 \leq P_{max}, \tag{4.14}$$

$$\tau_0 \geq 0, \tag{4.15}$$

where η_R is the energy conversion efficiency of the IRS. Also e_i in (4.1) is modified as

$$e_i = \tau_0 \eta_i |\boldsymbol{f}_i^H \boldsymbol{w}_0|^2 + \tau_1 \eta_i |(\boldsymbol{h}_i^H \boldsymbol{\Theta}_1 \boldsymbol{F}_R + \boldsymbol{f}_i^H)\boldsymbol{w}|^2, \tag{4.16}$$

and constraint (C4.3) in problem (P4.1) is replaced by the following constraint:

$$\tau_0 + \tau_1 + \sum_{i=1}^{K} \tau_{2,i} \leq 1. \tag{4.17}$$

We now want to see how the addition of energy harvesting capability at the IRS affects the network performance. Figure 4.9 shows the total throughput as a function of the power consumption of IRS elements. This figure shows that as the IRS power consumption increases, the performance superiority of the proposed IRS-empowered

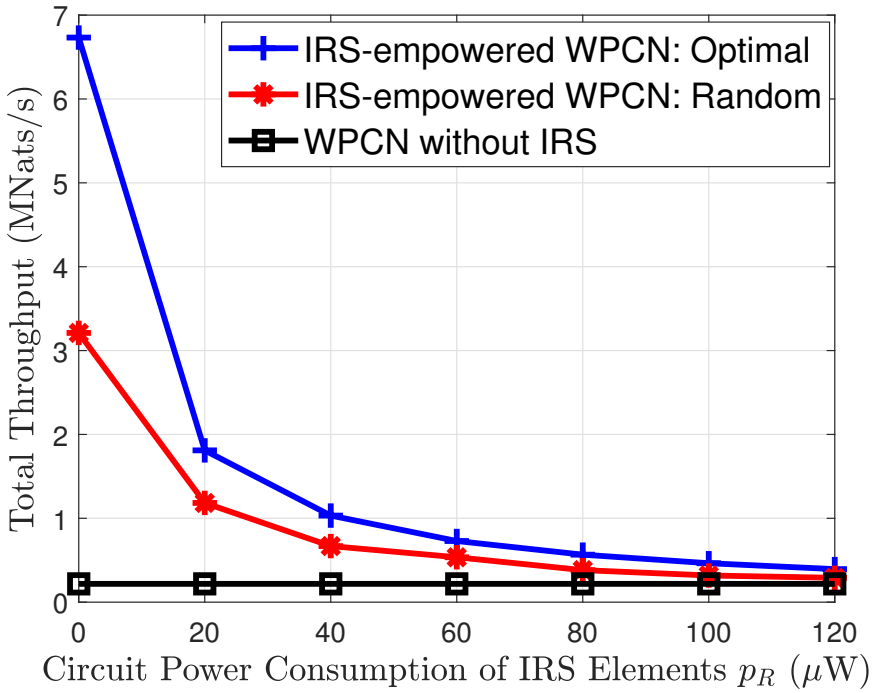

Figure 4.9: Total throughput vs. power consumption of IRS elements.

WPCN over the WPCN without IRS declines. The reason for this observation is that when the power consumption of IRS elements gets larger, more time needs to be allocated for the energy harvesting process of the IRS (i.e., the duration of τ_0 needs to be increased), which means that less time will be left for the IRS to aid the energy and information transmissions in the WPCN.

4.4 Conclusion

This chapter investigated the integration of the newly-emerged IRS technology into the conventional WPCN in order to improve the performance of wireless energy transfer and information transmission. The network considered in this chapter consists of several energy-constrained users, a PS for powering the users, an AP for receiving users' information, and an IRS which modifies the energy and information signals incident on the surface and reflects them towards the destined receivers. The problem

of maximizing the total network throughput is studied, where the objective is to optimize the IRS reflection coefficients in both energy and information transfer phases, PS beamforming vector, users' power allocation, and network time allocation. As the formulated problem is non-convex, a two-stage algorithm is presented, where the optimal solution to IRS reflection coefficients in the information transmission phase is provided in the first stage and the near-optimal solution to other optimization variables is obtained in the second stage. Numerical results study the impact of various network parameters on the performance of the system, reveal the gains that can be achieved by incorporating IRS into WPCN, and show the importance of optimizing the phase shift values of IRS elements. Finally, the performance of an IRS-assisted WPCN with energy harvesting IRS elements is evaluated, in which the IRS needs to obtain its required energy from the energy signals transmitted by the PS. It is disclosed that the benefits of using IRS in WPCN would be diminished if the power consumption of IRS elements for assisting the network operations is high, because IRS has to spend much time on energy collection and would not be able to aid the energy and information transfer until it harvests adequate energy.

Chapter 5

Intelligent Reflecting Surface-Empowered Backscatter-Assisted Wireless Powered Communication Networks

In this chapter, we study an IRS-empowered BS-WPCN, where a number of users which are powered by energy transmissions of the PS communicate with the AP via backscatter and active wireless information transmissions. An IRS is employed which assists both backscatter and active communications of the users with the AP by adjusting amplitude and phase of the impinging signals. In this chapter, a practical energy conversion model is assumed for energy harvesting of the users, where the limitations of practical energy harvesters including sensitivity and saturation are taken into consideration. Further, the AP is assumed to be equipped with multiple antennas, which is more realistic and practical than the single-antenna AP considered in previous chapters. The transmission block consists of two phases; the first

phase is divided into time-slots and the PS transmits downlink energy signals in each time-slot of this phase. Each user is assigned with a time-slot in which it backscatters the PS signal to transmit its own information to the AP. All other users which are not scheduled for backscatter transmission harvest energy from the PS signal. The second phase is dedicated to users' active information transmission in which the users exploit their previously collected energy to actively generate information signals and send them to the AP. Unlike previous chapters where the users adopted a TDMA scheme for their active information transfer, in this chapter, all users simultaneously transmit to the AP via SDMA in the active information transmission phase, which allows us to design the receive beamforming at the AP. As mentioned above, IRS elements empower the backscatter and active information transmission of the users by inducing amplitude and phase changes to the incident signal and reflecting it towards AP. The objective of this chapter is to maximize the total network throughput which is the summation of the throughputs attained in first and second phases. With this aim, we investigate the optimization of IRS amplitude reflection coefficients and phase shifts in all time-slots of the first phase as well as the single time-slot of the second phase, along with time and power allocation, PS transmit beamforming and AP receive beamforming vectors. We propose a two-stage algorithm for solving the throughput maximization problem, with IRS reflection coefficients for assisting users' backscatter information transmission being optimized in the first stage, while optimizing the remaining variables in the second stage. Specifically, we propose two different methods for optimizing IRS reflection amplitudes and phase shifts in all time-slots of the backscatter transmission phase. Thereafter, assuming that the AP uses minimum mean square error (MMSE) receive beamforming for decoding users' information in the second phase, we optimize PS beamforming vectors, time and power allocation, IRS reflection coefficients for assisting users' active information transmission, and AP

MMSE receive beamforming vectors by utilizing the techniques of SDR, SCA, BCD, AO, Lagrange duality, and by exploiting the relationship between MSE and SNR in MMSE receivers. Numerical simulations are finally conducted to evaluate the performance of the presented IRS-empowered BS-WPCN and validate the efficiency and accuracy of the proposed algorithms. The contents of this chapter have appeared in our recent paper [100].

5.1 System Model and Problem Formulation

The system model and transmission block structure for the IRS-empowered BS-WPCN are shown in Figure 5.1 and Figure 5.2, respectively. The considered network consists of K single-antenna users, an AP with M_A antennas, a PS with M_P antennas, and an IRS having N reflecting elements. The network operation consists of two phases, as depicted in Figure 5.2, with the first phase being dedicated to energy harvesting and backscatter transmission and the second phase being assigned for active information transmission. The details of network operation will be explained later in this section.

In previous chapters, we used a linear model for energy conversion at the users, where the harvested power was assumed to have a linear relationship with the received power. In practice, the relationship between the harvested and received powers is not linear and the conversion efficiency varies depending on the received power. Therefore, we aim to use a more realistic model for energy conversion in this chapter by taking into account the practical limitations of energy harvesting systems. The details will be elaborated in the next subsection.

In what follows, we present the system model including the energy conversion model and communication model, and formulate the total throughput maximization

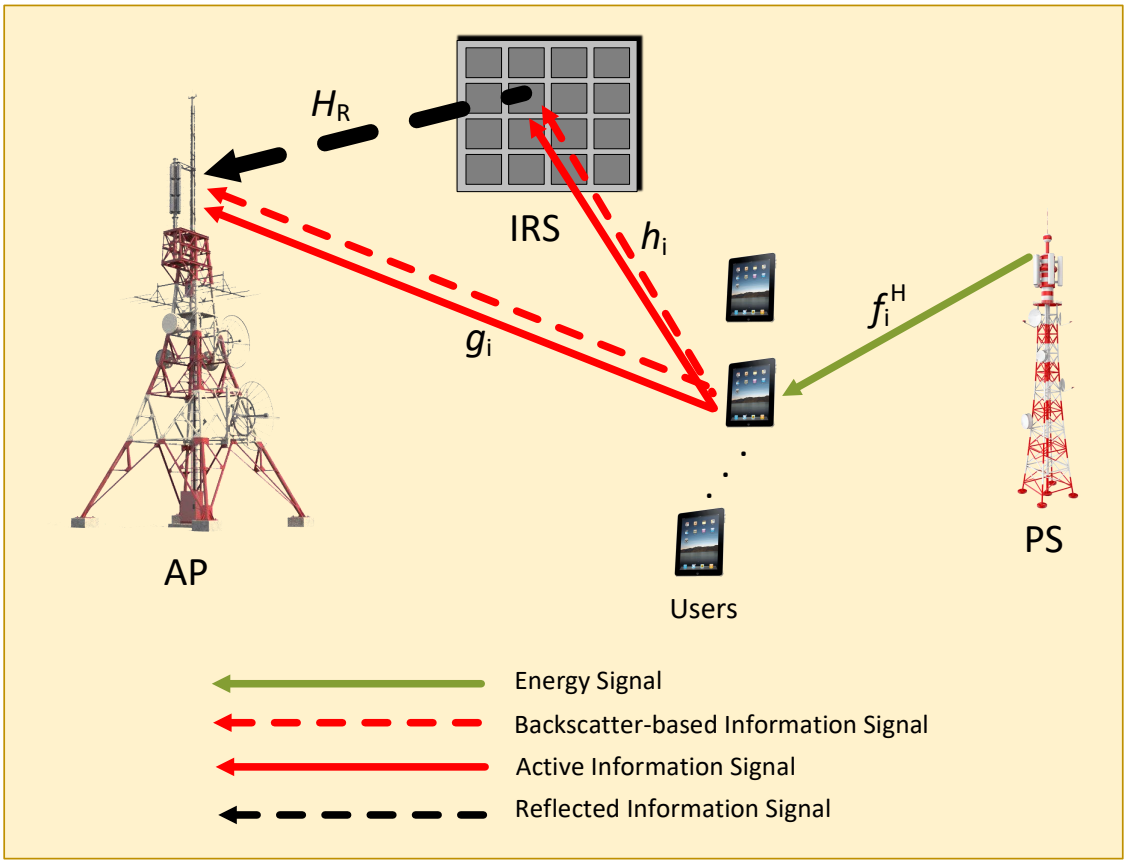

Figure 5.1: System model for IRS-empowered backscatter-assisted wireless powered communication network.

problem.

5.1.1 Energy Conversion Model

Most energy harvesting circuits use diode-based rectifiers to convert the received RF power into direct current (DC) power. The efficiency of diode-based energy harvesters highly depends on the level of the received power. Specifically, when the received power is below the sensitivity of the energy harvester, the output power is zero because low input powers cannot turn on the diode. More importantly, when the received power exceeds some specific levels, the energy conversion efficiency is greatly degraded [101]; however, the output DC power remains constant and becomes sat-

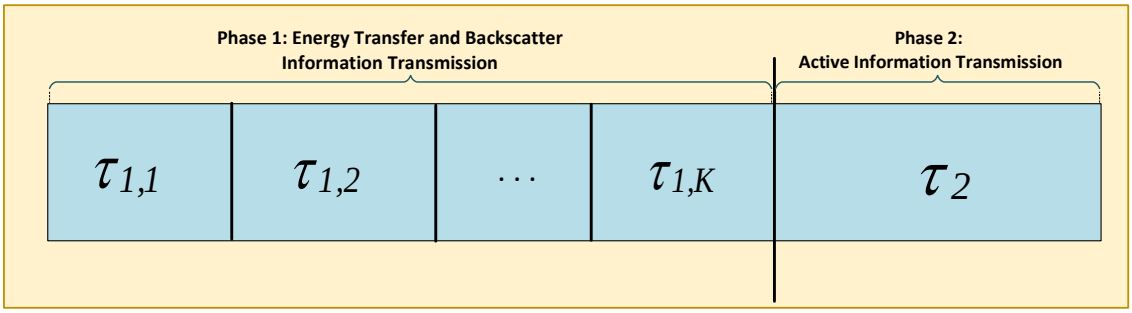

Figure 5.2: Transmission block for IRS-empowered backscatter-assisted wireless powered communication network.

urated [102]. This saturation point depends on the reverse breakdown voltage. As the reverse breakdown voltage increases, the maximum achievable output power also increases; however, saturation is unavoidable and there always exists a maximum level for the output power. Taking into account the saturation effect is pivotal when studying networks with energy harvesting devices. Without considering this effect, the theoretical optimal design fails to perform properly in practice. Therefore, the conventional linear energy conversion model, in which the output power linearly increases with the received power, cannot be relied on for studying the behavior of energy harvesting circuits.

The sigmoidal energy conversion model has been recently used by many researchers for designing resource allocation schemes in energy harvesting-enabled networks [56–59]. However, this model cannot be easily implemented in convex optimization toolboxes such as CVX without further approximations and transformations, especially when the received power varies over the harvesting period and the harvested power becomes a sum-of-ratios expression. Another energy conversion model has been used in the literature which models the input-output power relationship of an energy harvester with a piece-wise linear function with two pieces, where the output power linearly increases with the input power up to the saturation point, beyond which the output power remains constant [51, 97]. This model is more tractable than the

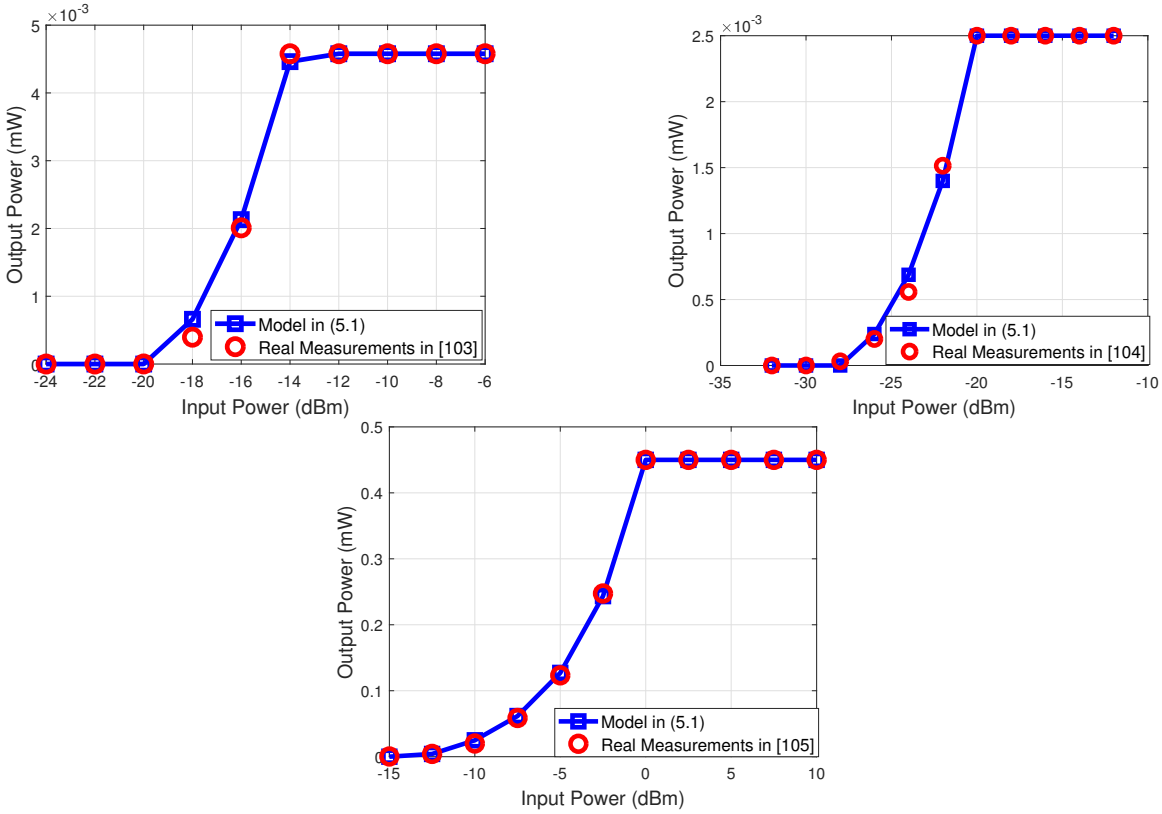

Figure 5.3: Comparison between the model in (5.1) and real measurements in [103–105].

sigmoidal model, however, it does not account for the sensitivity of energy harvesting circuits.

In this chapter, we use a piece-wise linear energy conversion model with three pieces, where both sensitivity and saturation effects are taken into consideration. The harvested power in this model is given by

$$p_h = \min\left(\max(0, \eta p_r - \xi), P_{sat}\right), \tag{5.1}$$

where p_h and p_r are the harvested power and the received power, respectively, P_{sat} is the saturation power and $\frac{\xi}{\eta}$ is the diode turn-on power.

In Figure 5.3, we have plotted the curve fitting results for the piece-wise linear energy conversion model in (5.1) using real measurements from [103–105]. The figure shows the good match between the model in (5.1) and real data, which confirms that

this model is accurate enough for modeling the behavior of realistic energy harvesting circuits.

5.1.2 Communication Model

The communication takes place over two phases, where the backscatter transmission of the users to the AP is carried out in the first phase, while the second phase is allocated for their active information transmission. Particularly, the first phase is split into K time-slots and the PS transmits the signal $\hat{\boldsymbol{x}}_i = \boldsymbol{w}_i \hat{s}_i$, with $\boldsymbol{w}_i \in \mathbb{C}^{M_P \times 1}$ and $\hat{s}_i$ being respectively the beamforming vector and the transmitted symbol in the ith time-slot of the first phase of duration $\tau_{1,i}$ and $\mathbb{E}\{|\hat{s}_i|^2\} = 1$. This signal is used by the users for energy harvesting and backscatter transmission purposes. To elaborate, U_i uses the transmitted signal of PS during $\tau_{1,i}$ for backscattering its information to the AP, while other $K-1$ users use this signal for harvesting energy. The backscatter transmission of the users is supported by IRS elements which induce phase and amplitude changes to the signal backscattered by the users and reflect it towards the AP. The harvested energy of U_i in the first phase is given by

$$e_i = \sum_{\substack{j=1 \\ j \neq i}}^{K} \tau_{1,j} p_{i,j}^h, \tag{5.2}$$

where $p_{i,j}^h$ is the harvested power of U_i during $\tau_{1,j}$. According to the model presented in (5.1), the expression for the harvested power of U_i in $\tau_{1,j}$ is obtained as

$$p_{i,j}^h = \min\left(\max(0, \eta_i |\boldsymbol{f}_i^H \boldsymbol{w}_j|^2 - \xi_i), P_{sat,i}\right), \tag{5.3}$$

where $P_{sat,i}$ is the saturation power of U_i's energy harvesting circuit, η_i and ξ_i are the energy harvesting circuit parameters. Also, $\boldsymbol{f}_i^H \in \mathbb{C}^{1 \times M_P}$ is the channel between the PS and U_i.

The transmitted signal of U_i during $\tau_{1,i}$ is given by $x_{1,i} = \sqrt{\beta_i}\boldsymbol{f}_i^H \boldsymbol{w}_i \hat{s}_i s_{1,i}$, where β_i is the backscatter coefficient of U_i and $s_{1,i}$ is its information-bearing symbol with $\mathbb{E}\{|s_{1,i}|^2\} = 1$. As previously stated, the backscatter transmission of U_i during $\tau_{1,i}$ is empowered by IRS. Denote the reflection matrix of IRS during $\tau_{1,i}$ by $\boldsymbol{\Theta}_{1,i} = \text{diag}(\alpha_{1,i,1}e^{j\theta_{1,i,1}}, ..., \alpha_{1,i,N}e^{j\theta_{1,i,N}})$, where $\alpha_{1,i,n}$ and $\theta_{1,i,n}$ are respectively the amplitude reflection coefficient and phase shift induced by the nth IRS element to the transmitted signal of U_i. The real-time amplitude and phase adjustment of IRS elements are performed by a smart controller which is powered by a stable energy source (e.g., battery or grid). This model can be easily extended to the scenario where IRS elements are enabled to harvest their required energy from existing RF sources (e.g., AP, PS, etc.) by assuming that a portion of the transmission block (e.g., τ_0) is dedicated for the energy harvesting of IRS. The received signal at the AP in $\tau_{1,i}$ is then expressed as

$$\begin{aligned} \boldsymbol{y}_{1,i} &= (\boldsymbol{H}_R \boldsymbol{\Theta}_{1,i} \boldsymbol{h}_i + \boldsymbol{g}_i) x_{1,i} + \boldsymbol{n}_A, \\ &= (\boldsymbol{H}_R \boldsymbol{\Theta}_{1,i} \boldsymbol{h}_i + \boldsymbol{g}_i) \sqrt{\beta_i} \boldsymbol{f}_i^H \boldsymbol{w}_i \hat{s}_i s_{1,i} + \boldsymbol{n}_A, \end{aligned} \tag{5.4}$$

where $\boldsymbol{H}_R \in \mathbb{C}^{M_A \times N}$ is the channel between IRS and AP, $\boldsymbol{h}_i \in \mathbb{C}^{N \times 1}$ is the channel between IRS and U_i, and $\boldsymbol{g}_i \in \mathbb{C}^{M_A \times 1}$ is the channel between AP and U_i. Also, $\boldsymbol{n}_A \sim \mathcal{CN}(0, \sigma_A^2 \boldsymbol{I}_{M_A})$ is the noise at the AP. After maximum ratio combining (MRC) at the AP, the SNR and achievable throughput of U_i in this phase are obtained as

$$\gamma_{1,i} = \frac{\beta_i |\boldsymbol{f}_i^H \boldsymbol{w}_i|^2 ||\boldsymbol{H}_R \boldsymbol{\Theta}_{1,i} \boldsymbol{h}_i + \boldsymbol{g}_i||^2}{\sigma_A^2}, \tag{5.5}$$

$$R_{1,i} = \tau_{1,i} \log(1 + \gamma_{1,i}) = \tau_{1,i} \log\Big(1 + \frac{\beta_i |\boldsymbol{f}_i^H \boldsymbol{w}_i|^2 ||\boldsymbol{H}_R \boldsymbol{\Theta}_{1,i} \boldsymbol{h}_i + \boldsymbol{g}_i||^2}{\sigma_A^2}\Big). \tag{5.6}$$

In the second phase of duration τ_2, all users actively transmit to the AP at the same

time and their transmission is again empowered by IRS elements. The transmitted signal of U_i in this phase is given by $x_{2,i} = \sqrt{p_i} s_{2,i}$ with p_i and $s_{2,i}$ being the transmit power and information-bearing symbol of U_i and $\mathbb{E}\{|s_{2,i}|^2\} = 1$. The transmitted signal of the users is reflected by IRS which applies the reflection matrix $\boldsymbol{\Theta}_2 = \text{diag}(\alpha_{2,1} e^{j\theta_{2,1}}, ..., \alpha_{2,N} e^{j\theta_{2,N}})$ to the signal and reflects it to the AP. The received signal at the AP in this phase is given by

$$\boldsymbol{y}_2 = \sum_{i=1}^{K} (\boldsymbol{H}_R \boldsymbol{\Theta}_2 \boldsymbol{h}_i + \boldsymbol{g}_i) x_{2,i} + \boldsymbol{n}_A = \sum_{i=1}^{K} \sqrt{p_i} (\boldsymbol{H}_R \boldsymbol{\Theta}_2 \boldsymbol{h}_i + \boldsymbol{g}_i) s_{2,i} + \boldsymbol{n}_A. \tag{5.7}$$

AP applies the receive beamforming vector $\boldsymbol{a}_i$ for decoding the signal of U_i. The signal-to-interference-plus-noise ratio (SINR) and achievable throughput of U_i for active information transmission are respectively obtained as

$$\gamma_{2,i} = \frac{p_i |\boldsymbol{a}_i^H (\boldsymbol{H}_R \boldsymbol{\Theta}_2 \boldsymbol{h}_i + \boldsymbol{g}_i)|^2}{\sum_{j \neq i} p_j |\boldsymbol{a}_i^H (\boldsymbol{H}_R \boldsymbol{\Theta}_2 \boldsymbol{h}_j + \boldsymbol{g}_j)|^2 + ||\boldsymbol{a}_i||^2 \sigma_A^2}, \tag{5.8}$$

$$R_{2,i} = \tau_2 \log(1 + \gamma_{2,i}) = \tau_2 \log \Big(1 + \frac{p_i |\boldsymbol{a}_i^H (\boldsymbol{H}_R \boldsymbol{\Theta}_2 \boldsymbol{h}_i + \boldsymbol{g}_i)|^2}{\sum_{j \neq i} p_j |\boldsymbol{a}_i^H (\boldsymbol{H}_R \boldsymbol{\Theta}_2 \boldsymbol{h}_j + \boldsymbol{g}_j)|^2 + ||\boldsymbol{a}_i||^2 \sigma_A^2}\Big). \tag{5.9}$$

We aim to maximize the total throughput of the network by optimizing IRS reflection coefficients, PS transmit beamforming vectors, AP receive beamforming vectors, power allocation for the users' active information transmission, and the time allocation for energy transfer, backscattering, and active information transmission. The throughput maximization problem is thus formulated as follows:

$$\max_{\substack{\{\boldsymbol{\Theta}_{1,i}\}_{i=1}^K, \boldsymbol{\Theta}_2, \{\boldsymbol{w}_i\}_{i=1}^K, \\ \{\boldsymbol{a}_i\}_{i=1}^K, \boldsymbol{p}, \boldsymbol{\tau}_1, \tau_2}} \quad \sum_{i=1}^{K} (R_{1,i} + R_{2,i}) \tag{P5.1}$$

$$\text{s.t.} \quad \text{(C5.1)} \; p_i \tau_2 + p_i' \tau_2 \leq e_i, \; \forall i,$$

$$\text{(C5.2)} \; ||\boldsymbol{w}_i||^2 \leq P_{max}, \; \forall i,$$

$$\text{(C5.3)}\ \sum_{i=1}^{K} \tau_{1,i}||\boldsymbol{w}_i||^2 \leq P_{avg},$$

$$\text{(C5.4)}\ \sum_{i=1}^{K} \tau_{1,i} + \tau_2 \leq 1,$$

$$\text{(C5.5)}\ \tau_{1,i} \geq 0\ \forall i, \tau_2 \geq 0,$$

$$\text{(C5.6)}\ p_i \geq 0\ \forall i,$$

$$\text{(C5.7)}\ 0 \leq \alpha_{1,i,n} \leq 1\ \forall i, n, \quad 0 \leq \theta_{1,i,n} < 2\pi\ \forall i, n,$$

$$\text{(C5.8)}\ 0 \leq \alpha_{2,n} \leq 1\ \forall n, \quad 0 \leq \theta_{2,n} < 2\pi\ \forall n,$$

where $\boldsymbol{p} = [p_1, ..., p_K]$, $\boldsymbol{\tau}_1 = [\tau_{1,1}, ..., \tau_{1,K}]$, and p_i' is the circuit power consumption of U_i. (C5.1) is the energy causality constraint indicating that the energy consumed by users cannot exceed their harvested energy. (C5.2) and (C5.3) are the maximum transmit power constraint and average transmit power constraint at the PS, (C5.4) and (C5.5) are the time allocation constraints assuming a normalized transmission block, (C5.6) indicates that the users' transmit power must be non-negative, (C5.7) and (C5.8) determine the acceptable range for the IRS amplitude reflection coefficients and phase shifts.

5.2 Total Throughput Maximization

Problem (P5.1) is not convex due to the structure of the objective function and coupling of variables in the objective function and constraints. Therefore, convex optimization techniques cannot be used for solving (P5.1). In the following, we propose a two-stage scheme, where the IRS reflection coefficients in the first phase are optimized in the first stage and the optimization of other variables is performed in the second stage.

5.2.1 Optimization of IRS Reflection Coefficients for Assisting Users' Backscatter Transmission

The problem of optimizing IRS reflection coefficients for assisting users' backscatter transmission is given by

$$\max_{\{\boldsymbol{\Theta}_{1,i}\}_{i=1}^{K}} \quad \sum_{i=1}^{K} \tau_{1,i} \log\left(1+\hat{\beta}_i||\boldsymbol{H}_R\boldsymbol{\Theta}_{1,i}\boldsymbol{h}_i+\boldsymbol{g}_i||^2\right), \tag{P5.2}$$
$$\text{s.t.} \quad \text{(C5.7)},$$

where $\hat{\beta}_i = \frac{\beta_i|\boldsymbol{f}_i^H\boldsymbol{w}_i|^2}{\sigma_A^2}$.

We can split problem (P5.2) into K separate sub-problems, each dealing with the optimization of IRS reflection coefficients in one of the time-slots of the first phase. Specifically, the ith sub-problem will be

$$\max_{\boldsymbol{\Theta}_{1,i}} \quad ||\boldsymbol{H}_R\boldsymbol{\Theta}_{1,i}\boldsymbol{h}_i+\boldsymbol{g}_i||^2, \tag{P5.3}$$
$$\text{s.t.} \quad \text{(C5.9)}\ 0 \le \alpha_{1,i,n} \le 1\ \forall n, \quad 0 \le \theta_{1,i,n} < 2\pi\ \forall n.$$

We define $\boldsymbol{\Phi}_i = \boldsymbol{H}_R\text{diag}(\boldsymbol{h}_i)$ and $\boldsymbol{v}_{1,i} = [v_{1,i,1},...,v_{1,i,N}]^T$ with $v_{1,i,n} = \alpha_{1,i,n}e^{j\theta_{1,i,n}}$. Then we have

$$\begin{aligned}||\boldsymbol{H}_R\boldsymbol{\Theta}_{1,i}\boldsymbol{h}_i+\boldsymbol{g}_i||^2 &= (\boldsymbol{\Phi}_i\boldsymbol{v}_{1,i}+g_i)^H(\boldsymbol{\Phi}_i\boldsymbol{v}_{1,i}+g_i)\\ &= \boldsymbol{v}_{1,i}^H\boldsymbol{\Phi}_i^H\boldsymbol{\Phi}_i\boldsymbol{v}_{1,i}+2\text{Re}\{\boldsymbol{v}_{1,i}^H\boldsymbol{\Phi}_i^H\boldsymbol{g}_i\}+||\boldsymbol{g}_i||^2,\end{aligned} \tag{5.10}$$

and problem (P5.3) can be re-written as

$$\max_{\boldsymbol{v}_{1,i}} \quad \boldsymbol{v}_{1,i}^H\boldsymbol{\Phi}_i^H\boldsymbol{\Phi}_i\boldsymbol{v}_{1,i}+2\text{Re}\{\boldsymbol{v}_{1,i}^H\boldsymbol{\Phi}_i^H\boldsymbol{g}_i\}+||\boldsymbol{g}_i||^2, \tag{P5.4}$$

$$\text{s.t.} \quad \text{(C5.10)} \ |v_{1,i,n}| \leq 1 \ \forall n.$$

Problem (P5.4) is a non-convex optimization problem because of the quadratic term $\boldsymbol{v}_{1,i}^H \boldsymbol{\Phi}_i^H \boldsymbol{\Phi}_i \boldsymbol{v}_{1,i}$ in the objective function. Here, we propose an AO-based design, where we alternately optimize the reflection coefficient of one IRS element having other reflection coefficients fixed, in an iterative manner.

Expanding the first two terms of the objective function in (P5.4), we have

$$\boldsymbol{v}_{1,i}^H \boldsymbol{\Phi}_i^H \boldsymbol{\Phi}_i \boldsymbol{v}_{1,i} + 2\text{Re}\{\boldsymbol{v}_{1,i}^H \boldsymbol{\Phi}_i^H \boldsymbol{g}_i\} = \sum_{n=1}^{N} \Big(|v_{1,i.n}|^2 \sum_{m=1}^{M_A} |[\boldsymbol{\Phi}_i]_{m,n}|^2 + 2\text{Re}\{v_{1,i,n} (\sum_{q=n+1}^{N} \bar{v}_{1,i,q} (\sum_{m=1}^{M_A} [\boldsymbol{\Phi}_i]_{m,n} [\boldsymbol{\Phi}_i^H]_{q,m}) + \sum_{m=1}^{M_A} \bar{g}_{i,m} [\boldsymbol{\Phi}_i]_{m,n}) \} \Big), \tag{5.11}$$

where $g_{i,m}$ is the mth element of $\boldsymbol{g}_i$.

The objective is to alternately optimize the reflection coefficients of IRS elements. The optimization problem for the nth reflection coefficient in the ith time-slot is formulated as

$$\max_{v_{1,i,n}} \ t_{i,n} |v_{1,i,n}|^2 + 2\text{Re}\{z_{i,n} v_{1,i,n}\} \tag{P5.5}$$
$$\text{s.t.} \quad \text{(C5.11)} \ |v_{1,i,n}| \leq 1,$$

where

$$t_{i,n} = \sum_{m=1}^{M_A} |[\boldsymbol{\Phi}_i]_{m,n}|^2, \tag{5.12}$$

$$z_{i,n} = \sum_{\substack{q=1 \\ q \neq n}}^{N} \bar{v}_{1,i,q} (\sum_{m=1}^{M_A} [\boldsymbol{\Phi}_i]_{m,n} [\boldsymbol{\Phi}_i^H]_{q,m}) + \sum_{m=1}^{M_A} \bar{g}_{i,m} [\boldsymbol{\Phi}_i]_{m,n}, \tag{5.13}$$

and the terms independent of $v_{1,i,n}$ have been discarded. The optimal solution to

(P5.5) is readily obtained as

$$v_{1,i,n} = e^{-j\arg(z_{i,n})}. \tag{5.14}$$

Algorithm 3 describes the alternating procedure for optimizing the IRS reflection coefficients.

Algorithm 3 AO-Based Optimization of IRS Reflection Coefficients for Assisting Backscatter Transmission

1: Set $v_{1,i,n}^{(0)} = 1 \ \forall i, n$.

2: **For** $i = 1 : K$ do

$l = 0$.

Repeat

Update iteration index $l = l + 1$.

For $n = 1 : N$ do

Given $v_{1,i,n'}^{(l)}$ for $n' = 1, ..., n-1$ and $v_{1,i,n'}^{(l-1)}$ for $n' = n+1, ..., N$ calculate $z_{i,n}$.

Find $v_{1,i,n}$ from (5.14).

Until $||\boldsymbol{v}_{1,i}^{(l)} - \boldsymbol{v}_{1,i}^{(l-1)}|| \leq \epsilon$.

3: Set $\alpha_{1,i,n}^{\text{opt}} = |v_{1,i,n}^{(l)}| \ \forall i, n$ and $\theta_{1,i,n}^{\text{opt}} = \arg(v_{1,i,n}) \ \forall i, n$.

Although the optimization of $v_{1,i,n}$ in (P5.5) ensures that the power of the combined signal from the direct path and the nth reflected path is improved, it does not necessarily mean that the power of the collective signal received at the AP is also increased. In other words, the separate optimization of IRS reflection coefficients may fail to result in coherent combination of the individually reflected signals at the AP. Therefore, the improvement of throughput over iterations is not guaranteed and the algorithm may converge to a sub-optimal solution. In what follows, we propose another method for finding the reflection coefficients of IRS elements based on the

SCA technique, which simultaneously updates the reflection coefficients of all IRS elements and thus, guarantees that the throughout increases after each update and a near-optimal solution for IRS reflection coefficients is obtained.

As mentioned earlier, the non-convexity of problem (P5.4) is due to the objective function being quadratic, which is convex in $\boldsymbol{v}_{1,i}$. At any feasible point $\boldsymbol{v}_{1,i}^{(0)}$, the term $\boldsymbol{v}_{1,i}^H \boldsymbol{\Phi}_i^H \boldsymbol{\Phi}_i \boldsymbol{v}_{1,i}$ is lower-bounded by its first-order Taylor expansion $2\text{Re}\{\boldsymbol{v}_{1,i}^H \boldsymbol{\Phi}_i^H \boldsymbol{\Phi}_i \boldsymbol{v}_{1,i}^{(0)}\} - \boldsymbol{v}_{1,i}^{(0)H} \boldsymbol{\Phi}_i^H \boldsymbol{\Phi}_i \boldsymbol{v}_{1,i}^{(0)}$. We can therefore apply the SCA technique and iteratively maximize the lower-bound of the objective function in (P5.4) until convergence. In the lth iteration, we will have the following optimization problem:

$$\begin{aligned} \max_{\boldsymbol{v}_{1,i}} \quad & 2\text{Re}\{\boldsymbol{v}_{1,i}^H (\boldsymbol{\Phi}_i^H \boldsymbol{\Phi}_i \boldsymbol{v}_{1,i}^{(l-1)} + \boldsymbol{\Phi}_i^H \boldsymbol{g}_i)\} + c_i^{(l-1)}, \\ \text{s.t.} \quad & \text{(C5.10)}, \end{aligned} \tag{P5.6}$$

where $\boldsymbol{v}_{1,i}^{(l-1)}$ is obtained in the $(l-1)$th iteration and $c_i^{(l-1)} = ||\boldsymbol{g}_i||^2 - \boldsymbol{v}_{1,i}^{(l-1)H} \boldsymbol{\Phi}_i^H \boldsymbol{\Phi}_i \boldsymbol{v}_{1,i}^{(l-1)}$. Problem (P5.6) is equivalent to

$$\begin{aligned} \max_{\boldsymbol{v}_{1,i}} \quad & \text{Re}\{\sum_{n=1}^{N} \bar{v}_{1,i,n} \psi_{i,n}^{(l-1)}\}, \\ \text{s.t.} \quad & \text{(C5.10)}, \end{aligned} \tag{P5.7}$$

where $\psi_{i,n}^{(l-1)}$ is the nth element of $\boldsymbol{\psi}_i^{(l-1)} = \boldsymbol{\Phi}_i^H \boldsymbol{\Phi}_i \boldsymbol{v}_{1,i}^{(l-1)} + \boldsymbol{\Phi}_i^H \boldsymbol{g}_i$. It is straightforward to see that the optimal solution to problem (P5.7) is given by

$$v_{1,i,n} = e^{j\text{arg}(\psi_{i,n}^{(l-1)})}. \tag{5.15}$$

The procedure for optimizing the IRS reflection coefficients using the SCA-based method is given in Algorithm 4.

Algorithm 4 SCA-Based Optimization of IRS Reflection Coefficients for Assisting Backscatter Transmission

1: Set $v_{1,i,n}^{(0)} = 1 \ \forall i, n$.

2: **For** $i = 1 : K$ do

$l = 0$.

Repeat

Update iteration index $l = l + 1$.

Calculate $\boldsymbol{\psi}_i^{(l-1)} = \boldsymbol{\Phi}_i^H \boldsymbol{\Phi}_i \boldsymbol{v}_{1,i}^{(l-1)} + \boldsymbol{\Phi}_i^H \boldsymbol{g}_i$.

Find $v_{1,i,n}^{(l)} \ \forall n$ from (5.15).

Until $||\boldsymbol{v}_{1,i}^{(l)} - \boldsymbol{v}_{1,i}^{(l-1)}|| \leq \epsilon$.

3: Set $\alpha_{1,i,n}^{\text{opt}} = |v_{1,i,n}^{(l)}| \ \forall i, n$ and $\theta_{1,i.n}^{\text{opt}} = \arg(v_{1,i,n}) \ \forall i, n$.

The objective function is guaranteed to improve after each iteration of Algorithm 4. Specifically, setting $\mathcal{F}(\boldsymbol{v}_{1,i}) = \boldsymbol{v}_{1,i}^H \boldsymbol{\Phi}_i^H \boldsymbol{\Phi}_i \boldsymbol{v}_{1,i} + 2\text{Re}\{\boldsymbol{v}_{1,i}^H \boldsymbol{\Phi}_i^H \boldsymbol{g}_i\} + ||\boldsymbol{g}_i||^2$, we have

$$\begin{aligned}
\mathcal{F}(\boldsymbol{v}_{1,i}^{(l)}) &\overset{(\varpi_1)}{\geq} 2\text{Re}\{\boldsymbol{v}_{1,i}^{(l)H}(\boldsymbol{\Phi}_i^H \boldsymbol{\Phi}_i \boldsymbol{v}_{1,i}^{(l-1)} + \boldsymbol{\Phi}_i^H \boldsymbol{g}_i)\} + c_i^{(l-1)} \\
&\overset{(\varpi_2)}{\geq} 2\text{Re}\{\boldsymbol{v}_{1,i}^{(l-1)H}(\boldsymbol{\Phi}_i^H \boldsymbol{\Phi}_i \boldsymbol{v}_{1,i}^{(l-1)} + \boldsymbol{\Phi}_i^H \boldsymbol{g}_i)\} + c_i^{(l-1)} = \mathcal{F}(\boldsymbol{v}_{1,i}^{(l-1)}) \\
&\overset{(\varpi_3)}{\geq} 2\text{Re}\{\boldsymbol{v}_{1,i}^{(l-1)H}(\boldsymbol{\Phi}_i^H \boldsymbol{\Phi}_i \boldsymbol{v}_{1,i}^{(l-2)} + \boldsymbol{\Phi}_i^H \boldsymbol{g}_i)\} + c_i^{(l-2)}, \quad \forall l,
\end{aligned} \tag{5.16}$$

where (ϖ_1) and (ϖ_3) hold because $\mathcal{F}(\boldsymbol{v}_{1,i})$ is lower-bounded by its first-order Taylor expansion, and (ϖ_2) is due to the fact that $\boldsymbol{v}_{1,i}^{(l)}$ is the optimal solution to (P5.6). Therefore, both the objective function in (P5.4) and its lower-bound in (P5.6) increase after each iteration.

5.2.2 Optimization of Other Variables

For the optimization of other variables including the IRS reflection coefficients in the second phase (i.e., active information transmission phase), transmit beamforming

vectors of the PS, receive beamforming vectors of the AP, power allocation of the users, and time allocation, we utilize the AO technique by dividing the variables into groups and alternately optimizing them in an iterative manner.

We first investigate the optimization of transmit beamforming vectors of the PS and resource allocation including power and time allocation. We have the following optimization problem:

$$\begin{aligned}\max_{\{\boldsymbol{w}_i\}_{i=1}^K,\boldsymbol{p},\boldsymbol{\tau}_1,\tau_2} \quad & \sum_{i=1}^{K}\Big(\tau_{1,i}\log\left(1+\tilde{\beta}_i|\boldsymbol{f}_i^H\boldsymbol{w}_i|^2\right) \\ & +\tau_2\log\left(1+\frac{p_i|\boldsymbol{a}_i^H(\boldsymbol{H}_R\boldsymbol{\Theta}_2\boldsymbol{h}_i+\boldsymbol{g}_i)|^2}{\sum_{j\neq i}p_j|\boldsymbol{a}_i^H(\boldsymbol{H}_R\boldsymbol{\Theta}_2\boldsymbol{h}_j+\boldsymbol{g}_j)|^2+||\boldsymbol{a}_i||^2\sigma_A^2}\right)\Big), \qquad \text{(P5.8)} \\ \text{s.t.} \quad & \text{(C5.1)-(C5.6)},\end{aligned}$$

where $\tilde{\beta}_i=\frac{\beta_i||\boldsymbol{H}_R\boldsymbol{\Theta}_{1,i}^{\text{opt}}\boldsymbol{h}_i+\boldsymbol{g}_i||^2}{\sigma_A^2}$.

The above problem is not a convex optimization problem because the objective function is not concave and the variables are coupled in the objective function and the constraints. We define $\tilde{\boldsymbol{W}}_i=\tau_{1,i}\boldsymbol{w}_i\boldsymbol{w}_i^H\ \forall i$, $E_i=p_i\tau_2\ \forall i$, and introduce auxiliary matrix $\boldsymbol{\Pi}$. Problem (P5.8) is now re-formulated as

$$\begin{aligned}\max_{\{\tilde{\boldsymbol{W}}_i\}_{i=1}^K,\boldsymbol{E},\boldsymbol{\tau}_1,\tau_2,\boldsymbol{\Pi}} \quad & \sum_{i=1}^{K}\Big(\tau_{1,i}\log\left(1+\tilde{\beta}_i\frac{\text{Tr}(\boldsymbol{F}_i\tilde{\boldsymbol{W}}_i)}{\tau_{1,i}}\right)+\tau_2\log\left(1+\frac{\tilde{a}_{i,i}\frac{E_i}{\tau_2}}{\sum_{j\neq i}\tilde{a}_{i,j}\frac{E_j}{\tau_2}+\hat{a}_i}\right)\Big), \qquad \text{(P5.9)} \\ \text{s.t.} \quad & \text{(C5.4) and (C5.5)}, \\ & \text{(C5.12)}\ E_i+p_i'\tau_2\leq\sum_{\substack{j=1\\j\neq i}}^{K}[\boldsymbol{\Pi}]_{i,j}\ \forall i, \\ & \text{(C5.13)}\ [\boldsymbol{\Pi}]_{i,j}+\tau_{1,j}\xi_i\leq\eta_i\text{Tr}(\boldsymbol{F}_i\tilde{\boldsymbol{W}}_j),\ \forall i,j\neq i, \\ & \text{(C5.14)}\ [\boldsymbol{\Pi}]_{i,j}\leq\tau_{1,j}P_{sat,i},\ \forall i,j\neq i,\end{aligned}$$

$$\text{(C5.15)}\ \mathrm{Tr}(\tilde{\boldsymbol{W}}_i) \leq \tau_{1,i} P_{max},\ \forall i,$$

$$\text{(C5.16)}\ \sum_{i=1}^{K} \mathrm{Tr}(\tilde{\boldsymbol{W}}_i) \leq P_{avg},$$

$$\text{(C5.17)}\ E_i \geq 0,\ \forall i,$$

$$\text{(C5.18)}\ \tilde{\boldsymbol{W}}_i \geq \boldsymbol{0},\ \forall i,$$

$$\text{(C5.19)}\ \mathrm{Rank}(\tilde{\boldsymbol{W}}_i) \leq 1,\ \forall i,$$

where $\boldsymbol{E} = [E_1, ..., E_K]$, $\boldsymbol{F}_i = \boldsymbol{f}_i \boldsymbol{f}_i^H\ \forall i$, $\tilde{a}_{i,j} = |\boldsymbol{a}_i^H(\boldsymbol{H}_R \boldsymbol{\Theta}_2 \boldsymbol{h}_j + \boldsymbol{g}_j)|^2\ \forall i, j$, $\hat{a}_i = ||\boldsymbol{a}_i||^2 \sigma_A^2,\ \forall i$.

Problem (P5.9) is still non-convex because the second term of the objective function is not concave and also the rank constraints in (C5.19) are not convex. To deal with the non-concavity in the objective function, we write the second term as a sum of concave and convex functions and apply the SCA technique to iteratively maximize a lower-bound of the objective function. Specifically we have

$$\tau_2 \log\left(1 + \frac{\tilde{a}_{i,i}\dfrac{E_i}{\tau_2}}{\sum_{j\neq i} \tilde{a}_{i,j}\dfrac{E_j}{\tau_2} + \hat{a}_i}\right) =$$

$$\tau_2 \log\left(\sum_{j=1}^{K} \tilde{a}_{i,j}\frac{E_j}{\tau_2} + \hat{a}_i\right) - \tau_2 \log\left(\sum_{\substack{j=1 \\ j\neq i}}^{K} \tilde{a}_{i,j}\frac{E_j}{\tau_2} + \hat{a}_i\right). \tag{5.17}$$

In (5.17), $\tau_2 \log(\sum_{j=1}^{K} \tilde{a}_{i,j}(E_j/\tau_2) + \hat{a}_i)$ is a concave function since it is obtained by applying the perspective operation to the concave function $\log(\sum_{j=1}^{K} \tilde{a}_{i,j} E_j + \hat{a}_i)$ and the perspective operation preserves concavity. On the other hand, $-\tau_2 \log(\sum_{j\neq i} \tilde{a}_{i,j}(E_j/\tau_2) + \hat{a}_i)$ is a jointly convex function of τ_2 and $\boldsymbol{E}$, which motivates us to use the SCA technique for solving (P5.9). Based on the first-order Taylor series expansion, this convex function can be approximated by its lower-bound as

$$
\begin{aligned}
&-\tau_2 \log(\sum_{j\neq i} \tilde{a}_{i,j}\frac{E_j}{\tau_2}+\hat{a}_i) \approx \\
&-\tau_2^{(0)} \log(\sum_{j\neq i} \tilde{a}_{i,j}\frac{E_j^{(0)}}{\tau_2^{(0)}}+\hat{a}_i) + \Big(\frac{\sum_{j\neq i}\tilde{a}_{i,j}\frac{E_j^{(0)}}{\tau_2^{(0)}}}{\sum_{j\neq i}\tilde{a}_{i,j}\frac{E_j^{(0)}}{\tau_2^{(0)}}+\hat{a}_i} - \log(\sum_{j\neq i} \tilde{a}_{i,j}\frac{E_j^{(0)}}{\tau_2^{(0)}}+\hat{a}_i)\Big)(\tau_2-\tau_2^{(0)}) \\
&+\Big(\frac{1}{\sum_{j\neq i}\tilde{a}_{i,j}\frac{E_j^{(0)}}{\tau_2^{(0)}}+\hat{a}_i}\Big)(\sum_{j\neq i}\tilde{a}_{i,j}(E_j-E_j^{(0)})),
\end{aligned} \tag{5.18}
$$

where $\tau_2^{(0)}$ and $E_j^{(0)}$ are feasible values for τ_2 and E_j, respectively. Applying the SCA method, the corresponding optimization problem in iteration l can be formulated as follows:

$$
\begin{aligned}
\max_{\{\tilde{\boldsymbol{W}}_i\}_{i=1}^K, \boldsymbol{E}, \boldsymbol{\tau}_1, \tau_2, \boldsymbol{\Pi}} \quad & R_{new}^{(l)}, \\
\text{s.t.} \quad & \text{(C5.4) and (C5.5), (C5.12)-(C5.19),}
\end{aligned} \tag{P5.10}
$$

where $R_{new}^{(l)}$ is given in (5.19) and superscript $(l-1)$ indicates the value obtained in the $(l-1)$th iteration.

$$
\begin{aligned}
R_{new}^{(l)} = \sum_{i=1}^{K} \Big(&\tau_{1,i}\log(1+\tilde{\beta}_i\frac{\mathrm{Tr}(\boldsymbol{F}_i\tilde{\boldsymbol{W}}_i)}{\tau_{1,i}}) + \tau_2\log(1+\sum_{j=1}^{K}\frac{\tilde{a}_{i,j}}{\hat{a}_i}\frac{E_j}{\tau_2}) \\
&+ \delta_{E,i}^{(l-1)}(\sum_{j\neq i}\tilde{a}_{i,j}E_j) + \delta_{\tau,i}^{(l-1)}\tau_2\Big),
\end{aligned} \tag{5.19}
$$

with

$$
\delta_{E,i}^{(l-1)} = -\frac{1}{\sum_{j\neq i}\tilde{a}_{i,j}\frac{E_j^{(l-1)}}{\tau_2^{(l-1)}}+\hat{a}_i}, \tag{5.20}
$$

$$
\delta_{\tau,i}^{(l-1)} = \frac{\sum_{j\neq i}\tilde{a}_{i,j}\frac{E_j^{(l-1)}}{\tau_2^{(l-1)}}}{\sum_{j\neq i}\tilde{a}_{i,j}\frac{E_j^{(l-1)}}{\tau_2^{(l-1)}}+\hat{a}_i} - \log\big(\sum_{j\neq i}\tilde{a}_{i,j}\frac{E_j^{(l-1)}}{\tau_2^{(l-1)}}+\hat{a}_i\big) + \log(\hat{a}_i). \tag{5.21}
$$

Now, the only source of non-convexity for problem (P5.10) is the rank constraint in (C5.19), which can be relaxed using the SDR technique. The relaxed problem will be a convex optimization problem, which can be solved by convex optimization toolboxes such as CVX [60]. We iteratively maximize the lower-bound of the total throughput by solving the relaxed version of (P5.10) until a satisfactory convergence is achieved.

In problems (P5.9) and (P5.10), we have ignored the sensitivity of the energy harvesting circuits of the users. Specifically, the received power at some users in some time-slots may be smaller than the sensitivity of their energy harvesting circuits, which must yield zero harvested power. However, as we have not accounted for the sensitivity of energy harvesting circuits in our problem formulations, the obtained value for some of $[\mathbf{\Pi}]_{i,j}$'s may be negative, which is not acceptable. We thus have to perform one more step to optimize time and energy allocation. Setting $[\tilde{\mathbf{\Pi}}]_{i,j} = \max(0, [\mathbf{\Pi}]_{i,j})\ \forall i, j,\ j \neq i$, we will have the following problem for optimizing time and energy allocation:

$$\begin{aligned}
\max_{\boldsymbol{E},\boldsymbol{\tau}_1,\tau_2}\ & R_{new}^{(l)}, && \text{(P5.11)}\\
\text{s.t.}\ & \text{(C5.4), (C5.5), and (C5.17)},\\
& \text{(C5.20)}\ E_i + p_2'\tau_2 \leq \sum_{\substack{j=1\\ j\neq i}}^{K} [\tilde{\mathbf{\Pi}}]_{i,j}\ \forall i, && (5.22)\\
& \text{(C5.21)}\ \mathrm{Tr}(\tilde{\boldsymbol{W}}_i^{\star}) \leq \tau_{1,i} P_{max}\ \forall i,
\end{aligned}$$

where $\tilde{\boldsymbol{W}}_i^{\star}$ is the solution obtained for $\tilde{\boldsymbol{W}}_i$ by solving problem (P5.10). Problem (P5.11) is a convex problem and can be solved either analytically or by CVX. After iteratively solving problem (P5.11) until convergence, the near-optimal energy and time allocation are obtained, which are denoted as $\boldsymbol{E}^{\star}$, $\boldsymbol{\tau}_1^{\star}$, and $\tau_2^{\star}$. The near-optimal power allocation is then readily calculated as $p_i^{\star} = \frac{E_i^{\star}}{\tau_2^{\star}}\ \forall i$.

If $\tilde{\boldsymbol{W}}_i^\star \ \forall i$ does not satisfy the rank constraint in (C5.19), we use the Eigen-decomposition technique to obtain the corresponding near-optimal beamforming vector. To elaborate, assume that $\tilde{\boldsymbol{W}}_i^\star$ is of rank greater than one. Then, based on the Eigen-decomposition technique, the ith beamforming vector of the PS is approximated as $\boldsymbol{w}_i^\star = \sqrt{\frac{\lambda_{i,1}}{\tau_{1,i}^\star}}\boldsymbol{u}_{i,1}$, where $\lambda_{i,1}$ is the largest eigen-value of $\tilde{\boldsymbol{W}}_i^\star$ and $\boldsymbol{u}_{i,1}$ is the corresponding eigen-vectors.

Algorithm 5 summarizes the procedure for optimizing the PS beamforming vectors and network resource allocation.

The next step is to optimize IRS reflection coefficients and AP receive beamforming vectors in τ_2. First, fixing the AP receive beamforming vectors, the problem for optimizing IRS reflection coefficients during τ_2 can be formulated as

$$\begin{aligned} \max_{\boldsymbol{\Theta}_2} \quad & \sum_{i=1}^{K} \log\left(1 + \frac{p_i|\boldsymbol{a}_i^H(\boldsymbol{H}_R\boldsymbol{\Theta}_2\boldsymbol{h}_i + \boldsymbol{g}_i)|^2}{\sum_{j\neq i} p_j|\boldsymbol{a}_i^H(\boldsymbol{H}_R\boldsymbol{\Theta}_2\boldsymbol{h}_j + \boldsymbol{g}_j)|^2 + ||\boldsymbol{a}_i||^2\sigma_A^2}\right)\Big), \qquad \text{(P5.12)} \\ \text{s.t.} \quad & \text{(C5.8)}. \end{aligned}$$

Problem (P5.12) is not convex and finding its optimal solution is not straightforward. A sub-optimal solution may be obtained using the techniques of SDR and SCA as will be briefly discussed in the following.

Setting $\boldsymbol{\Phi}_i = \boldsymbol{H}_R\text{diag}(\boldsymbol{h}_i)$, $\boldsymbol{v}_2 = [v_{2,1}, ..., v_{2,N}]^T$ with $v_{2,n} = \alpha_{2,n}e^{j\theta_{2,n}}$, $\tilde{\boldsymbol{v}}_2 = [\boldsymbol{v}_2^T \ 1]^T$, and $\tilde{\boldsymbol{V}}_2 = \tilde{\boldsymbol{v}}_2\tilde{\boldsymbol{v}}_2^H$, and after dropping the rank-one constraint on $\tilde{\boldsymbol{V}}_2$, problem (P5.12) is re-formulated as

$$\begin{aligned} \max_{\tilde{\boldsymbol{V}}_2} \quad & \sum_{i=1}^{K} \log\left(1 + \frac{\text{Tr}(\boldsymbol{A}_{i,i}\tilde{\boldsymbol{V}}_2)}{\text{Tr}(\tilde{\boldsymbol{A}}_i\tilde{\boldsymbol{V}}_2) + ||\boldsymbol{a}_i||^2\sigma_A^2}\right), \qquad \text{(P5.13)} \\ \text{s.t.} \quad & \text{(C5.22)} \ [\tilde{\boldsymbol{V}}_2]_{n,n} \leq 1 \ n = 1, ..., N, \\ & \text{(C5.23)} \ [\tilde{\boldsymbol{V}}_2]_{N+1,N+1} = 1, \end{aligned}$$

Algorithm 5 Optimization of Transmit Beamforming and Resource Allocation

1: Set $l = 0$ and $R_{new}^{(0)} = 0$.

2: Initialize $\boldsymbol{E}^{(0)}$, $\boldsymbol{\tau}_1^{(0)}$ and $\tau_2^{(0)}$.

3: **Repeat**

Update iteration index $l = l + 1$.

Update $\delta_{E,i}^{(l-1)}$ $\forall i$ and $\delta_{\tau,i}^{(l-1)}$ $\forall i$ from (5.20) and (5.21).

Solve the relaxed version of (P5.10) using CVX.

4: **Until** $|R_{new}^{(l)} - R_{new}^{(l-1)}| \leq \epsilon$.

5: Set $\tilde{\boldsymbol{W}}_i^{\star} = \tilde{\boldsymbol{W}}_i^{(l)}$ $\forall i$.

6: Set $[\tilde{\boldsymbol{\Pi}}]_{i,j} = \max(0, [\boldsymbol{\Pi}]_{i,j})$ $\forall i, j,\ j \neq i$.

7: Set $l = 0$ and $R_{new}^{(0)} = 0$.

8: Initialize $\boldsymbol{E}^{(0)}$, $\boldsymbol{\tau}_1^{(0)}$ and $\tau_2^{(0)}$.

9: **Repeat**

Update iteration index $l = l + 1$.

Update $\delta_{E,i}^{(l-1)}$ $\forall i$ and $\delta_{\tau,i}^{(l-1)}$ $\forall i$ from (5.20) and (5.21).

Solve the relaxed version of (P5.11).

10: **Until** $|R_{new}^{(l)} - R_{new}^{(l-1)}| \leq \epsilon$.

11: Set $\boldsymbol{E}^{\star} = \boldsymbol{E}^{(l)}$, $\boldsymbol{\tau}_1^{\star} = \boldsymbol{\tau}_1^{(l)}$, $\tau_2^{\star} = \tau_2^{(l)}$, $\boldsymbol{p}^{\star} = \boldsymbol{E}^{\star}/\tau_2^{\star}$.

12: Use Eigen-decomposition and extract $\boldsymbol{w}_i^{\star}$ $\forall i$ from $\tilde{\boldsymbol{W}}_i^{\star}$ $\forall i$.

where

$$\boldsymbol{A}_{i,j} = p_j \begin{bmatrix} \boldsymbol{\Phi}_j^H \boldsymbol{a}_i \boldsymbol{a}_i^H \boldsymbol{\Phi}_j^H & \boldsymbol{\Phi}_j^H \boldsymbol{a}_i \boldsymbol{a}_i^H \boldsymbol{g}_j \\ \boldsymbol{g}_j^H \boldsymbol{a}_i \boldsymbol{a}_i^H \boldsymbol{\Phi}_j & 0 \end{bmatrix}, \ \forall i, j,$$

and $\tilde{\boldsymbol{A}}_i = \sum_{j \neq i} \boldsymbol{A}_{i,j}$.

Clearly, problem (P5.13) is still non-convex. Based on the product rule for loga-

rithms, (P5.13) is re-written as

$$\max_{\tilde{\boldsymbol{V}}_2} \quad \sum_{i=1}^{K} \Big(\log\left(\mathrm{Tr}(\boldsymbol{A}_{i,i}\tilde{\boldsymbol{V}}_2) + \mathrm{Tr}(\tilde{\boldsymbol{A}}_i\tilde{\boldsymbol{V}}_2) + ||\boldsymbol{a}_i||^2\sigma_A^2\right) - \log\zeta_i \Big), \tag{P5.14}$$

$$\text{s.t.} \quad \text{(C5.22) and (C5.23)},$$

$$\text{(C5.24)} \ \mathrm{Tr}(\tilde{\boldsymbol{A}}_i\tilde{\boldsymbol{V}}_2) + ||\boldsymbol{a}_i||^2\sigma_A^2 \leq \zeta_i, \forall i.$$

The objective function in problem (P5.14) involves summation of concave and convex functions. This issue can be dealt with through the SCA technique. Specifically, the convex term $-\log\zeta_i$ can be approximated by a lower-bound. The resulting problem will be an SDP which can be iteratively solved via CVX, updating ζ_i $\forall i$ in each iteration until convergence is attained. Eventually, the rank-one extraction procedure must be performed to find a feasible rank-one solution for $\tilde{\boldsymbol{V}}_2$, from which a sub-optimal $\boldsymbol{v}_2$ is obtained. A similar process as above can be applied for optimizing the receive beamformers at the AP, $\{\boldsymbol{a}_i\}_{i=1}^K$, fixing other optimization variables. Finally, the AO algorithm is applied for iteratively solving the three sub-problems (sub-problem for transmit beamforming and resource allocation, sub-problem for IRS reflection during τ_2, and sub-problem for receive beamforming) until an acceptable convergence is achieved.

The above procedure incurs considerable complexity since SDP problems must be solved numerous times in each iteration. Specifically, as the optimization of $\boldsymbol{v}_2$ and $\{\boldsymbol{a}_i\}_{i=1}^K$ requires the application of SCA technique, several SDP problems must be solved for finding the sub-optimal solution for $\boldsymbol{v}_2$ and $\{\boldsymbol{a}_i\}_{i=1}^K$ in each iteration, which results in significant complexity for the whole algorithm. This complexity increases with increasing the number of users, antennas at the AP, and IRS elements, and can be prohibitively high in large-scale networks.

Herein, we propose an algorithm with lower complexity for optimizing IRS reflec-

tion coefficients in τ_2, assuming MMSE receive beamforming at the AP. Particularly, using the relationship between MSE and SINR in MMSE receivers, we can jointly optimize the receive beamforming vectors at the AP and IRS reflection coefficients in τ_2, using the BCD technique.

Under the assumption of independence between different $s_{2,i}$'s and also between $s_{2,i}$ $\forall i$ and each element of the noise vector $\boldsymbol{n}_A$, the MSE for U_i's information signal is given by

$$\mathcal{E}_i = \mathbb{E}[|\boldsymbol{a}_i^H \boldsymbol{y}_2 - s_{2,i}|^2] = \sum_{j=1}^{K} p_j |\boldsymbol{a}_i^H (\boldsymbol{H}_R \boldsymbol{\Theta}_2 \boldsymbol{h}_j + \boldsymbol{g}_j)|^2$$
$$- \sqrt{p_i}(\boldsymbol{a}_i^H (\boldsymbol{H}_R \boldsymbol{\Theta}_2 \boldsymbol{h}_i + \boldsymbol{g}_i) + (\boldsymbol{H}_R \boldsymbol{\Theta}_2 \boldsymbol{h}_i + \boldsymbol{g}_i)^H \boldsymbol{a}_i) + ||\boldsymbol{a}_i||^2 \sigma_A^2 + 1. \tag{5.23}$$

The following theorem establishes an equivalence between throughput maximization and MSE minimization problems.

Theorem 1. *The problem in* (P5.12) *is equivalent to the following problem*

$$\min_{\{\boldsymbol{a}_i\}_{i=1}^K, \boldsymbol{\omega}, \boldsymbol{\Theta}_2} \sum_{i=1}^{K} (\omega_i \mathcal{E}_i - \log \omega_i) \tag{5.24}$$
$$s.t. \quad \textit{(C5.8)},$$

where $\boldsymbol{\omega} = [\omega_1, ..., \omega_K]$*, and* ω_i *is a weight associated with* U_i*.*

Proof. Fixing $\boldsymbol{\omega}$ and $\boldsymbol{\Theta}_2$, (5.24) is convex with respect to $\boldsymbol{a}_i$, $\forall i \in \mathcal{K}$, the optimal value of which can be obtained from the first-order optimality condition as

$$\boldsymbol{a}_i^\star = \sqrt{p_i}(\sum_{j=1}^{K} p_j \tilde{\boldsymbol{g}}_j \tilde{\boldsymbol{g}}_j^H + \sigma_A^2 \boldsymbol{I}_{M_A})^{-1} \tilde{\boldsymbol{g}}_i, \tag{5.25}$$

where $\tilde{\boldsymbol{g}}_i = \boldsymbol{H}_R \boldsymbol{\Theta}_2 \boldsymbol{h}_i + \boldsymbol{g}_i$ and the receive beamforming vector in (5.25) is the well-

known MMSE receiver which minimizes the MSE as

$$\mathcal{E}_{i,min} = 1 - p_i \tilde{\boldsymbol{g}}_i^H J^{-1} \tilde{\boldsymbol{g}}_i, \tag{5.26}$$

with $J = \sum_{j=1}^{K} p_j \tilde{\boldsymbol{g}}_j \tilde{\boldsymbol{g}}_j^H + \sigma_A^2 \boldsymbol{I}_{M_A}$.

Having $\{\boldsymbol{a}_i^\star\}_{i=1}^K$ and $\boldsymbol{\Theta}_2$ fixed, the weight ω_i for minimizing (5.24) is obtained as

$$\omega_i^\star = \mathcal{E}_{i,min}^{-1}. \tag{5.27}$$

Now, the problem for optimizing $\boldsymbol{\Theta}_2$ is obtained by substituting (5.25) and (5.27) into (5.24) as

$$\min_{\boldsymbol{\Theta}_2} \; -\sum_{i=1}^{K} \log(\mathcal{E}_{i,min}^{-1}) = \max_{\boldsymbol{\Theta}_2} \sum_{i=1}^{K} \log(\mathcal{E}_{i,min}^{-1}) \tag{5.28}$$

$$\text{s.t.} \;\; \text{(C5.8)}.$$

We now have

$$\begin{aligned}
\mathcal{E}_{i,min}^{-1} &= (1 - p_i \tilde{\boldsymbol{g}}_i^H J^{-1} \tilde{\boldsymbol{g}}_i)^{-1} = \left(\frac{p_i \tilde{\boldsymbol{g}}_i^H J^{-1} \tilde{\boldsymbol{g}}_i - (p_i \tilde{\boldsymbol{g}}_i^H J^{-1} \tilde{\boldsymbol{g}}_i)^2}{p_i \tilde{\boldsymbol{g}}_i^H J^{-1} \tilde{\boldsymbol{g}}_i}\right)^{-1} \\
&= \frac{p_i \tilde{\boldsymbol{g}}_i^H J^{-1} \tilde{\boldsymbol{g}}_i}{p_i \tilde{\boldsymbol{g}}_i^H J^{-1} \tilde{\boldsymbol{g}}_i - (p_i \tilde{\boldsymbol{g}}_i^H J^{-1} \tilde{\boldsymbol{g}}_i)^2} = 1 + \frac{(p_i \tilde{\boldsymbol{g}}_i^H J^{-1} \tilde{\boldsymbol{g}}_i)^2}{p_i \tilde{\boldsymbol{g}}_i^H J^{-1} \tilde{\boldsymbol{g}}_i - (p_i \tilde{\boldsymbol{g}}_i^H J^{-1} \tilde{\boldsymbol{g}}_i)^2} \\
&\overset{(\varpi_4)}{=} 1 + \frac{(p_i \tilde{\boldsymbol{g}}_i^H J^{-1} \tilde{\boldsymbol{g}}_i)^2}{p_i \tilde{\boldsymbol{g}}_i^H J^{-1} J J^{-1} \tilde{\boldsymbol{g}}_i - (p_i \tilde{\boldsymbol{g}}_i^H J^{-1} \tilde{\boldsymbol{g}}_i)^2} \\
&= 1 + \frac{(p_i \tilde{\boldsymbol{g}}_i^H J^{-1} \tilde{\boldsymbol{g}}_i)^2}{p_i \tilde{\boldsymbol{g}}_i^H J^{-1} (J - p_i \tilde{\boldsymbol{g}}_i \tilde{\boldsymbol{g}}_i^H) J^{-1} \tilde{\boldsymbol{g}}_i} \\
&= 1 + \frac{(p_i \tilde{\boldsymbol{g}}_i^H J^{-1} \tilde{\boldsymbol{g}}_i)^2}{p_i \tilde{\boldsymbol{g}}_i^H J^{-1} (\sum_{j \neq i} p_j \tilde{\boldsymbol{g}}_j \tilde{\boldsymbol{g}}_j^H + \sigma_A^2 \boldsymbol{I}_{M_A}) J^{-1} \tilde{\boldsymbol{g}}_i} \\
&\overset{(\varpi_5)}{=} 1 + \frac{p_i |\boldsymbol{a}_i^{\star H} (\boldsymbol{H}_R \boldsymbol{\Theta}_2 \boldsymbol{h}_i + \boldsymbol{g}_i)|^2}{\sum_{j \neq i} p_j |\boldsymbol{a}_i^{\star H} (\boldsymbol{H}_R \boldsymbol{\Theta}_2 \boldsymbol{h}_j + \boldsymbol{g}_j)|^2 + ||\boldsymbol{a}_i||^2 \sigma_A^2} = 1 + \gamma_{2,i,\text{mmse}},
\end{aligned} \tag{5.29}$$

where $\gamma_{2,i,\text{mmse}}$ is the SINR of U_i for active information transmission, when MMSE re-

ceive beamforming is employed at the AP. In (5.29), (ϖ_4) holds because $p_i\tilde{\boldsymbol{g}}_i^H J^{-1}JJ^{-1}\tilde{\boldsymbol{g}}_i = p_i\tilde{\boldsymbol{g}}_i^H J^{-1}\tilde{\boldsymbol{g}}_i$ and (ϖ_5) holds because $\boldsymbol{a}_i^\star = \sqrt{p_i}J^{-1}\tilde{\boldsymbol{g}}_i$. The proof is completed by substituting (5.29) into (5.28). □

Re-writing the MSE in (5.23) with respect to $\boldsymbol{\Phi}_i$'s and $\boldsymbol{v}_2$, we have

$$\mathcal{E}_i = \boldsymbol{v}_2^H(\sum_{j=1}^{K} p_j\boldsymbol{\Phi}_j^H\boldsymbol{a}_i\boldsymbol{a}_i^H\boldsymbol{\Phi}_j)\boldsymbol{v}_2 + \boldsymbol{v}_2^H(\sum_{j=1}^{K} p_j\boldsymbol{\Phi}_j^H\boldsymbol{a}_i\boldsymbol{a}_i^H\boldsymbol{g}_j - \sqrt{p_i}\boldsymbol{\Phi}_i^H\boldsymbol{a}_i)+$$
$$(\sum_{j=1}^{K} p_j\boldsymbol{\Phi}_j^H\boldsymbol{a}_i\boldsymbol{a}_i^H\boldsymbol{g}_j - \sqrt{p_i}\boldsymbol{\Phi}_i^H\boldsymbol{a}_i)^H\boldsymbol{v}_2 + \sum_{j=1}^{K} p_j\boldsymbol{g}_j^H\boldsymbol{a}_i\boldsymbol{a}_i^H\boldsymbol{g}_j - \sqrt{p_i}(\boldsymbol{a}_i^H\boldsymbol{g}_i + \boldsymbol{g}_i^H\boldsymbol{a}_i) + ||\boldsymbol{a}_i^H||^2\sigma_A^2 + 1. \tag{5.30}$$

According to Theorem 1, problem (P5.12) can be re-formulated as

$$\min_{\{\boldsymbol{a}_i\}_{i=1}^K,\boldsymbol{\omega},\boldsymbol{v}_2} \sum_{i=1}^{K}(\omega_i\mathcal{E}_i - \log\omega_i) \tag{P5.15}$$
$$\text{s.t. } (\text{C5.25}) \ |v_{2,n}| \leq 1, \ \forall n.$$

Applying the BCD method, problem (P5.15) can be alternately solved for $\{\boldsymbol{a}_i\}_{i=1}^K$, $\boldsymbol{\omega}$, and $\boldsymbol{v}_2$ in an iterative manner, where the optimum value for each variable is found in each iteration. Particularly, denoting by $\boldsymbol{v}_2^{(l-1)}$ the optimal value for $\boldsymbol{v}_2$ in the $(l-1)$th iteration, the optimal receive beamforming vector for U_i in the lth iteration is given by

$$\boldsymbol{a}_i^{(l)} =$$
$$\sqrt{p_i}\Big(\sum_{j=1}^{K} p_j((\boldsymbol{\Phi}_j\boldsymbol{v}_2^{(l-1)} + \boldsymbol{g}_j)(\boldsymbol{\Phi}_j\boldsymbol{v}_2^{(l-1)} + \boldsymbol{g}_j)^H) + \sigma_A^2\boldsymbol{I}_{M_A}\Big)^{-1}(\boldsymbol{\Phi}_i\boldsymbol{v}_2^{(l-1)} + \boldsymbol{g}_i), \ \forall i, \tag{5.31}$$

and the optimal value for ω_i in the lth iteration is given by

$$\omega_i^{(l)} = \frac{1}{\mathcal{E}_i^{(l)}}, \quad \forall i, \tag{5.32}$$

where $\mathcal{E}_i^{(l)}$ is obtained by substituting $\boldsymbol{v}_2^{(l-1)}$ and $\boldsymbol{a}_i^{(l)}$ into (5.30). Finally, with $\{\boldsymbol{a}_i^{(l)}\}_{i=1}^K$ and $\boldsymbol{\omega}^{(l)}$, the problem for optimizing $\boldsymbol{v}_2$ in the lth iteration is formulated as

$$\begin{aligned} &\min_{\boldsymbol{v}_2} \ \boldsymbol{v}_2^H \boldsymbol{B}^{(l)} \boldsymbol{v}_2 - 2\mathrm{Re}\{\boldsymbol{b}^{(l)H} \boldsymbol{v}_2\}, \\ &\text{s.t.} \ \ (\text{C5.26}) \ \boldsymbol{v}_2^H \boldsymbol{D}_n \boldsymbol{v}_2 \leq 1, \ \forall n, \end{aligned} \tag{P5.16}$$

where

$$\begin{aligned} \boldsymbol{B}^{(l)} &= \sum_{i=1}^K \omega_i \sum_{j=1}^K p_j \boldsymbol{\Phi}_j^H \boldsymbol{a}_i^{(l)} \boldsymbol{a}_i^{(l)H} \boldsymbol{\Phi}_j \\ \boldsymbol{b}^{(l)} &= \sum_{i=1}^K \omega_i (\sqrt{p_i} \boldsymbol{\Phi}_i^H \boldsymbol{a}_i^{(l)} - \sum_{j=1}^K p_j \boldsymbol{\Phi}_j^H \boldsymbol{a}_i^{(l)} \boldsymbol{a}_i^{(l)H} \boldsymbol{g}_j), \end{aligned}$$

and $\boldsymbol{D}_n$ is a diagonal matrix with 1 on its nth diagonal element and 0 elsewhere. Problem (P5.16) is a convex quadratically-constrained quadratic program (QCQP) and can be solved using convex optimization techniques. We use the Lagrange duality method to solve (P5.16) for which the Lagrangian is given by

$$\mathcal{L} = \boldsymbol{v}_2^H \boldsymbol{B}^{(l)} \boldsymbol{v}_2 - 2\mathrm{Re}\{\boldsymbol{b}^{(l)H} \boldsymbol{v}_2\} + \sum_{n=1}^N \mu_n (\boldsymbol{v}_2^H \boldsymbol{D}_n \boldsymbol{v}_2 - 1), \tag{5.33}$$

with $\boldsymbol{\mu} = [\mu_1, ..., \mu_N]$ being the Lagrange multiplier associated with the constraint (C5.26). The first-order optimality condition of $\mathcal{L}$ with respect to $\boldsymbol{v}_2$ yields

$$\boldsymbol{v}_2(\boldsymbol{\mu}) = (\boldsymbol{B}^{(l)} + \sum_{n=1}^N \mu_n \boldsymbol{D}_n)^{-1} \boldsymbol{b}^{(l)}. \tag{5.34}$$

$\boldsymbol{\mu}$ can be updated via the ellipsoid method with the subgradient of μ_n being given by $|v_{2,n}|^2-1$.

Matrix $\boldsymbol{B}^{(l)}$ is the summation of K^2 rank-one matrices. If $K^2 \geq N$, matrix $\boldsymbol{B}^{(l)}$ is full-rank and invertible and so is $\boldsymbol{B}^{(l)} + \sum_{n=1}^{N} \mu_n \boldsymbol{D}_n$. If $K^2 < N$, the invertibility of $\boldsymbol{B}^{(l)} + \sum_{n=1}^{N} \mu_n \boldsymbol{D}_n$ depends on the value of μ_n's and is not guaranteed; but problem (P5.16) is still a QCQP and can be solved using CVX solvers.

Algorithm 6 describes the steps for optimizing the MMSE receive beamforming vectors at the AP and IRS reflection coefficients for assisting users' active information transfer.

Algorithm 6 Optimization of MMSE Receive Beamforming and IRS Reflection for Assisting Active Information Transfer

1: Initialize $\boldsymbol{\omega}^{(0)}$. Set $l = 0$.

2: **Repeat**

Update iteration index $l = l + 1$.

Obtain $\boldsymbol{a}_i^{(l)}$ $\forall i$ from (5.31).

Obtain $\omega_i^{(l)}$ $\forall i$ from (5.32).

Obtain $\boldsymbol{v}_2^{(l)}$ by solving the QCQP in (P5.16).

3: **Until** $\sum_{i=1}^{K} \left| \log(\omega_i^{(l)}) - \log(\omega_i^{(l-1)}) \right| \leq \epsilon$.

4: Set $\alpha_{2,n}^{\star} = |v_{2,n}^{(l)}|$ $\forall n$, $\theta_{2,n}^{\star} = \arg(v_{2,n}^{(l)})$ $\forall n$, and $\boldsymbol{a}_i^{\star} = \boldsymbol{a}_i^{(l)}$ $\forall i$.

The optimal IRS amplitude reflection coefficients in the active information phase are not necessarily equal to 1. The reason is that the users simultaneously transmit to the AP and as is clear from the throughput expression of the users in the active information transfer phase (Equation (5.9)), the power of the received signal from each user at the AP affects the throughput of other users. Therefore, optimizing the amplitude reflection of IRS elements in addition to their phase shifts is important for maximizing the total throughput. This is in contrast to the backscatter transmission

phase, where the optimal amplitude reflection coefficients are 1 (Equations (5.14) and (5.15)) because each user individually transmits to the AP in its assigned time-slot and maximizing the received power for each user's signal maximizes its own throughput and the total throughput.

5.2.3 Overall Throughput Maximization Algorithm

The overall two-stage algorithm for maximizing the total network throughput is given in Algorithm 7, where the first stage deals with the optimization of IRS amplitude reflection coefficients and phase shifts for assisting the users' backscatter transmission to the AP, and the optimization of other variables is relegated to the second stage, in which we use the techniques of AO, SDR, BCD, and Lagrange duality for finding a near-optimal solution to the time and power allocation, PS transmit beamforming, IRS reflection coefficients for aiding the active information transfer of the users, and MMSE receive beamforming vectors at the AP.

Algorithm 7 Total Throughput Maximization Algorithm for Solving (P5.1)

1: Find the optimized amplitude reflection coefficients and phase shifts of IRS elements in all time-slots of the first phase through Algorithm 3 or Algorithm 4.

2: Return $\boldsymbol{\Theta}_{1,i}^{\text{opt}}$ $\forall i$.

3: Initialize $\boldsymbol{\Theta}_2^{(0)}$ and $\{\boldsymbol{a}_i^{(0)}\}_{i=1}^K$. Set $R_{1,i}^{(0)} = 0$ $\forall i$, $R_{2,i}^{(0)} = 0$ $\forall i$, $R^{(0)} = \sum_{i=1}^K (R_{1,i}^{(0)} + R_{2,i}^{(0)}) = 0$, $l = 0$.

4: **Repeat**

Update iteration index $l = l + 1$.

Find $\{\boldsymbol{w}_i^{(l)}\}_{i=1}^K$, $\boldsymbol{p}^{(l)}$, $\boldsymbol{\tau}_1^{(l)}$, and $\tau_2^{(l)}$ from Algorithm 5.

Find $\boldsymbol{\Theta}_2^{(l)}$ and $\{\boldsymbol{a}_i^{(l)}\}_{i=1}^K$ from Algorithm 6.

Calculate $R^{(l)} = \sum_{i=1}^K (R_{1,i}^{(l)} + R_{2,i}^{(l)})$.

5: **Until** $|R^{(l)} - R^{(l-1)}| \leq \epsilon$.

6: Return $R_{\max} = R^{(l)}$, $\boldsymbol{\Theta}_2^{\text{opt}} = \boldsymbol{\Theta}_2^{(l)}$, $\boldsymbol{w}_i^{\text{opt}} = \boldsymbol{w}_i^{(l)}$ $\forall i$, $\boldsymbol{a}_i^{\text{opt}} = \boldsymbol{a}_i^{(l)}$ $\forall i$, $\boldsymbol{p}^{\text{opt}} = \boldsymbol{p}^{(l)}$, $\boldsymbol{\tau}_1^{\text{opt}} = \boldsymbol{\tau}_1^{(l)}$, $\tau_2^{\text{opt}} = \tau_2^{(l)}$.

5.3 Performance Evaluation

In this section, we assess the performance of our proposed IRS-empowered BS-WPCN by comparing it to four benchmark schemes labeled as "IRS-empowered WPCN", "Random IRS reflection matrices", "Pre-configured IRS reflection matrices", and "Equal time allocation" on the figures. In particular, "IRS-empowered WPCN" is the scheme proposed in Chapter 4, where the conventional WPCN is upgraded by adding an IRS for assisting in downlink energy transfer and uplink information transmission. To make comparisons fair, we modify the IRS-assisted WPCN model in Chapter 4 to have a multi-antenna AP. "Random IRS reflection matrices" is the scheme in which the IRS phase shifts are randomly chosen in all $K+1$ time-slots, while other variables

are optimized based on the techniques discussed throughout this chapter. In "Pre-configured IRS reflection matrices", the phase shifts are once selected randomly and the same selected phase shifts are used in all time-slots and throughout the whole simulations. This resembles the scenario where IRS elements are pre-configured and cannot be reconfigured after IRS is deployed. Finally, "Equal time allocation" refers to the case with equal time-slot length for all $K+1$ slots, i.e., the duration of each time-slot is $\frac{1}{K+1}$ in this scheme. We also plot the graph for the proposed scheme after applying a 2-bit-resolution phase quantization to the optimized phase shifts of IRS elements in each time-slot. Particularly, each optimized continuous phase shift is quantized to its closest value from the set $\mathcal{P} = \{\frac{\pi}{4}, \frac{3\pi}{4}, \frac{5\pi}{4}, \frac{7\pi}{4}\}$, i.e.,

$$\theta_{n,i}^{(q)} = \arg\min_{\theta \in \mathcal{P}} |\theta - \theta_{n,i}^{\text{opt}}|, \ n = 1, .., N, \ i = 1, ..., K+1, \tag{5.35}$$

where $\theta_{n,i}^{(q)}$ denotes the quantized phase shift for the nth IRS element in the ith time-slot. The throughput is then calculated based on the quantized phase shifts with all other variables taking the same optimized values as before. This scheme is tagged as "IRS-empowered BS-WPCN: 2-bit" on the figures.

5.3.1 Simulation Setup

We consider a 2-D Cartesian coordinate system, as shown in Figure 5.4, where the AP is located at the origin, the reference element of the IRS is placed at (x_{IRS}, y_{IRS}) and the PS is positioned at $(x_{PS}, 0)$. K users are evenly placed on the left half-circle centered at the PS with radius r. Parameters η, ξ, and P_{sat} for the energy conversion model at the users are obtained by fitting the model in (5.1) to the real measurements reported in [105]. All channels are modeled by the Rician fading channel model. For example, the channel between AP and IRS is given by

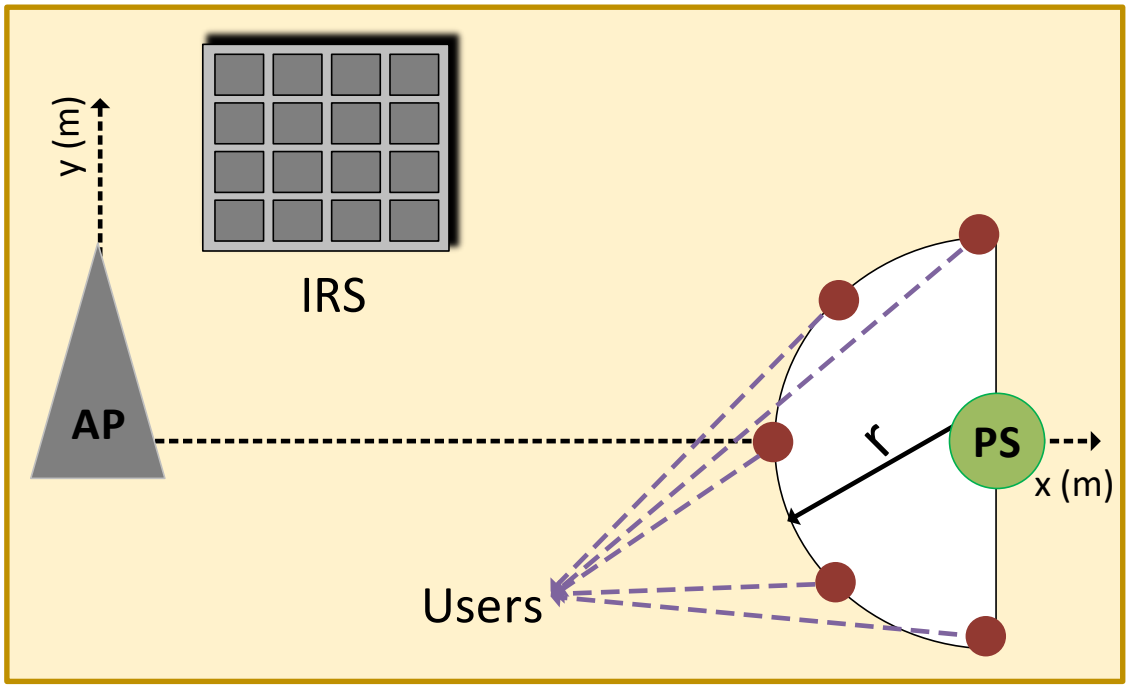

Figure 5.4: Simulation setup.

$$\boldsymbol{H}_R = \sqrt{\frac{\kappa_{h,r}}{\kappa_{h,r}+1}}\boldsymbol{H}_R^{\text{LoS}} + \sqrt{\frac{1}{\kappa_{h,r}+1}}\boldsymbol{H}_R^{\text{NLoS}}, \tag{5.36}$$

where $\kappa_{h,r}$ is the Rician factor, and $\boldsymbol{H}_R^{\text{LoS}} \in \mathbb{C}^{M_A \times N}$ and $\boldsymbol{H}_R^{\text{NLoS}} \in \mathbb{C}^{M_A \times N}$ are the LoS and NLoS components of $\boldsymbol{H}_R$. The LoS channel matrix is modeled as $\boldsymbol{H}_R^{\text{LoS}} = \hat{\boldsymbol{h}}_R^{(M_A)}(\varphi_{\text{AoA}})\hat{\boldsymbol{h}}_R^{(N)H}(\varphi_{\text{AoD}})$, where φ_{AoA} and φ_{AoD} denote the angle of arrival and angle of departure, respectively, and $\hat{\boldsymbol{h}}_R^{(X)}(\varphi) = [1, e^{j\pi\sin(\varphi)}, e^{j2\pi\sin(\varphi)}, ..., e^{j(X-1)\pi\sin(\varphi)}]^T$. The elements of $\boldsymbol{H}_R^{\text{NLoS}}$ follow the standard Rayleigh fading. $\boldsymbol{H}_R$ is then multiplied by the square root of the distance-dependent path-loss $C_0(d_{h,r}/d_0)^{-\rho_{h,r}}$, where C_0 is the path-loss at the reference distance of $d_0 = 1$ m, set as $C_0 = -20$ dB, $d_{h,r}$ represents the distance between AP and IRS, and $\rho_{h,r}$ is the path-loss exponent of the channel between AP and IRS. Channels $\boldsymbol{f}_i^H$, $\forall i$, $\boldsymbol{h}_i$, $\forall i$, and $\boldsymbol{g}_i$, $\forall i$ are modeled in a similar way as $\boldsymbol{H}_R$ with κ_f, κ_h, and κ_g being the corresponding Rician factors, and ρ_f, ρ_h, and ρ_g denoting the path-loss exponents of the corresponding channels.

Unless otherwise stated, the following set of parameters are used in all simulations: The number of users K is assumed to be 10. The number of antennas at the PS and the AP is set as 5, i.e., $M_P = M_A = 5$, and the number of elements at the IRS is set to be 25, i.e., $N = 25$. The following coordinates are used for the IRS and the PS: $x_{IRS} = y_{IRS} = 5$ m, $x_{PS} = 30$ m. Also, the distance from the users to the PS is set as $r = 10$ m. The channel-related parameters used in simulations are $\kappa_{h,r} = \kappa_f = \infty$, $\kappa_h = 3$, $\kappa_g = 0$, $\rho_{h,r} = \rho_f = 2$, $\rho_h = 2.8$, $\rho_g = 3.5$. Energy harvesting circuit parameters are obtained as $\eta_i = 0.47,\ \forall i$, $\xi_i = 2.24 \times 10^{-5},\ \forall i$, and $P_{sat,i} = 45$ mW, $\forall i$. Average power at the PS is set as $P_{avg} = 1$ W and for the maximum power at the PS, we always set $P_{max} = 2P_{avg}$. Backscatter coefficient is set as $\beta_i = 0.6,\ \forall i$ and the circuit power consumption for active information transmission is assumed to be $p_i' = 1$ mW, $\forall i$. The noise power spectral density at the AP is -160 dBm/Hz, the bandwidth is 1 MHz, and the stopping threshold for convergence is set as $\epsilon = 0.001$ in all algorithms. The AP is assumed to apply MMSE receive beamforming for detecting users' active information signals. The results are based on the average of 1000 different channel realizations. The parameter settings for the simulations of this chapter are provided in Table 5.1.

5.3.2 Numerical Results

Figures 5.5 - 5.9 evaluate the performance of the proposed IRS-empowered BS-WPCN in different network settings and compare its throughput with the benchmark schemes previously described.

As expected, the throughput improves with increasing the average PS transmit power, number of IRS reflecting elements, and number of antennas at the AP and the PS (Figures 5.5-5.8). It is worth mentioning that although the energy harvesting circuits of some or all of the users enter the saturation region with increasing P_{avg} in

Table 5.1: Simulation parameters for IRS-empowered BS-WPCN.

Parameter	**Description**	**Setting**
K	Number of users	10
M_P	Number of PS antennas	5
M_A	Number of AP antennas	5
N	Number of IRS elements	25
P_{avg}	Average PS transmit power	1 W
P_{max}	Maximum PS transmit power	2 W
x_{PS}	X-coordinate of the PS	30 m
x_{IRS}	X-coordinate of the reference element of IRS	5 m
y_{IRS}	Y-coordinate of the reference element of IRS	5 m
r	Distance between PS and users	10 m
$\beta_i,\ \forall i$	Backscatter coefficient of all users	0.6
$\eta_i,\ \forall i$	Users' energy harvesting circuit parameter	0.47
$\xi_i,\ \forall i$	Users' energy harvesting circuit parameter	2.24×10^{-5}
$P_{sat,i},\ \forall i$	Users' energy harvesting circuit saturation power	45 mW
$p_i',\ \forall i$	Circuit power consumption of all users	1 mW
κ_f	Rician factor for the channel between PS and users	∞
κ_g	Rician factor for the channel between users and AP	0
κ_h	Rician factor for the channel between IRS and users	3
$\kappa_{h,r}$	Rician factor for the channel between IRS and AP	∞
ρ_f	Path-loss exponent for the channel between PS and users	2
ρ_g	Path-loss exponent for the channel between users and AP	3.5
ρ_h	Path-loss exponent for the channel between IRS and users	2.8
$\rho_{h,r}$	Path-loss exponent for the channel between IRS and AP	2
d_0	Reference distance	1 m
C_0	Path-loss at the reference distance	-20 dBm
σ_A^2	Noise power at the AP	-100 dBm
ϵ	Convergence threshold for all algorithms	0.001

Figure 5.5, the performance of the proposed model continues to improve with increasing the PS average transmit power. This is because the performance of backscatter communication is not constrained by the limitations of the energy harvesting circuits and the throughput obtained from backscatter transmission always gets better with more transmit power at the PS. On the other hand, the performance of "IRS-empowered WPCN" becomes saturated at $P_{avg} = 30$ dBm because the users cannot harvest more energy and the throughput, which is merely based on active wireless

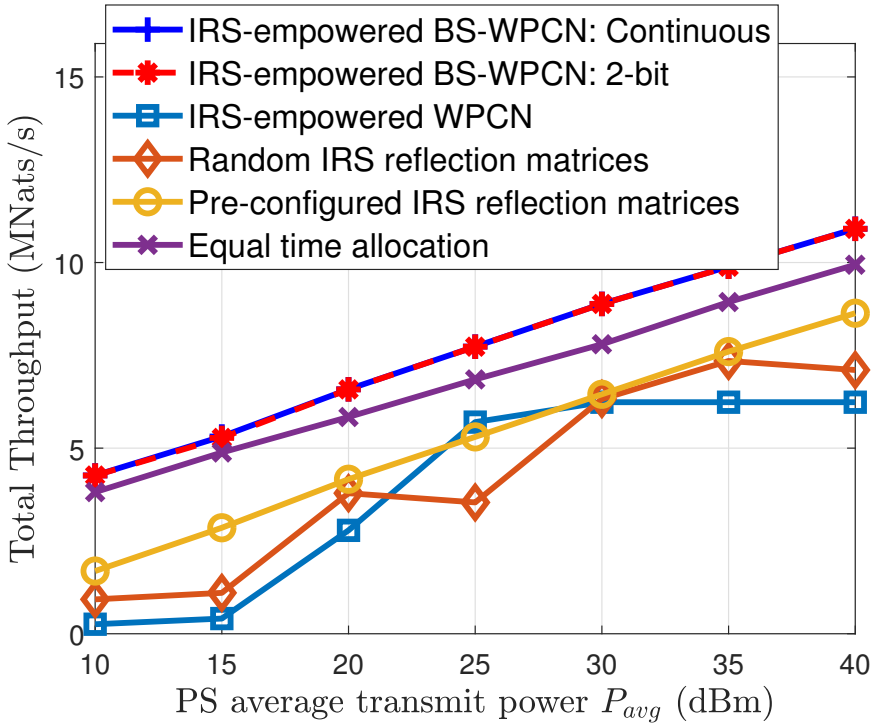

Figure 5.5: Total throughput vs. average transmit power of the PS.

powered transmission, cannot be further enhanced.

With increasing the x-coordinate of IRS in Figure 5.9, the throughput first decreases because of the longer distance between IRS and AP. However, the throughout begins to increase after some point since IRS gets closer to the users and the impinging signals on the IRS become stronger. This compensates for the increased distance between IRS and AP and improves the throughput. Hence, the IRS is better to be located either close to the AP or close to the users for achieving high network throughputs.

It is well observed that our proposed method performs remarkably better than the benchmark schemes, which endorses the efficiency of the proposed model and algorithms. Specifically, our proposed IRS-empowered BS-WPCN considerably outperforms the IRS-empowered WPCN presented in the previous chapter, which demonstrates the potential of backscatter communication for improving the performance of

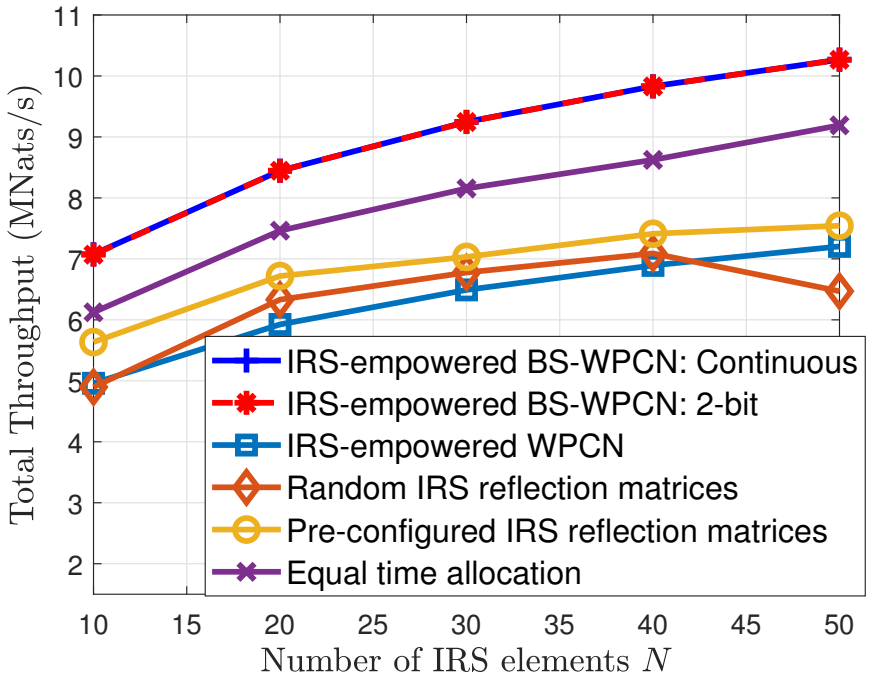

Figure 5.6: Total throughput vs. number of IRS elements.

WPCNs. Moreover, the performance of the proposed scheme is much superior to that of "Random IRS reflection matrices" and "Pre-configured IRS reflection matrices" schemes, showing the importance of real-time optimization and dynamic reconfiguration of IRS reflecting parameters. It can also be seen that the scheme with random selection of IRS phase shifts undergoes fluctuations, which is due to the fact that the randomly-chosen phase shifts may not result in constructive combination of the reflected signals with the signals of the direct path at the AP. In fact, with random phase shifts for IRS elements in each time-slot, different levels of constructiveness/destructiveness can be expected for combination of signals and thus, a monotonic behavior for the "Random IRS reflection matrices" cannot be obtained. Finally, the gap between the proposed and "Equal time allocation" schemes confirms that optimizing time allocation is also important for enhancing the performance.

Another important observation is that the scheme with 2-bit-resolution quantized phase shifts almost overlaps with the one with continuous phase shifts, which indicates

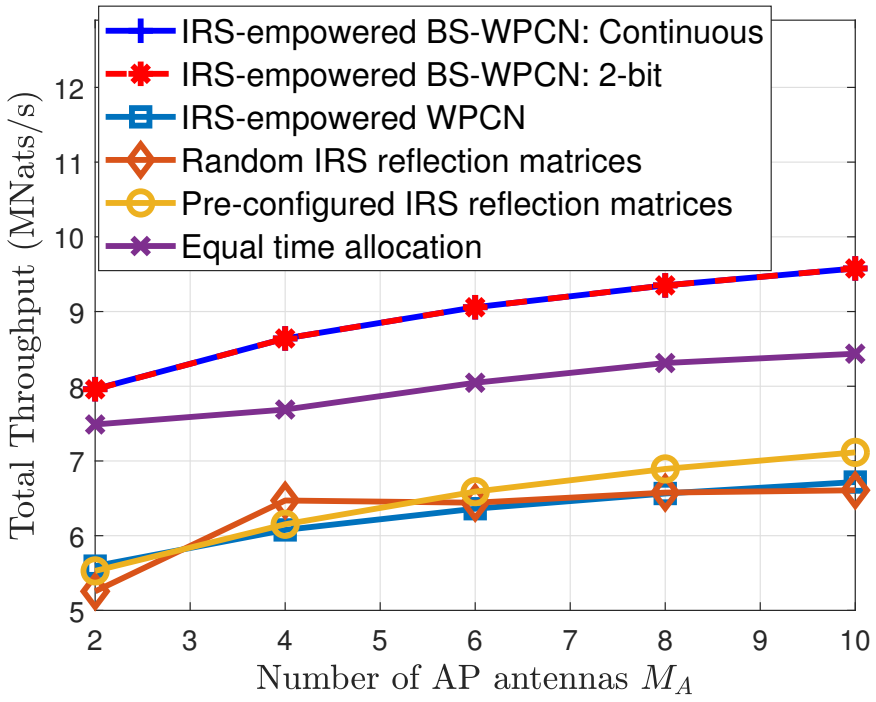

Figure 5.7: Total throughput vs. number of AP antennas.

that our proposed algorithms can be applied to practical IRS-assisted systems with discrete phase shift values for the IRS elements.

Similar to what we did in Chapter 3, we show the normalized throughput for backscatter and active wireless powered communications at the end of this chapter. The normalized throughput is depicted in Figure 5.10 as a function of the average transmit power at the PS. The observation is consistent with that of Chapter 3 in that the shares of backscatter transmission and wireless powered transmission respectively increases and decreases with increasing the PS transmit power.

5.4 Conclusion

This chapter studied an IRS-empowered BS-WPCN, where the backscatter and active information transmission of the users to the AP are assisted by an IRS. We investigated the optimization of IRS reflection coefficients, power allocation for the users'

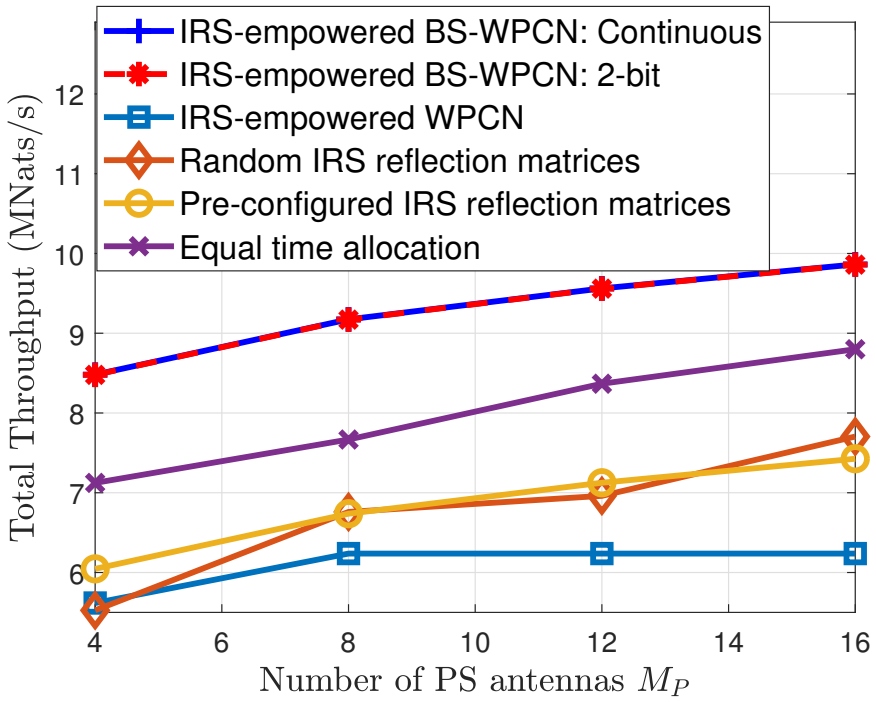

Figure 5.8: Total throughput vs. number of PS antennas.

active information transmission, transmit beamforming of the PS, receive beamforming of the AP, and time allocation, for maximizing the total throughput of the network. We presented a two-stage solution, where in the first stage, two methods based on AO and SCA techniques have been proposed for optimizing the IRS reflection coefficients in the backscatter information transmission phase. In the second stage, we have used the SDR and SCA techniques for optimizing AP transmit beamforming vectors, power and time allocation. Also, assuming an MMSE receiver at the AP, an efficient algorithm based on the BCD technique has been presented for jointly optimizing the AP receive beamforming vectors and IRS reflection coefficients when assisting the users' active communication. Numerical results have confirmed the effectiveness of the proposed model and scheme, and demonstrated the performance enhancements achieved by simultaneous integration of backscatter communication and IRS technologies into WPCN.

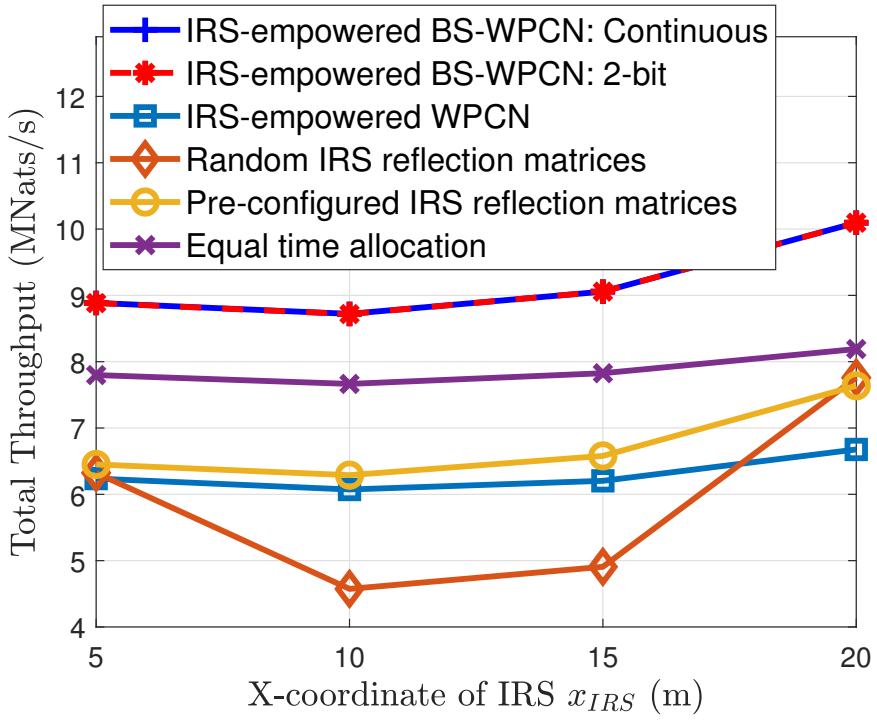

Figure 5.9: Total throughput vs. IRS x-coordinate.

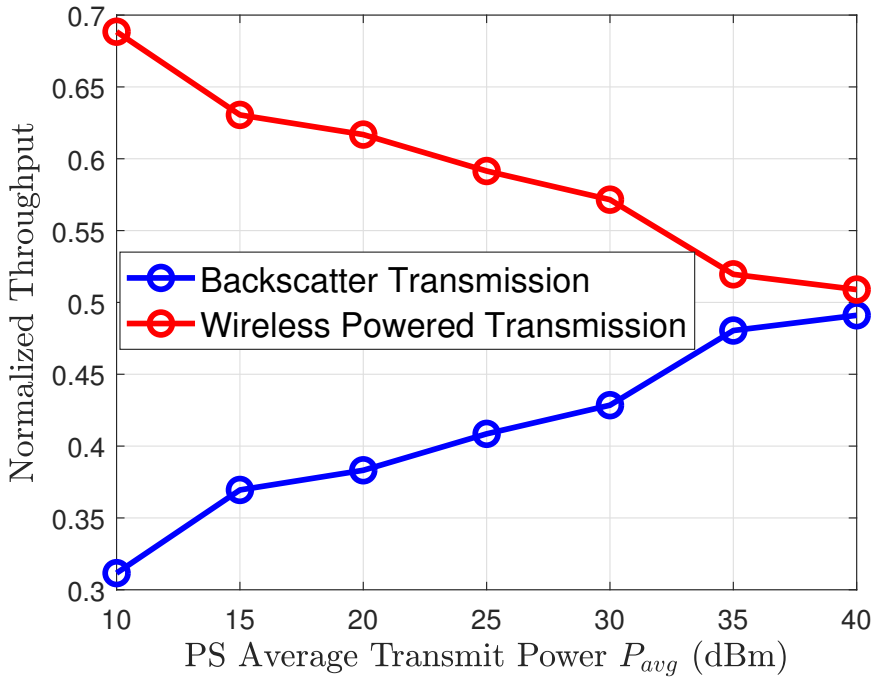

Figure 5.10: Normalized throughput of backscatter and wireless powered transmissions in the proposed IRS-empowered backscatter-assisted wireless powered communication network.

Chapter 6

Conclusions and Future Outlook

6.1 Concluding Remarks

While 5G wireless systems offer significant enhancements to their 4G counterparts in terms of bandwidth, connectivity, latency, etc. they are unable to meet the requirements of the applications envisioned for the next decade. The demands of applications such as super-smart city, autonomous vehicles, smart health-care, etc. are much greater than what 5G systems can afford. This means that we cannot yet expect the widespread realization of IoT/IoE and have to wait for 6G to finally fulfill this long-awaited promise. As an enabler and a key player for the success of IoT/IoE, WPCN has been the center of attention in the past decade and attracted a large number of journal and conference publications. Despite the extensive efforts in this area, WPCN still lacks the required performance for being seamlessly fitted into the next generation IoT/IoE environments. The main objective of this thesis has been to present ideas for improving the performance of WPCNs. Specifically, we proposed to integrate other novel technologies such as backscatter communication and IRS into WPCNs for enhancing their efficiency and making better use of the available

resources, without putting much extra burden in terms of deployment cost and implementation complexity on the network. The chapter-wise summary of this thesis is provided in the following.

In Chapter 1, we have discussed the requirements of the next generation of wireless systems, i.e., 6G, and explained why WPCN can be regarded as one of the enablers for the applications of this generation. We have presented the practical limitations of WPCNs and introduced backscatter communication and IRS as two groundbreaking technologies which have the potential to noticeably improve the performance of WPCNs. Followed by this, the motivations, objectives, and contributions of this thesis have been elucidated in detail.

In Chapter 2, we have reviewed the literature on WPCNs and the efforts which have been made for enhancing these networks. The backscatter communication and IRS technologies have also been overviewed in this chapter, along with a detailed discussion on the comparison between IRS and traditional relays.

In Chapter 3, we have proposed the idea of integrating backscatter communication with the traditional WPCN and enhancing the well-known HTT protocol to HBTT protocol. In particular, the energy transfer phase in the HTT protocol has been upgraded to an energy transfer and backscatter information transmission phase, and the users, which conventionally used the PS signal for only energy harvesting, have been enabled to utilize the signal for backscatter information transmission to the AP as well. The inclusion of backscatter transmission in the energy transfer phase results in a more efficient use of resources because the time and the energy signal, which have been only exploited for the purpose of energy collection, are now being used for two purposes. In this chapter, we have investigated the optimization of PS beamforming vector and network time allocation for maximizing the total network throughput. The extensive numerical simulations of this chapter have demonstrated

that integrating the two technologies of WPCN and backscatter communication can substantially improve the throughput compared to the scenarios where the users only use one of the mentioned technologies for communicating to the AP.

In Chapter 4, the integration of the IRS technology into WPCN has been studied, where the energy transfer from the PS to the users and the information transmission from the users to the AP have been empowered by the elements of an IRS. Specifically, an IRS has been added to the WPCN with the capability of modifying the energy and information signals and reflecting them towards the desired direction. The modification of signals is performed in a unified manner by IRS elements such that the signals that directly travel from the sender to the receiver are constructively combined with those modified and reflected by IRS elements, thus boosting the power of the received signals at the receiver. The focus of this chapter has been to optimize the reflection coefficients of IRS for assisting the energy transfer and information transmission, transmit beamforming vector of the PS, power and time allocation in order to maximize the throughput. Numerical results of this chapter have confirmed that an IRS-empowered WPCN remarkably outperforms a WPCN without IRS, even when the IRS reflection coefficients are not optimized. However, it has been shown that an IRS-empowered WPCN with optimized IRS reflection coefficients has much superior performance as compared to the case where the reflection coefficients are not optimized. At the end of this chapter, we have studied the performance of an IRS-empowered WPCN assuming that the IRS itself needs to harvest energy before being able to aid the energy and information transmissions. It has been revealed that the benefits of using IRS will diminish if the power consumption of IRS elements is high because IRS would not be able to assist the network operations until it has collected sufficient energy. This important observation needs to be taken into consideration in the design of future self-sustainable IRS-empowered WPCNs.

In Chapter 5, we have investigated the integration of both backscatter communication and IRS into WPCNs. The model studied in this chapter is similar to the one considered in Chapter 3 in that WPCN users are powered by the PS and communicate with the AP by both backscatter and active information transmission. However, the model differs from that of Chapter 3 as the AP is assumed to be equipped with multiple antennas and an IRS is also deployed for assisting the backscatter and active information transfer of the users. The objective of this chapter has been maximizing the overall throughput through the optimization of the reflection coefficients of IRS for assisting in both backscatter and active information transmissions, PS transmit beamforming vectors in the backscatter transmission phase, AP receive beamforming vectors in the active information transmission phase, power allocation for users' active information transfer, and network time allocation. It is worth mentioning that we jointly optimized the amplitude reflection coefficients and phase shifts of IRS elements in Chapters 4 and 5. While in Chapter 4 and the backscatter information transmission phase of Chapter 5, we can simply set the amplitude reflection coefficients to 1 in order to maximize reflection, this assumption is not applicable to the active information transfer of the IRS-empowered BS-WPCN in Chapter 5. In particular, as the users simultaneously transmit information in the active information transfer phase, the AP receives a combination of the users' signals. In such as case, each user's received information signal is treated as interference for other users' signals and the amplitude of the received signal for each user affects the performance of other users as well. Therefore, setting the amplitude reflections to 1 in this scenario would not provide us with the optimal solution. We have conducted extensive numerical simulations to evaluate the performance of the proposed algorithms and compared the throughput achieved in the proposed model with that obtained in the benchmark schemes. We have also validated the applicability of the proposed algorithms to practical scenarios

where there are only a limited number of available phase shifts for IRS elements and the phase shift values must be chosen from a discrete set instead of a continuous one.

The results and findings of this thesis along with the potential research directions which are subsequently discussed can serve as a useful resource for interested readers and spark further research in this area so that we can finally see large-scale implementations of WPCN in the emerging 6G-enabled IoT/IoE ecosystem.

6.2 The Way Forward

The incorporation of backscattering and IRS into WPCNs has been proved very useful for improving the performance of energy transfer and information transmission and taking WPCNs one step closer to full-scale deployment in the IoT/IoE era. Herein, we present the opportunities ahead for further extensions and performance improvements of WPCNs, wishing to light up the way for researchers in their future investigations.

- **Placement Optimization of IRS:** In the numerical simulations of Chapter 5, it has been revealed that the IRS should be placed either close to the users or close to the AP for achieving high network throughput. As IRS plays a significant role in improving the performance of WPCNs, the location of the IRS can add another degree of freedom for further performance enhancements. Therefore, placement optimization of IRS in IRS-empowered WPCN and IRS-empowered BS-WPCN is an important direction for future research.

- **Intelligent Transmitting Surface (ITS)-Enabled Passive Beamforming:** ITS is another type of intelligent surface in which the surface is co-located with the transmitter, enabling smart and reconfigurable passive beamforming. In this thesis, we have assumed active transmit beamforming at the PS and investigated the optimization of the PS beamforming vectors. With ITS, the

benefits of intelligent surfaces can also be exploited at the PS and performance gains can be achieved without needing to use excessive power. We thus believe that the joint design of passive beamforming at the PS and IRS is a worthwhile topic for future investigation.

- **Optimization of the Number of Active IRS Elements for Self-Sustainable Operation:** In numerical simulations of Chapter 4, we have investigated the scenario with energy harvesting IRS elements. It has been disclosed that the benefits of using IRS can be limited if the power consumption of the elements is high. To enable self-sustainable operation at the IRS without losing its advantages, the number of elements at the IRS which are activated for assisting the network can be reduced. Indeed, as the total power consumption of IRS directly depends on the number of reflecting elements, reducing the number of elements that are "on" can lower the total power consumption of the IRS and the network can still benefit from the assistance provided by the IRS "on" elements. This, however, needs deeper investigation to find the optimal number of IRS elements which are activated in each time-slot.

- **Multi-Purpose Employment of IRS:** In Chapters 4 and 5 of this thesis, IRS has been employed for assisting the network. Specifically, in Chapter 4, IRS elements has collaboratively worked for assisting in energy transfer in the first phase, while they cooperated to aid the information transmission in the second phase. Similarly, in Chapter 5, all IRS elements united for empowering the backscatter transmission of the users in the first phase, whereas they collaborated for assisting in active information transfer in the second phase. Therefore, we have assumed that IRS elements always unite for one objective which has been assisting in either energy transfer or information transmission. However, IRS elements can be used more dynamically to simultaneously serve

several purposes. For example, in the IRS-empowered BS-WPCN studied in Chapter 5, IRS elements can be divided into groups with each group working for a specific purpose. To elaborate, one group can be used for assisting in backscatter transmission of the users, while another group aids the energy transfer. This can be a very important direction of research because future 6G systems are expected to comprise heterogeneous devices. A device with urgent data may need the assistance of IRS to transmit the data to its receiver, while at the same time, another device is in desperate need for harvesting more energy to sustain its operations. We therefore highly recommend future researchers to look into the possibility of utilizing IRS for serving different purposes.

- **Multiple Cooperative IRSs for Assisting the Network:** In IRS-empowered WPCN and BS-WPCN models studied in Chapters 4 and 5, the IRS must be close to the PS, users, and AP to effectively aid the network. This may not be feasible in real-life large-scale WPCNs with numerous users and possibly multiple APs and PSs. In such cases, a single IRS is not sufficient for assisting the network due to large distances between different network elements. We thus need to exploit multiple cooperative IRSs which collaboratively serve the network. We therefore suggest multi-IRS-empowered large-scale WPCN as an important topic for future research.

- **Practical and Realistic Assumptions for Network Elements:** In order to gain useful insights and make theoretical studies applicable to practical scenarios, we have to use realistic models and make practical assumptions. In Chapter 5 of this thesis, we have used a practical model for energy conversion at WPCN users; however, we have ignored channel estimation errors and other hardware imperfections. Our work in this thesis can thus be extended to account for imperfect CSI and hardware impairments.

- **Rigorous and Lightweight Optimization Schemes:** In this thesis, like most of the works on IRS-aided wireless systems, we have resorted to the well-known techniques of SDR, SCA, and AO for optimizing variables. These methods, although widely used for performance optimization in wireless networks, fail to provide global optimum solutions. What's more, they incur considerable complexity which increases with the number of active antennas, passive elements, and users. Lack of robust and lightweight optimization algorithms is a large gap which needs to be filled for future large-scale implementation of IRS-empowered WPCN and BS-WPCN.

- **FD AP for Simultaneous Information Transmission and Reception:** This thesis only studied uplink information transfer from the users to the AP. However, downlink information transmission from the AP to the users is also important and needs to investigated. To this end, an FD AP can be used which can simultaneously send and receiver information. Under such a setting, the elements of IRS can be divided into two groups to support both downlink and uplink transmissions at the same time. For example, one group of IRS elements assists in downlink information transmission of the AP to user i and the other aids the uplink information transfer from user j to the AP. We think that this novel model is worthy of future investigation.

- **Efficient Channel Estimation Techniques:** The practicality of the proposed schemes and algorithms highly depends on the efficiency and accuracy of channel estimation methods. As IRS elements are almost passive and WPCN users are energy-constrained, channel acquisition in the IRS-empowered WPCN and BS-WPCN is not straightforward. We hence need novel channel estimation methods with low overhead and satisfactory accuracy.

- **Sensing-Enabled IRS:** In addition to its ability to enhance the performance of wireless systems, IRS can also be used as a sensing platform for monitoring the environment through its elements. By piggybacking the sensed data into the signals impinging on the surface, IRS presents an energy- and spectrum-efficient alternative to conventional sensors which need to consume extra power and bandwidth for reporting their data. Under the assumption of sensing-enabled IRS elements, it is worthwhile to study the performance of the IRS-empowered WPCN and BS-WPCN and revisit the schemes and algorithms proposed for performance optimization in these networks.

Bibliography

[1] H. Tataria, M. Shafi, A. F. Molisch, M. Dohler, H. Sjoland, and F. Tufvesson, "6G Wireless Systems: Vision, Requirements, Challenges, Insights, and Opportunities," *Proceedings of the IEEE*, vol. 109, no. 9, pp. 1166 - 1199, July 2021.

[2] K. David and H. Berndt, "6G Vision and Requirements: Is There Any Need for Beyond 5G," *IEEE Vehicular Technology Magazine*, vol. 13, no. 3, pp. 72 - 80, July 2018.

[3] W. Saad, M. Bennis, and M. Chen, "A Vision of 6G Wireless Systems: Applications, Trends, Technologies, and Open Research Problems," *IEEE Network*, vol. 34, no. 3, pp. 134 - 142, May/June 2020.

[4] S. Dang, O. Amin, B. Shihada, and M-S. Alouini, "What should 6G be?," *Nature Electronics*, vol. 3, pp. 20 - 29, January 2020.

[5] I. F. Akyildiz, A. Kak, and S. Nie, "6G and Beyond: The Future of Wireless Communications Systems," *IEEE Access*, vol. 8, pp. 133995 - 134030, July 2020.

[6] N. Rajatheva *et al.*, "White Paper on Broadband Connectivity in 6G," *Available Online: arxiv.org/abs/2004.14247*, April 2020.

[7] S. Nayak and R. Patgiri, "6G Communication Technology: A Vision on Intelligent Healthcare," *Health Informatics: A Computational Perspective in Health-*

care. Studies in Computational Intelligence, Springer, vol. 932, pp. 1 - 18, January 2021.

[8] E. C. Strinati, S. Barbarossa, J. L. Gonzalez-Jimenez, D. Ktenas, N. Cassiau, L. Maret, and C. Dehos, "6G: The Next Frontier: From Holographic Messaging to Artificial Intelligence Using Subterahertz and Visible Light Communication," *IEEE Vehicular Technology Magazine*, vol. 14, no. 3, pp. 42 - 50, September 2019.

[9] S. Elmeadawy and R. M. Shubair, "6G Wireless Communications: Future Technologies and Research Challenges," *2019 International Conference on Electrical and Computing Technologies and Applications (ICECTA)*, Ras Al Khaimah, UAE, November 2019, pp. 1 - 5.

[10] M. Z. Chowdhury, M. Shahjalal, S. Ahmed, and Y. M. Jang, "6G Wireless Communication Systems: Applications, Requirements, Technologies, Challenges, and Research Directions," *IEEE Open Journal of the Communication Society*, vol. 1, pp. 957 - 975, July 2020.

[11] J. He, K. Yang, and H-H. Chen, "6G Cellular Networks and Connected Autonomous Vehicles," *IEEE Network*, pp. 1 - 7, 2021.

[12] X. Lu, P. Wang, D. Niyato, D. I. Kim, and Z. Han , "Wireless Networks With RF Energy Harvesting: A Contemporary Survey," *IEEE Communication Surveys and Tutorials*, vol. 17, no. 2, pp. 757 - 789, Second Quarter 2015.

[13] M. K. Watfa, H. Alhassanieh, and S. Selman, "Multi-Hop Wireless Energy Transfer in WSNs," *IEEE Communications Letters*, vol. 15, no. 12, pp. 1275 - 1277, December 2011.

[14] S. Kashyap, E. Bjornson, and E. G. Larsson, "On the Feasibility of Wireless Energy Transfer Using Massive Antenna Arrays," *IEEE Transactions on Wireless Communications*, vol. 15, no. 5, pp. 3466 - 3480, May 2016.

[15] J. Xu and R. Zhang, "A General Design Framework for MIMO Wireless Energy Transfer With Limited Feedback," *IEEE Transactions on Signal Processing*, vol. 64, no. 10, pp. 2475 - 2488, May 2016.

[16] L. Shi, L. Zhao, K. Liang, and H-H. Chen, "Wireless Energy Transfer Enabled D2D in Underlaying Cellular Networks," *IEEE Transactions on Vehicular Technology*, vol. 67, no. 2, pp. 1845 - 1849, February 2018.

[17] J. Wang, Y. Li, Y. Jia, J. Zhang, S. Zhin, T. Q. S. Quek, "Wireless Energy Transfer in Extra-Large Massive MIMO Rician Channels," *IEEE Transactions on Wireless Communications*, pp. 1 - 14, 2021.

[18] P. Ramezani and A. Jamalipour, "Toward the Evolution of Wireless Powered Communication Networks for the Future Internet of Things," *IEEE Network*, vol. 31, no. 6, pp. 62 - 69, November/December 2017.

[19] H. Ju and R. Zhang, "Throughput Maximization in Wireless Powered Communication Networks," *IEEE Transactions on Wireless Communications*, vol. 13, no. 1, pp. 418 - 428, January 2014.

[20] S. Bi and R. Zhang, "Placement Optimization of Energy and Information Access Points in Wireless Powered Communication Networks," *IEEE Transactions on Wireless Communications*, vol. 15, no. 3, pp. 2351 - 2364, March 2016.

[21] S. Bi, Y. Zeng, and R. Zhang, "Wireless Powered Communication Networks: An Overview," *IEEE Wireless Communications*, vol. 23, no. 2, pp. 10 - 18, April 2016.

[22] P. Ramezani and A. Jamalipour, "Throughput Maximization in Dual-Hop Wireless Powered Communication Networks," *IEEE Transactions on Vehicular Technology*, vol. 66, no. 10, pp. 9304 - 9312, October 2017.

[23] P. Ramezani and A. Jamalipour, "Fairness Enhancement in Dual-Hop Wireless Powered Communication Networks," *2017 IEEE International Conference on Communications (ICC)*, Paris, France, May 2017, pp. 1 - 6.

[24] N. H. Mahmood *et al.*, "White paper on critical and massive machine type communication towards 6G," *Available Online: arxiv.org/abs/2004.14146*, May 2020.

[25] X. Lu, D. Niyato, H. Jiang, D. I. Kim, Y. Xiao, and Z. Han, "Ambient Backscatter Assisted Wireless Powered Communications," *IEEE Wireless Communications*, vol. 25, no. 2, pp. 170 - 177, April 2018.

[26] L. Bariah *et al.*, "A Prospective Look: Key Enabling Technologies, Applications and Open Research Topics in 6G Networks," *IEEE Access*, vol. 8, pp. 174792 - 174820, August 2020.

[27] C. Pan *et al.*, "Reconfigurable Intelligent Surfaces for 6G Systems: Principles, Applications, and Research Directions," *IEEE Communications Magazine*, vol. 59, no. 6, pp. 14 - 20, June 2021.

[28] P. Ramezani, B. Lyu, and A. Jamalipour, "Toward RIS-Enhanced Terrestrial/Non-Terrestrial Connectivity in 6G-Enabled IoE Era," Submitted to *IEEE Network*.

[29] Q. Sun, G. Zhu, C. Shen, X. Li, and Z. Zhong, "Joint Beamforming Design and Time Allocation for Wireless Powered Communication Networks," *IEEE Communications Letters*, vol. 18, no. 10, pp. 1783 - 1786, October 2014.

[30] L. Liu, R. Zhang, and K-C. Chua, "Multi-Antenna Wireless Powered Communication With Energy Beamforming," *IEEE Transactions on Communications*, vol. 62, no. 12, pp. 4349 - 4361, December 2014.

[31] G. Yang, C. K. Ho, R. Zhang, and Y. L. Guan, "Throughput Optimization for Massive MIMO Systems Powered by Wireless Energy Transfer," *IEEE Journal on Selected Areas in Communications*, vol. 33, no. 5, pp. 1640 - 1650, August 2015.

[32] I. Pehlivan and S. C. Ergen, "Scheduling of Energy Harvesting for MIMO Wireless Powered Communication Networks," *IEEE Communications Letters*, vol. 23, no. 1, pp. 152 - 155, January 2019.

[33] H. Ju and R. Zhang, "Optimal Resource Allocation in Full-Duplex Wireless-Powered Communication Network," *IEEE Transactions on Communications*, vol. 62, no. 10, pp. 3528 - 3540, October 2014.

[34] X. Kang, C. K. Ho, and S. Sun, "Full-Duplex Wireless-Powered Communication Network With Energy Causality," *IEEE Transactions on Wireless Communications*, vol. 14, no. 10, pp. 5539 - 5551, October 2015.

[35] H. Kim, H. Lee, M. Ahn, H-B. Kong, and I. Lee, "Subcarrier and Power Allocation Methods in Full Duplex Wireless Powered Communication Networks for OFDM Systems," *IEEE Transactions on Wireless Communications*, vol. 15, no. 7, pp. 4745 - 4753, July 2016.

[36] T. P. Do and Y. H. Kim, "Resource Allocation for a Full-Duplex Wireless-Powered Communication Network With Imperfect Self-Interference Cancelation," *IEEE Communications Letters*, vol. 20, no. 12, pp. 2482 - 2485, December 2016.

[37] D-H. Chen and Y-C. He, "Full-Duplex Secure Communications in Cellular Networks With Downlink Wireless Power Transfer," *IEEE Transactions on Communications*, vol. 66, no. 1, pp. 265 - 277, January 2018.

[38] R. Rezaei, S. Sun, X. Kang, Y. L. Guan, and M. R. Pakravan, "Secrecy Throughput Maximization for Full-Duple Wireless Powered IoT Networks Under Fairness Constraints," *IEEE Internet of Things J.*, vol. 6, no. 4, pp. 6964 - 6976, August 2019.

[39] J-H. Lee, Y-H. Cho, D-J. Park, and D. E. Chang, "Robust Beamforming and Time Allocation for Full-Duplex Wireless-Powered Communication Networks," *IEEE Communications Letters*, vol. 23, no. 9, pp. 1665 - 1669, September 2019.

[40] D. K. P. Asiedu, S. Mahama, C. Song, D. Kim, and K-J. Lee, "Beamforming and Resource Allocation for Multiuser Full-Duplex Wireless-Powered Communications in IoT Networks," *IEEE Internet of Things J.*, vol. 7, no. 12, pp. 11355 - 11370, December 2020.

[41] M. S. Iqbal, Y. Sadi, and S. Coleri, "Minimum Length Scheduling for Discrete-Rate Full-Duplex Wireless Powered Communication Networks," *IEEE Transactions on Wireless Communications*, 2021.

[42] Y. L. Che, L. Duan, and R. Zhang, "Spatial Throughput Maximization of Wireless Powered Communication Networks," *IEEE Journal on Selected Areas in Communications*, vol. 33, no. 8, pp. 1534 - 1548, August 2015.

[43] H. Ju and R. Zhang, "User Cooperation in Wireless Powered Communication Networks," *2014 IEEE Global Communications Conference*, Austin, TX, USA, December 2014, pp. 1430-1435.

[44] H. Chen, Y. Li, J. L. Rebelatto, B. F. Uchoa-Filho, and B. Vucetic "Harvest-Then-Cooperate: Wireless-Powered Cooperative Communications," *IEEE Transactions on Signal Processing*, vol. 63, no. 7, pp. 1700 - 1711, April 2015.

[45] X. Di, K. Xiong, P. Fan, H-C. Yang, and K. B. Letaief, "Optimal Resource Allocation in Wirelessly Powered Communication Networks With User Cooperation," *IEEE Transactions on Wireless Communications*, vol.16, no. 12, pp. 7936 - 7949, December 2017.

[46] W. Shin, M. Vaezi, J. Lee, and H. V. Poor, "Cooperative Wireless Powered Communication Networks With Interference Harvesting," *IEEE Transactions on Vehicular Technology*, vol.67, no. 4, pp. 3701 - 3705, April 2018.

[47] Y. Ma, H. Chen, Z. Lin, Y. Li, and B. Vucetic, "Distributed and Optimal Resource Allocation for Power Beacon-Assisted Wireless-Powered Communications," *IEEE Transactions on Vehicular Technology*, vol.68, no. 8, pp. 8243 - 8248, August 2019.

[48] Q. Wu, G. Zhang, D. W. K . Ng, W. Chen, and R. Schober, "Generalized Wireless-Powered Communications: When to Activate Wireless Power Transfer?," *IEEE Transactions on Communications*, vol.63, no. 10, pp. 3569 - 3583, October 2015.

[49] B. Lyu, T. Qi, H. Guo, and Z. Yang, "Throughput Maximization in Full-Duplex Dual-Hop Wireless Powered Communication Networks," *IEEE Access*, vol.7, pp. 158584 - 158593, October 2019.

[50] P. Ramezani, Y. Zeng, and A. Jamalipour, "Optimal Resource Allocation for Multiuser Internet of Things Network With Single Wireless-Powered Relay," *IEEE Internet of Things Journal*, vol.6, no. 2, pp. 3132 - 3142, April 2019.

[51] P. Ramezani and A. Jamalipour,"Two-Way Dual-Hop WPCN With A Practical Energy Harvesting Model," *IEEE Transactions on Vehicular Technology*, vol. 69, no. 7, pp. 8013- 8017, June 2020.

[52] S. Lee and R. Zhang,"Cognitive Wireless Powered Network: Spectrum Sharing Models and Throughput Maximization," *IEEE Transactions on Cognitive Communications and Networking*, vol. 1, no. 3, pp. 335- 846, September 2015.

[53] S. S. Kalamkar, J. P. Jeyaraj, A. Banerjee, and K. Rajawat,"Resource Allocation and Fairness in Wireless Powered Cooperative Cognitive Radio Networks," *IEEE Transactions on Communications*, vol. 64, no. 8, pp. 3246- 3261, August 2016.

[54] D. Xu and Q. Li,"Joint Power Control and Time Allocation for Wireless Powered Underlay Cognitive Radio Networks," *IEEE Wireless Communications Letters*, vol. 6, no. 3, pp. 294- 297, June 2017.

[55] D. Xu and Q. Li,"Resource Allocation for Secure Communications in Cooperative Cognitive Wireless Powered Communication Networks," *IEEE Systems Journal*, vol. 13, no. 3, pp. 2431- 2442, September 2019.

[56] E. Boshkovska, D. W. K. Ng, N. Zlatanov, and R. Schober, "Practical Non-Linear Energy Harvesting Model and Resource Allocation for SWIPT Systems," *IEEE Communications Letters*, vol.19, no. 12, pp. 2082 - 2085, December 2015.

[57] E. Boshkovska, D. W. K. Ng, L. Dai, and R. Schober, "Power-Efficient and Secure WPCNs With Hardware Impairments and Non-Linear EH Circuit," *IEEE Transactions on Communications*, vol.66, no. 6, pp. 2642 - 2657, June 2018.

[58] B. Clerckx, R. Zhang, R. Schober, D. W. K. Ng, D. I. Kim, and H. V. Poor, "Fundamentals of Wireless Information and Power Transfer: From RF Energy Harvester Models to Signal and System Designs," *IEEE Journal on Selected Areas in Communications*, vol.37, no. 1, pp. 4 - 33, January 2019.

[59] K. Xu *et al.*, "Beam-Domain SWIPT for mMIMO System With Nonlinear Energy Harvesting Legitimate Terminals and a Non-Cooperative Terminal," *IEEE Transactions on Green Communications and Networking*, vol.3, no. 3, pp. 703 - 720, September 2019.

[60] M. Grant and S. Boyd, "CVX: MATLAB Software for Disciplined Convex Programming," *Available Online: cvxr.com/cvx*, January 2020.

[61] C. Huang, A. Zappone, G. C. Alexandropoulos, M. Debbah, and C. Yuen, "Reconfigurable Intelligent Surfaces for Energy Efficiency in Wireless Communication," *IEEE Transactions on Wireless Communications*, vol. 18, no. 8, pp. 4157 - 4170, August 2019.

[62] Q. Wu and R. Zhang, "Intelligent Reflecting Surface Enhanced Wireless Network via Joint Active and Passive Beamforming," *IEEE Transactions on Wireless Communications*, vol. 18, no. 11, pp. 5394 - 5409, November 2019.

[63] M. Cui, G. Zhang, and R. Zhang, "Secure Wireless Communication via Intelligent Reflecting Surface," *IEEE Wireless Communications Letters*, vol. 8, no. 5, pp. 1410 - 1414, October 2019.

[64] C. Pan *et al.*, "Multicell MIMO Communications Relying on Intelligent Reflecting Surfaces," *IEEE Transactions on Wireless Communications*, vol. 19, no. 8, pp. 5218 - 5233, August 2020.

[65] Q. Wu and R. Zhang, "Weighted Sum Power Maximization for Intelligent Reflecting Surface Aided SWIPT," *IEEE Wireless Communications Letters*, vol. 9, no. 5, pp. 586 - 590, May 2020.

[66] C. Pan *et al.*, "Intelligent Reflecting Surface Aided MIMO Broadcasting for Simultaneous Wireless Information and Power Transfer," *IEEE Journal on Selected Areas in Communications*, vol. 38, no. 8, pp. 1719 - 1734, August 2020.

[67] S. Atapattu, R. Fan, P. Dharmawansa, G. Wang, J. Evans, T. A. Tsiftsis, "Reconfigurable Intelligent Surface Assisted Two–Way Communications: Performance Analysis and Optimization," *IEEE Transactions on Communications*, vol. 68, no. 10, pp. 6552 - 6567, October 2020.

[68] S. Lin, B. Zheng, B. C. Alexandropoulos, M. Wen, F. Chen, and S. Mumtaz, "Adaptive Transmission for Reconfigurable Intelligent Surface-Assisted OFDM Wireless Communications," *IEEE Journal on Selected Areas in Communications*, vol. 38, no. 11, pp. 2653 - 2665, November 2020.

[69] J. Yuan, Y-C. Liang, J. Joung, G. Feng, and E. G. Larsson, "Intelligent Reflecting Surface-Assisted Cognitive Radio System," *IEEE Transactions on Communications*, vol. 69, no. 1, pp. 675 - 687, January 2021.

[70] Q. Wu and R. Zhang, "Beamforming Optimization for Wireless Network Aided by Intelligent Reflecting Surface With Discrete Phase Shifts," *IEEE Transactions on Communications*, vol. 68, no. 3, pp. 1838 - 1851, March 2020.

[71] Y. Zeng and R. Zhang, "Optimized Training Design for Wireless Energy Transfer," in *IEEE Transactions on Wireless Communications*, vol. 63, no. 2, pp. 536-550, February 2015.

[72] D. Mishra and H. Johansson, "Channel Estimation and Low-complexity Beamforming Design for Passive Intelligent Surface Assisted MISO Wireless Energy Transfer," in *ICASSP 2019 - 2019 IEEE International Conference on Acoustics, Speech and Signal Processing (ICASSP)*, Brighton, U.K., May 2019, pp. 1-5.

[73] Z-Q. He and X. Yuan, "Cascaded Channel Estimation for Large Intelligent Metasurface Assisted Massive MIMO," in *IEEE Wireless Communications Letters*, vol. 9, no. 2, pp. 210-214, February 2020.

[74] Z. Wang, L. Liu, and S. Cui, "Channel Estimation for Intelligent Reflecting Surface Assisted Multiuser Communications: Framework, Algorithms, and Analysis," in *IEEE Transactions on Wireless Communications*, vol. 19, no. 10, pp. 6607-6620, October 2020.

[75] C. Hu, L. Dai, S. Han, and X. Wang, "Two-Timescale Channel Estimation for Reconfigurable Intelligent Surface Aided Wireless Communications," *IEEE Transactions on Communications*, pp. 1 - 12, 2021.

[76] A. P. Sample, D. J. Yeager, P. S. Powledge, and J. R. Smith, "Design of a Passively-Powered, Programmable Sensing Platform for UHF RFID Systems," *2007 IEEE International Conference on RFID*, Grapevine, TX, USA, March 2007, pp. 149 - 156.

[77] D. J. Yeager, P. S. Powledge, R. Prasad, D. Wetherall, and J. R. Smith, "Design of a Passively-Powered, Programmable Sensing Platform for UHF RFID Systems," *2008 IEEE International Conference on RFID*, Las Vegas, NV, US, April 2008, pp. 320 - 327.

[78] O. B. Akan, M. T. Isik, and B. Baykal,"Wireless Passive Sensor Networks," *IEEE Communications Magazine*, vol. 47, no. 8, pp. 92 - 99, August 2009.

[79] S. Roy *et al.*, "RFID: From Supply Chains to Sensor Nets," *Proceedings of the IEEE*, vol. 98, no. 9, pp. 1583 - 1592, September 2010.

[80] J. Kimionis, A. Bletsas, and J. N. Sahalos,"Increased Range Bistatic Scatter Radio," *IEEE Transactions on Communications*, vol. 62, no. 3, pp. 1091 - 1104, March 2014.

[81] V. Liu, A. Parks, V. Talla, S. Gollakota, D. Wetherall, and J. R. Smith,"Ambient Backscatter: Wireless Communication Out of Thin Air," *ACM SIGCOMM Computer Communication Review*, vol. 43, no. 4, pp. 39 - 50, October 2013.

[82] K. Lu, G. Wang, F. Qu, and Z. Zhong,"Signal Detection and BER Analysis for RF-Powered Devices Utilizing Ambient Backscatter," *2015 International Conference on Wireless Communications and Signal Processing (WCSP)*, Nanjing, China, October 2015, pp. 1 - 5.

[83] G. Wang, F. Gao, R. Fan, and C. Tellambura,"Ambient Backscatter Communication Systems: Detection and Performance Analysis," *IEEE Transactions on Communications*, vol. 64, no. 11, pp. 4836 - 4846, November 2016.

[84] B. Lyu, Z. Yang, G. Gui, and Y. Feng, "Wireless Powered Communication Networks Assisted by Backscatter Communication," *IEEE Access*, vol. 5, pp. 7254 - 7262, March 2017.

[85] D. T. Hoang, D. Niyato, P. Wang, and D. I. Kim,"Optimal Time Sharing in RF-Powered Backscatter Cognitive Radio Networks," *2017 IEEE International Conference on Communications (ICC)*, Paris, France, May 2017, pp. 1 - 6.

[86] D. T. Hoang, D. Niyato, P. Wang, D. I. Kim, and Z. Han,"Ambient Backscatter: A New Approach to Improve Network Performance for RF-Powered Cognitive

Radio Networks," *IEEE Transactions on Communications*, vol. 65, no. 9, pp. 3659 - 3674, September 2017.

[87] B. Lyu, H. Guo, Z. Yang, and G. Gui,"AThroughput Maximization for Hybrid Backscatter Assisted Cognitive Wireless Powered Radio Networks," *IEEE Internet of Things Journal*, vol. 5, no. 3, pp. 2015 - 2024, June 2018.

[88] S. H. Kim and D. I. Kim,"Hybrid Backscatter Communication for Wireless-Powered Heterogeneous Networks," *IEEE Transactions on Wireless Communications*, vol. 16, no. 10, pp. 6557 - 6570, October 2017.

[89] X. Lu, H. Jiang, D. Niyato, D. I. Kim, and Z. Han,"Wireless-Powered Device-to-Device Communications With Ambient Backscattering: Performance Modeling and Analysis," *IEEE Transactions on Wireless Communications*, vol. 17, no. 3, pp. 1528 - 1544, March 2018.

[90] X. Lu, G. Li, H. Jiang, D. Niyato, and P. Wang,"Performance Analysis of Wireless-Powered Relaying with Ambient Backscattering," *2018 IEEE International Conference on Communications (ICC)*, Kansas City, MO, USA, May 2018, pp. 1-6.

[91] M. D. Renzo *et al.*, "Smart radio environments empowered by reconfigurable AI meta-surfaces: an idea whose time has come," *EURASIP Journal on Wireless Communications and Networking*, vol. 2019, no. 1, pp. 1 - 20, May 2019.

[92] Q. Wu and R. Zhang, "Towards Smart and Reconfigurable Environment: Intelligent Reflecting Surface Aided Wireless Network," *IEEE Communications Magazine*, vol. 58, no. 1, pp. 106 - 112, January 2020.

[93] C. Huang *et al.*, "Holographic MIMO Surfaces for 6G Wireless Networks: Opportunities, Challenges, and Trends," *IEEE Wireless Communications*, vol. 27, no. 5, pp. 118 - 125, October 2020.

[94] B. Lyu, D. T. Hoang, S. Gong, and Z. Yang,"Intelligent Reflecting Surface Assisted Wireless Powered Communication Networks," *2020 IEEE Wireless Communications and Networking Conference Workshops (WCNCW)*, Seoul, Korea, April 2020, pp. 1-6.

[95] Y. Zheng, S. Bi, Y. J. Zhang, Z. Quan, and H. Wang,"Intelligent Reflecting Surface Enhanced User Cooperation in Wireless Powered Communication Networks," *IEEE Wireless Communications Letters* , vol. 9, no. 6, pp. 901- 905, June 2020.

[96] P. Ramezani and A. Jamalipour,"Throughput Maximization in Backscatter Assisted Wireless Powered Communication Networks," *2019 IEEE International Conference on Communications (ICC)*, Shanghai, China, May 2019, pp. 1-6.

[97] P. Ramezani and A. Jamalipour,"Optimal Resource Allocation in Backscatter Assisted WPCN With Practical Energy Harvesting Model," *IEEE Transactions on Vehicular Technology*, vol. 68, no. 12, pp. 12406- 12410, December 2019.

[98] Z-Q. Luo, W-K. Ma, A. M-C. So, Y. Ye, and S. Zhang,"Semidefinite Relaxation of Quadratic Optimization Problems," *IEEE Signal Processing Magazine*, vol. 27, no. 3, pp. 20- 34, May 2010.

[99] B. Lyu, P. Ramezani, D. T. Hoang, S. Gong, Z. Yang, and A. Jamalipour,"Optimized Energy and Information Relaying in Self-Sustainable IRS-Empowered WPCN," *IEEE Transactions on Communications*, vol. 69, no. 1, pp. 619 - 633, January 2021.

[100] P. Ramezani and A. Jamalipour,"Backscatter-Assisted Wireless Powered Communication Networks Empowered by Intelligent Reflecting Surface," *IEEE Transactions on Vehicular Technology*, vol. 70, no. 11, pp. 11908-11922, November 2021.

[101] J. Guo and X. Zhu,"An Improved Analytical Model for RF-DC Conversion Efficiency in Microwave Rectifiers," *2012 IEEE/MTT-S International Microwave Symposium Digest*, Montreal, QC, Canada, June 2012, pp. 1-3.

[102] C. R. Valenta and G. D. Durgin,"Harvesting Wireless Power: Survey of Energy-Harvester Conversion Efficiency in Far-Field, Wireless Power Transfer Systems," *IEEE Microwave Magazine*, vol. 15, no. 4, pp. 108- 120, June 2014.

[103] G. Papotto, F. Carrara, and G. Palmisano,"90-nm CMOS Threshold-Compensated RF Energy Harvester," *IEEE Journal of Solid-State Circuits*, vol. 46, no. 9, pp. 1985 - 1997, September 2011.

[104] M. Stoopman, S. Keyrouz, H. J. Visser, K. Philips, and W. A. Serdijn,"Co-Design of a CMOS Rectifier and Small Loop Antenna for Highly Sensitive RF Energy Harvesters," *IEEE Journal of Solid-State Circuits*, vol. 49, no. 3, pp. 622 - 634, March 2014.

[105] D. Khan *et al.*,"A CMOS RF Energy Harvester With 47% Peak Efficiency Using Internal Threshold Voltage Compensation," *IEEE Microwave and Wireless Components Letters*, vol. 29, no. 6, pp. 415 - 417, June 2019.